Application of a Modified k–ε Turbulence Model to Gas Turbine Combustor Geometries

by

Heather L. Relation

Thesis submitted to the Faculty of the
Virginia Polytechnic Institute and State University
in partial fulfillment of the requirements for the degree of
Master of Science
in
Mechanical Engineering

APPROVED:

Dr. W. F. Ng, Chairman

Dr. H. L. Moses

Dr. C. L. Dancey

April, 1993

Blacksburg, Virginia

Application of a Modified k–ε Turbulence Model

to Gas Turbine Combustor Geometries

by

Heather L. Relation

Dr. W. F. Ng, Chairman

Mechanical Engineering

(ABSTRACT)

The k–epsilon turbulence model yields inconsistent and diffusive results for swirling and recirculating flows, which are characteristic of combustor geometries. Y. S. Chen and S. W. Kim propose a modification to the k–epsilon turbulence model which has shown improved predictions for several complex flows. This study evaluates the application of the Chen modification of the k–epsilon turbulence model to combustor geometries by applying the modification to two burner test cases which contain the elemental flow characteristics of an industrial gas turbine combustor. The modification is implemented into a commercial computational fluid dynamics (CFD) code. The results show an improved prediction of the location, shape and size of the primary centerline recirculation zone for both cases. The large swirl and axial velocity gradients, which are diffused by the standard k–epsilon model, are preserved by the Chen model. The overprediction of turbulent eddy viscosity in regions of high shear, which is characteristic of k–epsilon, is controlled by the Chen modification. In industrial combustor design, the prediction of the location, size and shape of primary flow features is of paramount importance. The Chen modification can, therefore, be considered a successful improvement to the k–epsilon model and can be considered applicable to combustor geometries.

Acknowledgements

My sincerest thanks to Dr. Wing Fai Ng, whose support of my goals is much appreciated. His enthusiasm for my work and good general advice has guided me through the difficult times of my graduate studies.

My committee members, Dr. Clint L. Dancey and Dr. Hal L. Moses deserve a special note of appreciation for being so flexible and for supporting my late change of committee.

My research has been supported by General Electric Power Generation's Combustion Engineering. I have L. Berkeley Davis to thank for making this happen and for saving me from facing the imminent nightmare of conducting unfunded research. Stephen H. Black, who has overseen my project, has provided me with much appreciated advice and knowledge which has helped me along the way. What can I say about John L. Battaglioli? John has been both a teacher and a good friend. He has kept me from developing an ulcer in those extremely frustrating portions of my research. I am especially grateful for all that he has done for me. A special thanks to Margaret J. H. O'Brien, my officemate, friend, advisor, and proofreader. Without her I would still be sitting in the mail room pulling my hair out as I tried to

concentrate. For this, and much more, I am forever indebted to her. I would like to thank Elizabeth (Betty) A. Beaudoin for all the advice and thoughtful insight she has given me along the way. She is a fine engineer and an inspiration to me.

My greatest appreciation to my parents who have supported my decisions and encouraged my dreams throughout my life. I owe what I am today to them and hope that they can be proud.

A final thanks to my fiancé, David D. Chapman, for all of his love and support. I truly could not have made it this far without him.

Table of Contents

List of Illustrations

Nomenclature

C_i	convective term in the Navier–Stokes equations
C_μ	proportional coefficient in the Boussinesq approximation
f	body forces
f_+ and f_-	linear interpolation factors
F_i	flux in the i^{th} direction
g	metric tensor
k	turbulent kinetic energy
L	turbulent length scale
p	pressure
$\vec{s}$	surface vector
t	time
T	integrated time step
u	velocity
V_t	turbulent velocity scale
x	coordinate direction

Greek Letters

α	proportionality constant
δ_{ij}	Kronecker delta
ε	turbulent energy dissipation
μ	molecular or laminar viscosity
ν	kinematic viscosity
ϱ	density
τ_t	turbulent stress tensor
Φ	any of the dependent variables of the Navier–Stokes equations

Subscripts

i, j, or k	refers to the i_{th}, j_{th} or k_{th} coordinate direction
t	refers to a turbulent quantity

Superscripts

$(\ )'$	refers to the fluctuating component of the term
$\overline{(\ )}$	refers to the time averaged value of the term

1.0 Introduction

Computational fluid dynamics is a field that has made extraordinary progress in the past twenty years. Today, automotive and aerospace companies are using computational analyses to decrease the number of iterations in the design process [1,2]. CFD is a particularly attractive design tool to the gas turbine industry. Designing the combustor for a gas turbine requires expensive testing and many iterations. Previously, the combustion engineer has relied primarily on experience, test results and crude analyses based on empirical formulations to make final design decisions [3]. CFD has the potential to explain the physics of flow phenomena occurring in a combustor can, where experimental data are often not available. It is possible to acquire limited data in the combustor, but the process is cumbersome, expensive [4] and the results are non–comprehensive [5]. Numerical analysis can, thus, be used to reduce the number of iterations by providing insight on the changes that a design parameter or geometrical feature will have on the characteristics of the flow in the combustor.

The four things that are of primary importance in designing a gas turbine combustor are emissions, cooling, flame stabilization and dynamics. Dynamics are vibrations of the combustor can that occur because of the large pressure oscillations that result from the combustion process. This acoustics problem has been the

subject of many investigations, but still little is known about how to control it. Emissions are under strict regulation by federal and local government agencies, thereby forcing companies to design low emissions combustors. NOx, CO, and unburned hydrocarbon levels, which are under the most strict regulations, are dependent on the temperature and equivalence ratio at which the fuel–air mixture burns. Local equivalence ratio, a measure of fuel to air in the mixture, is highly dependent on turbulent motion in the flow. Cooling and flame stabilization, which both can be accomplished by a number of different methods, are also turbulent processes. This thesis has not attempted to address computational kinetics, but rather it focuses on the problem of accurately predicting turbulent flow structures in complex industrial geometries. This task can not be accomplished without the aid of numerical analysis, and is of significant importance to the combustion engineer.

Flame stabilization is a basic requirement of all gas turbine combustors [3]. For a flame to be stabilized, the fuel–air mixture entering the combustor must be supplied with a portion of the hot products of combustion which contain necessary catalysts for the reaction to occur [3]. This can be accomplished by inducing recirculation. A recirculation zone is characterized by a negative velocity in the streamwise, or axial, direction. One method by which this flow feature can develop is by introducing an axial flow to a large expansion, such as a backward facing step. The large adverse pressure gradient encountered will result in a flow reversal, or recirculation. Another method of inducing recirculation, popular in the gas turbine industry, is to introduce swirl to the flow. Axisymmetric swirl is defined as a tangential velocity component imposed on an axial flow. A swirling flow, when allowed to expand in the radial direction, will form a low pressure zone in the core region near

the flow's symmetry axis. The result is a flow reversal about the centerline. This phenomena is known as vortex breakdown and the resulting flow reversal is often described as a centerline recirculation [7]. Both methods of inducing recirculation are employed by the gas turbine industry. Thus, the study of recirculating and swirling flow, both complex turbulent flows, is important in this investigation.

The accuracy of a turbulent flow calculation is primarily dependent on the method of modeling turbulence. Presently, the most widely used turbulence model in commercial CFD codes is k–epsilon [8]. The k–epsilon model gives comprehensive results that are consistent with the experimental data for most turbulent flows. It is also computationally less time and memory intensive than Reynold's stress formulations and direct numerical simulations (DNS) which claim to be more accurate for most cases. Time and memory are factors which are limited by a company's design deadlines and computer resources. K–epsilon is, thus, implemented in many of the commercial CFD codes available today because it provides a combination of timely and comprehensive results for a broad range of complex turbulent flows. Although widely used, the k–epsilon turbulence model tends to underpredict large gradients in swirling and recirculating flows which are characteristic in a combustor. Many modifications have been made to the model to attempt to eliminate this problem. However, the applications of these improvements are limited to the narrow range of flow types for which they were developed [9]. Geometries that are dominant in engineering industries involve a multitude of flow types, making these modifications inapplicable.

Y. S. Chen and S. W. Kim present a modification to the k–epsilon turbulence model which is not flow specific and can be applied to a broad range of flow configurations [10]. Unlike previous modifications, the model is simple and takes a

more general approach to ascertaining a remedy to the problems associated with k–epsilon. Chen and Kim (referred to from hereon as just Chen) applied their modification to a number of complex flow types. Chen's model has demonstrated improved results for round and plane co–flowing jets, submerged jets, backward facing step flow and a swirling flow case. In particular, the predictions of the backward facing step and swirling flow cases Chen has chosen demonstrated a significant improvement from the standard k–epsilon model.

Flow in an industrial combustor is a combination of swirling, recirculating and turning flows. The recirculating flow which Chen had evaluated was formed when a two–dimensional axial flow encountered a backward facing step [10]. This application showed great improvement from the results obtained with the standard k–epsilon model. As previously discussed, swirl is often also used in combustors to create recirculation. Chen had applied his modification to a swirling flow which resulted in the development of a centerline recirculation [10]. The inlet boundary condition, however, had been applied within the recirculation zone. Therefore, Chen merely evaluated the ability of his modification to maintain a recirculation which had already been specified. This evaluation, is thus, an inadequate measure of the modification's ability to predict the development of a recirculation zone induced by swirl. Chen, also, had not tested his modification on a flow where the effects of curvature greatly influence the flow characteristics. Preliminary work for this thesis, discussed further in Appendix A, has determined that in these cases the Chen modification does not result in improved predictions. The application of the Chen modification to combustor geometries, however, can not be discounted. The flow patterns characteristic of an industrial combustor are much more complex than the classic physics cases tested by Chen and previously tested as preliminary work

for this thesis. The application of the Chen modification to gas turbine combustors, therefore, can not be evaluated based on these results.

The purpose of this study is to evaluate the application of the Chen modification of the k–epsilon turbulence model to combustor geometries by applying the modification to two quarled burner test cases which contain the elemental flow characteristics of an industrial combustor. Unlike Chen's analysis of a swirling flow, the quarled burner cases, whose geometries and flow characteristics are depicted in Figures 1 and 2, include a ramp, which turns the flow before it reaches the expansion. Because the flow is entering the expansion at an angle, recirculation will not occur as a function of the geometry, but of the swirl, making the quarled burner cases a much better evaluation of the Chen modification's ability to improve calculations for swirling and separating flows. This analysis also includes computation of the region before the expansion, whereas Chen begins computation within the recirculation zone. The flow in the region approaching the expansion is highly anisotropic, a characteristic which k–epsilon is unable to model. Also, in a practical industrial application the lack of availability of adequate test data makes it impossible to provide an inlet boundary condition in the recirculation zone where flame is stabilized. The modeling of this region, therefore, is important to determine the Chen modifications ability to give reasonable predictions of the basic flow characteristics in an anisotropic flow. This analysis involves no reaction, as it is the ability of the Chen modification to improve turbulent flowfield predictions that is being evaluated. The flow can be considered axisymmetric and incompressible. The quarled burner cases, overall, allow a thorough investigation of the Chen modification's applicability to analysis of industrial gas turbine combustor flows.

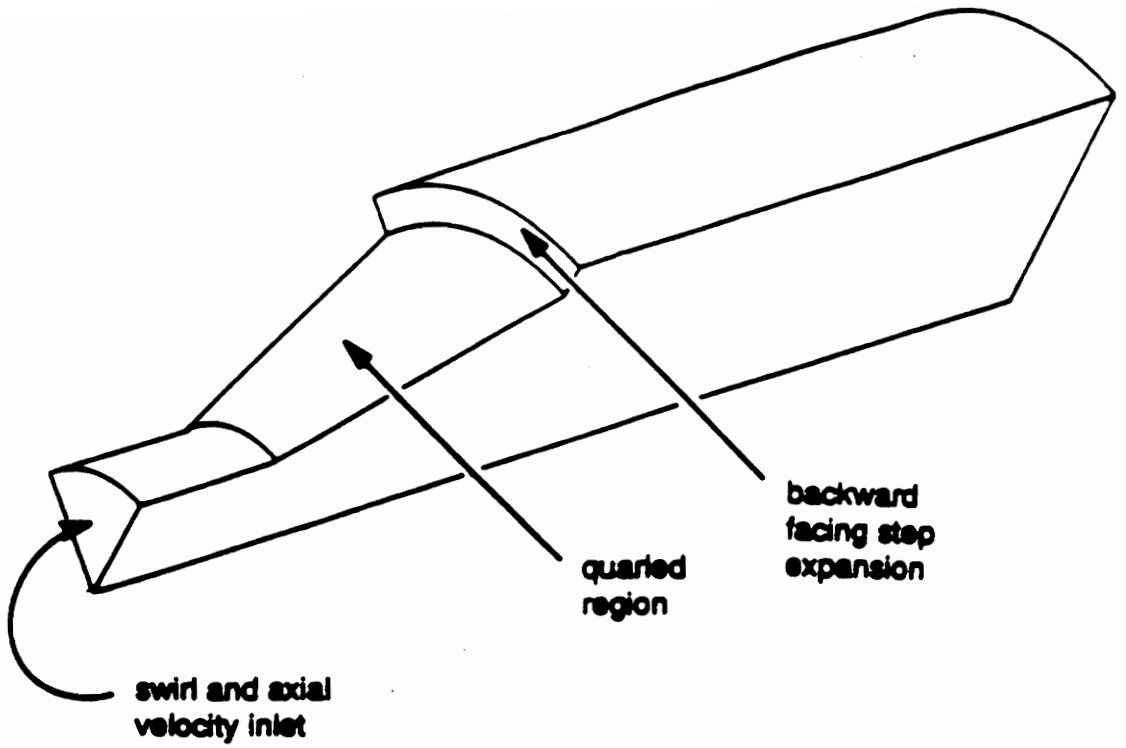

Figure 1a. Quarled Burner Case 1, Geometrical Features

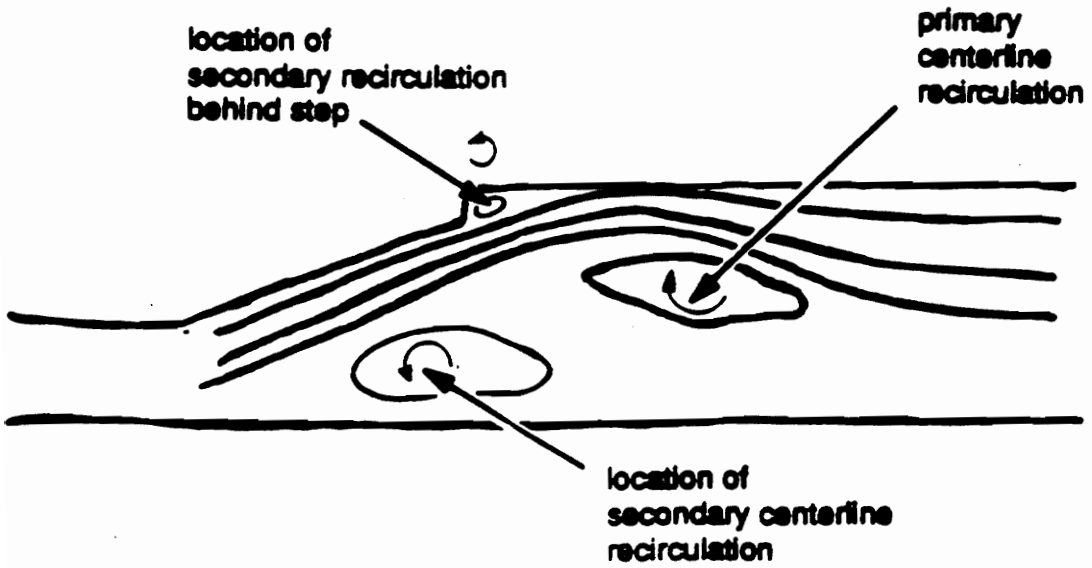

Figure 1b. Quarled Burner Case 1, Flow Features [11]

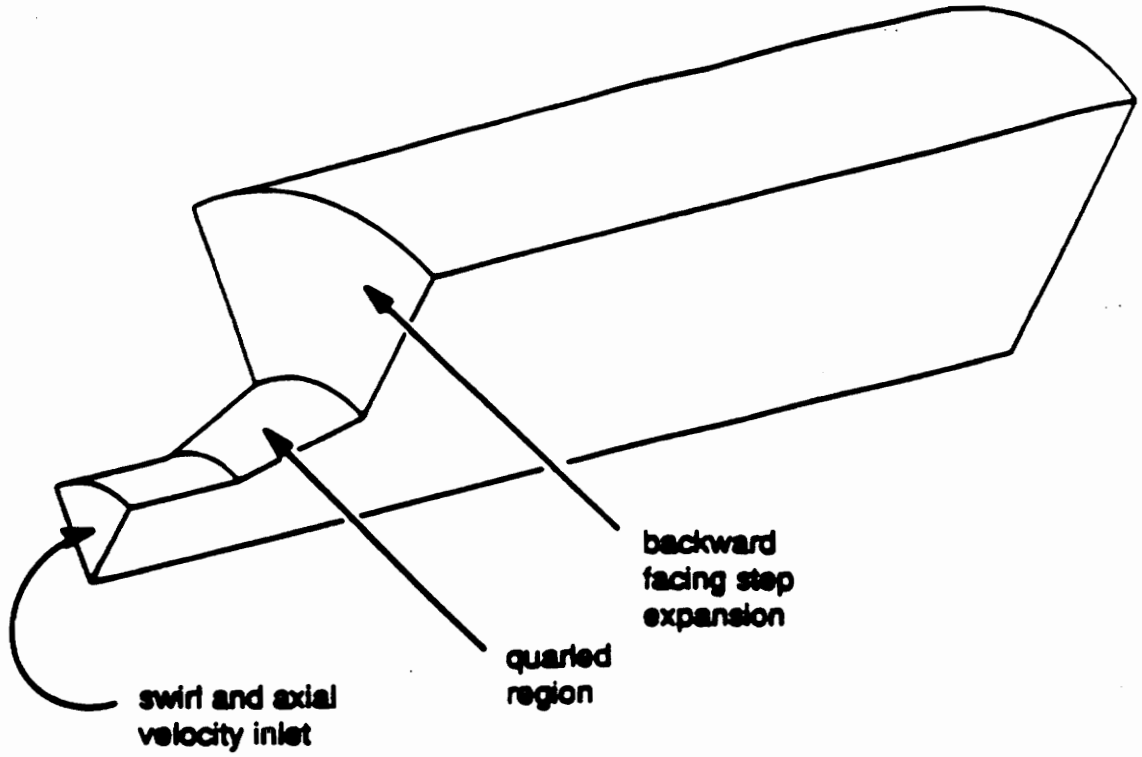

Fig. 2a. Quarled Burner Case 2, Geometrical Features

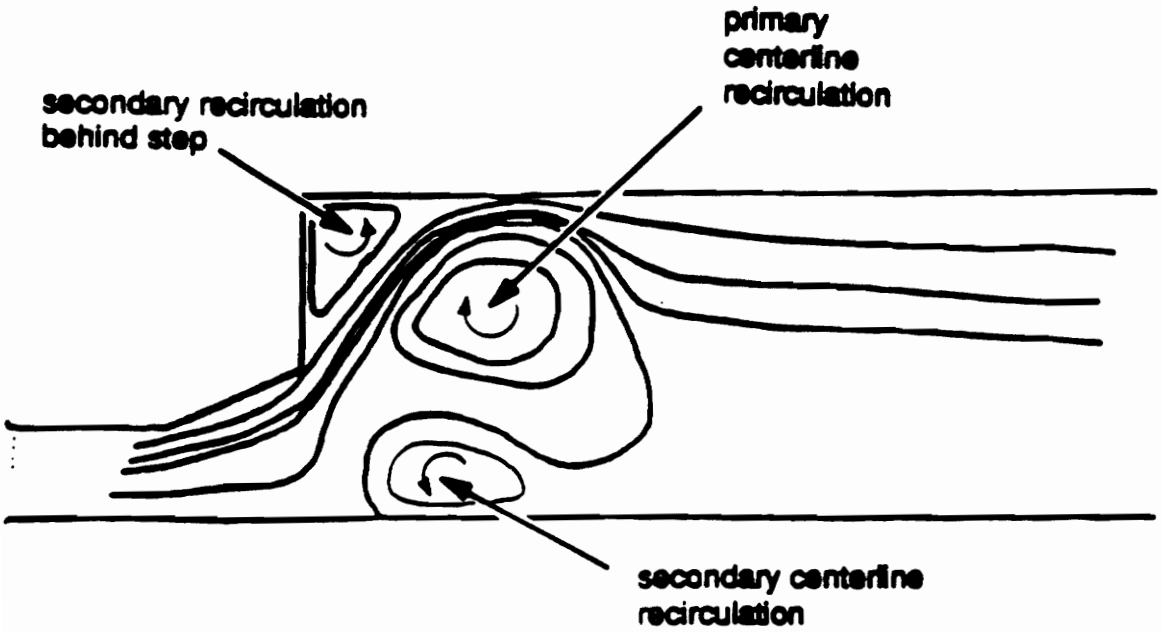

Fig. 2b. Quarled Burner Case 2, Flow Features

The modification has been implemented into STAR–CD, a commercial CFD code. A discussion of STAR–CD's capabilities and discretization methods is located in Appendix B. The details on the implementation of the Chen modification into STAR–CD and the use of the code with the Chen model can be found in Appendix C. The modification to the code was verified using a case similar to the one that Chen has shown to yield improved results. The case chosen is Vogel and Eaton's two dimensional rectangular backward facing step [12]. The details of the verification are discussed in Appendix D.

This thesis begins with a discussion of the deficiencies of the k–epsilon model. Previous improvements made to k–epsilon and their deficiencies are discussed. Also included in the background is an introduction to the Chen modification followed by a discussion of its advantages over the previously proposed improvements to the k–epsilon model. In addition, results from the evaluation of the quarled burner test cases with STAR–CD's standard k–epsilon model are presented. The application of the Chen modification and why it should improve predictions for these cases is then discussed. A brief introduction to turbulence modeling follows. The k–epsilon model is presented, precluding the introduction of the Chen modification. A description of the quarled burner test cases is included next. This chapter contains a detailed description of the geometry, the flow characteristics and experimental test locations of both burner cases. Also included is a description of the mesh, boundary conditions and discretization methods used for each case. Finally, the results of the computations performed with the Chen modification implemented in STAR–CD are presented, followed by a discussion of the predictions. Conclusions and recommendations complete the thesis.

2.0 Background

The standard k–epsilon model, while giving comprehensive and consistent predictions for most turbulent flows, produces highly diffusive results for certain classes of complex flows. By highly diffusive results, it is meant that the k–epsilon turbulence model tends to underpredict gradients in regions of high shear. Thus, the purpose of this chapter is to discuss the deficiencies of the k–epsilon model, introduce Chen's modification to k–epsilon and discuss why an improvement in the prediction of the flow characteristics of the quarled burner test cases should be expected with it's application. Since the k–epsilon model is commonly employed, this chapter assumes some familiarity with it. A further description of the k–epsilon turbulence model can be found in chapter 3.1.

As related to the current investigation, k–epsilon tends to underpredict the length of the recirculation zone behind a rectangular backward facing step and overpredict the decay of tangential momentum in a swirling flow. The diffusive characteristic of the k–epsilon model is most often attributed to the turbulent dissipation equation, which is highly empirical in nature. For this reason, most improvements have been achieved by altering the equation for epsilon.

A popular method of improving predictions in swirling flow and streamline curvature cases is the use of the Richardson correlation. Boysan and the team of

Launder, Pridden and Sharma propose models that add a source term to the dissipation equation [13]. The coefficient of this additional source term is based on the Richardson number and attempts to sensitize the dissipation to the effects of swirl and curvature. Both modifications require that an arbitrary limit be set on the magnitude of the Richardson number when it is negative to assure that an excessively large curvature correction will not cause a negative dissipation sink. Another fault of this type of modification is that the added coefficient is not optimized for general swirling flows and, therefore, is highly case specific. In an attempt to create a general modification to the k–epsilon model for turning flows, Pourahmadi and Humphrey modify C_μ to account for the effects of streamline curvature [14]. Their model experiences some success in predicting the coefficient of friction on the concave and convex surfaces of a curved duct, but makes only a slight improvement over the Richardson correlations in the prediction of velocity. Hanjalic and Launder attempt to improve predictions in flows with high adverse pressure gradients [15]. To do this, they choose to retain the irrotational contribution to production which is ordinarily neglected in the closure of the dissipation equation. Results obtained with this modification are improved for decelerated flows. However, to model the irrotational term, further empiricism is required which, as in the case of the four modifications discussed previously, limits the scope of application to the flows for which the coefficients were determined.

Chen approaches the modification of the k–epsilon turbulence model from a more general viewpoint. The diffusive nature of k–epsilon, as discussed before, is assumed to be a result of the highly empirical turbulent dissipation equation. In areas of high shear, the model predicts that the rate of production of turbulent kinetic energy increases much more quickly than the rate of turbulent dissipation. This does not accurately represent the reaction of the turbulence parameters to shear

flow and, hence, turbulent viscosity is overpredicted. Chen adds a second time scale, which is a function of production, to the dissipation equation to allow the model to respond to mean strain more effectively. The addition of the second time scale results in an extra source term and accompanying coefficient. The model constants were determined using experimental data of homogeneous turbulence decay with or without mean strain imposed, a near wall boundary conditions analysis and numerical optimization [10]. Thus, the empiricism does not limit the model to a specific case. Chen tested his modification on a wide variety of flow types to assess its generality. The model demonstrated improved results for round and plane co–flowing jets, submerged jets, backward facing step flow and confined swirling flow. Because of its applicability to a broad base of flow types and its success in improving results for these test cases, the Chen modification is attractive as a possibility for improved numerical predictions of more complex flow geometries such as combustor flows.

Calculations using the standard k–epsilon model of turbulence exhibit poor correlation to the experimental results of the two quarled burner cases. Details on the experiment and computational model can be found in chapter 4. Case 1 illustrates recirculation induced by swirling flow, whereas Case 2 also illustrates a secondary recirculation behind a stepped expansion. In both cases the flow is turned through a ramp or quarl which results in some expansion before the flow reaches the step. Figures 3 and 4 show comparisons of numerical and experimental results for the swirl and axial velocities of Case 1, respectively. The computational swirl and axial velocity are underpredicted at the outer radius and overpredicted in the intermediate region. This behavior clearly demonstrates the inability of the standard k–epsilon model to predict the large swirl and axial velocity gradients seen in this flow. Because swirl momentum is diffused over the entire

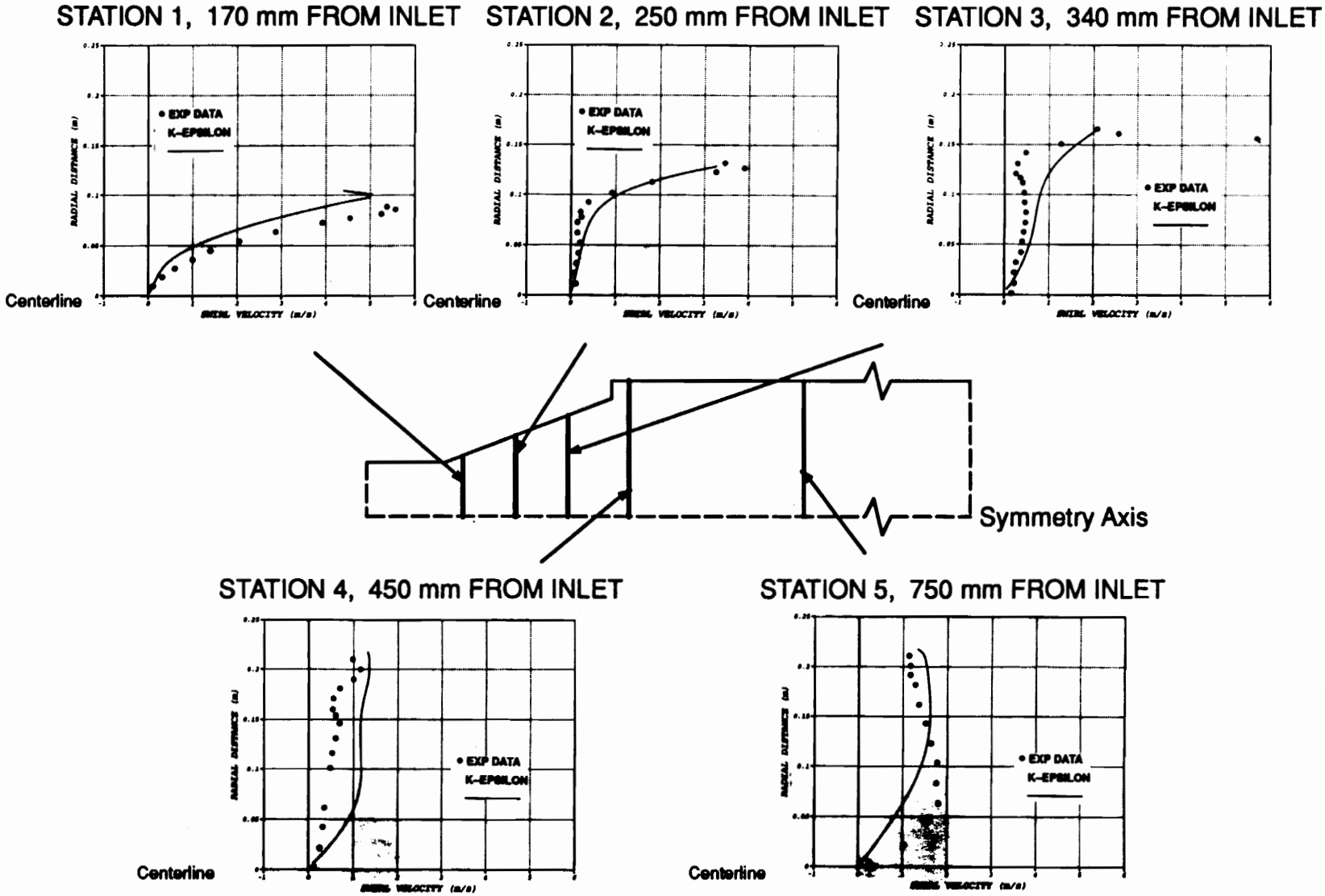

Figure 3. Quarled Burner Case 1, Swirl Velocity Predictions with the k–epsilon Turbulence Model

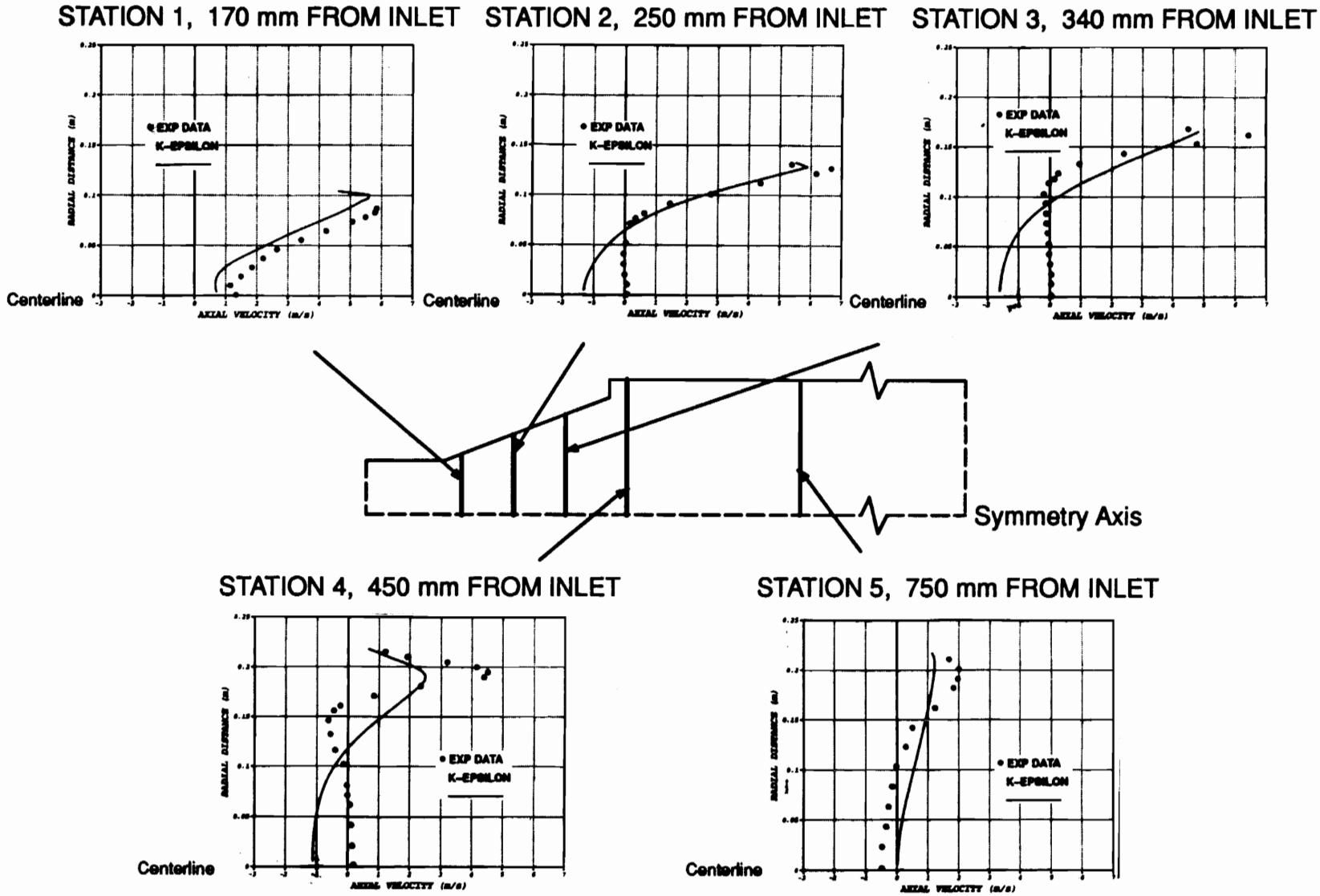

Figure 4. Quarled Burner Case 1, Axial Velocity Predictions with the k–epsilon Turbulence Model

radius, the jet moving along the outer edge of the quarl is less concentrated. This stream of flow begins to diffuse in the quarl which results in a lower maximum velocity entering the expansion. As Figure 5 illustrates, the center of recirculation is subsequently predicted to be closer to the axis of symmetry and further upstream than the experimental results dictate. Axial and swirl velocity profiles of both experimental and computational results for Case 2 are illustrated in Figures 6 and 7, respectively. Because there exists a recirculation behind the step, the peak in axial and swirl velocities is not seen at the outer radius, as in Case 1, but at mid–radius. Again, it is apparent that the k–epsilon model does not predict the large swirl velocity gradients in the flow and distributes the swirl momentum along the radial direction. Because the maximum velocity of the fluid moving over the centerline recirculation zone is underpredicted, the secondary recirculation zone behind the step is able to push out further into the expansion. The loss of the maximum velocity of this stream of flow also results in the displacement of the center of recirculation towards the axis of symmetry and further upstream. Figure 8 illustrates the failure of standard k–epsilon to reasonably model the characteristics of this geometry. Both Cases 1 and 2 demonstrate the diffusive nature of the standard k–epsilon model of turbulence. This quality greatly effects the consistency of predictions for complex flows and limits the use of the k–epsilon model to flows with no strong secondary flow patterns.

The Chen modification of the k–epsilon turbulence model has been shown to improve predictions for several configurations involving complex flow patterns. The success of this model is attributed to the addition of a second time scale to the dissipation equation. This extra term, put simply, lets the growth of turbulent dissipation catch up to the growth of kinetic energy. Standard k–epsilon tends to be especially diffusive in areas of high shear where the ratio of turbulent kinetic

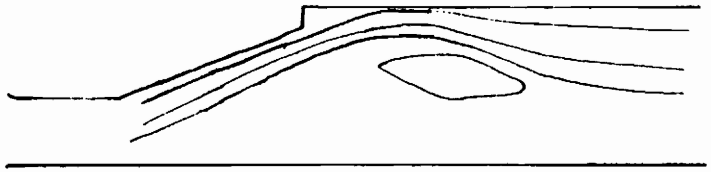

Figure 5a. Quarled Burner Case 1, Experimental Streamlines [11]

Figure 5b. Quarled Burner Case 1, k–epsilon Model Streamlines

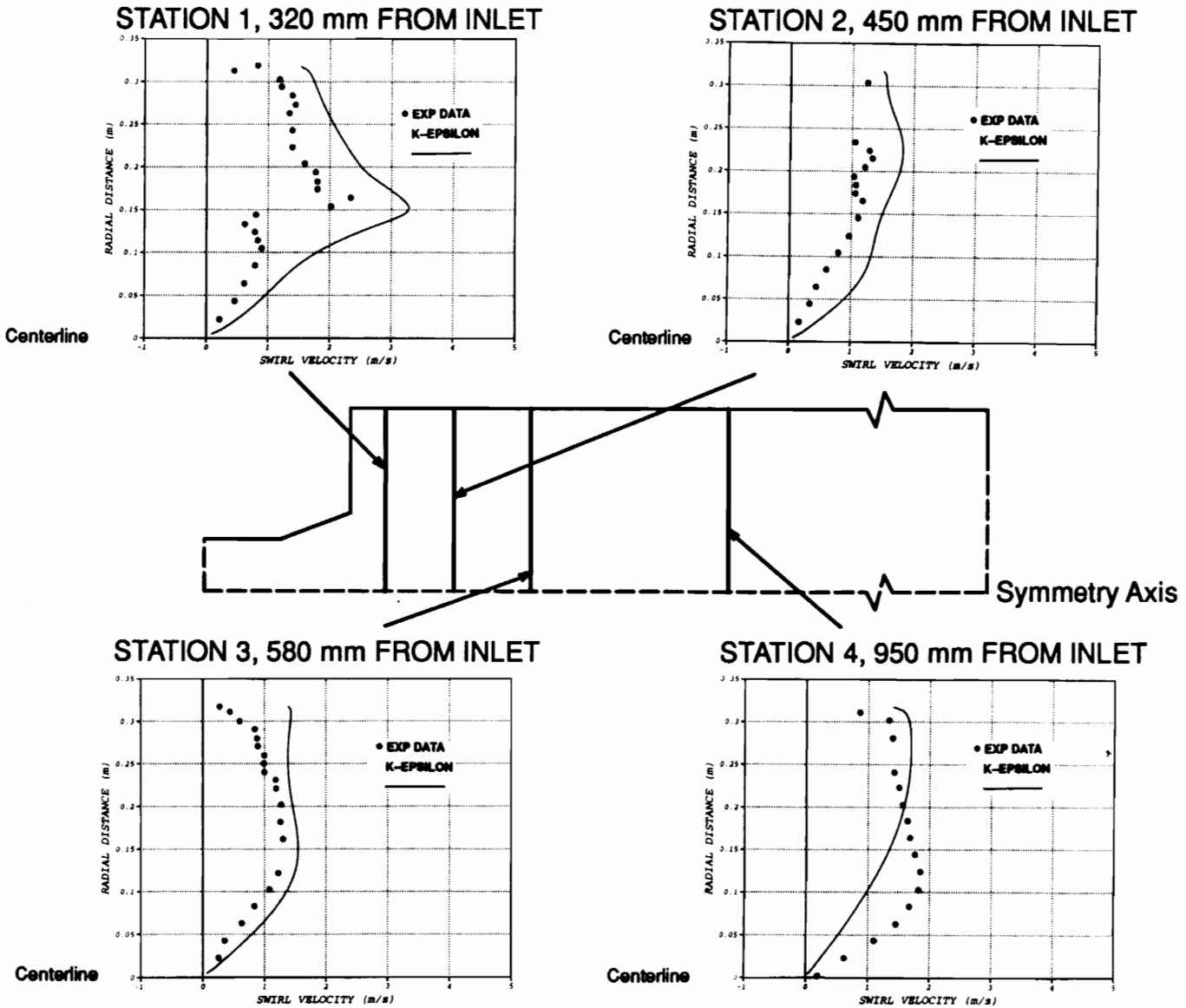

Figure 6. Quarled Burner Case 2, Swirl Velocity Predictions with the k–epsilon Turbulence Model

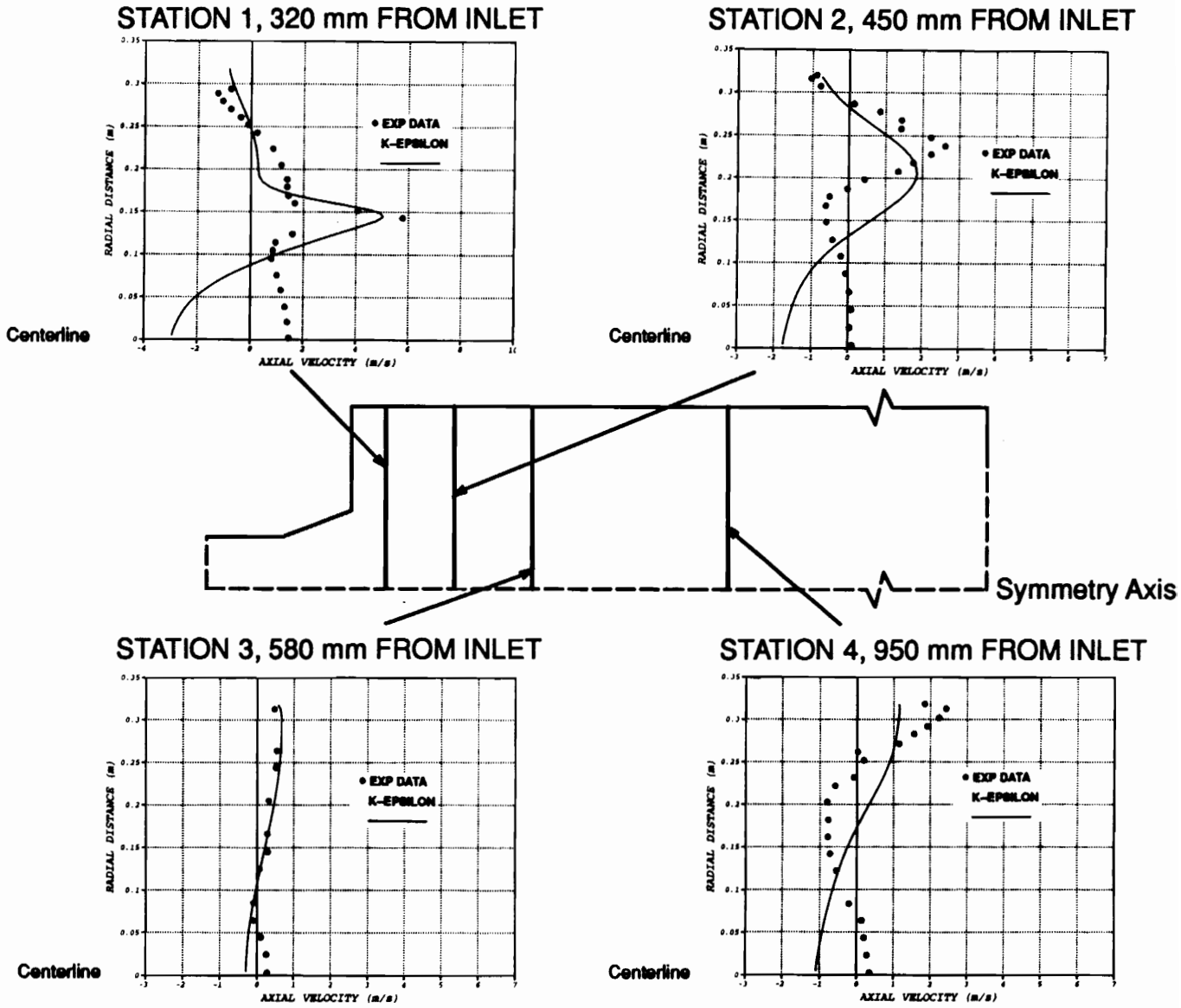

Figure 7. Quarled Burner Case 2, Axial Velocity Predictions with the k–epsilon Turbulence Model

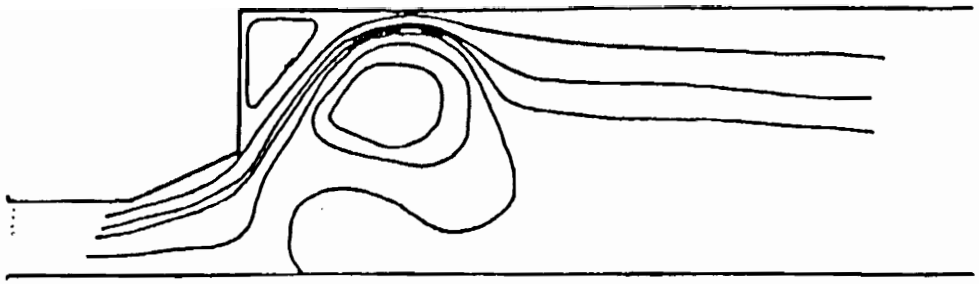

Figure 8a. Quarled Burner Case 2, Experimental Streamlines [11]

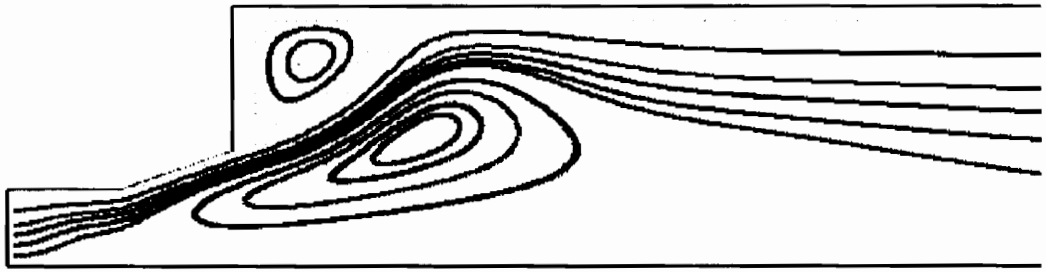

Figure 8b. Quarled Burner Case 2, k–epsilon Model Streamlines

energy to turbulent dissipation is overpredicted. This pattern, subsequently, results in the overprediction of turbulent viscosity in this region. The momentum of the flow passing over the recirculation zone is, thus, diffused more quickly. This slows down the stream which allows it to be turned more quickly towards the the low pressure region at the center of recirculation. Chen's modification will tend to decrease the ratio between turbulent kinetic energy and dissipation in regions of high shear which, in turn, will decrease the turbulent viscosity. This effect will concentrate the momentum of the core flow and allow the center of recirculation to be pushed further downstream and towards the outer radius. Comparing the computational streamline plots of cases 1 and 2 to their respective experimental streamline plots, it is clear that if the Chen modification effects the flow as expected predictions would be greatly improved.

The standard k–epsilon model, while the most widely used turbulence model in commercial CFD codes, is unable to produce consistent results for complex flow geometries. Many attempts have been made to modify the model to compensate for is overly diffusive character. Most modifications have proven to be either only partially successful or useful for only the cases for which they were designed. In industry, a case specific model is of little use, as analysis is not usually performed on a simple geometry with one characteristic flow type. The general nature of Chen's modification along with its proven success in improving predictions of cases where k–epsilon would give inconsistent results, presents this model as a candidate for use with more complex flow configurations. This study concentrates on the application of the Chen modification of the k–epsilon turbulence model to combustor geometries.

3.0 Turbulence Modeling

This investigation deals with the application of a modification of the k–epsilon model of turbulence to a particular geometry. This chapter discusses the various methods by which turbulence is modeled and why k–epsilon is the model chosen for this investigation. The k–epsilon model is derived, followed by the presentation of the Chen modification to k–epsilon.

The Navier–Stokes equations govern both laminar and turbulent flows. In order to fully resolve the turbulent structures of the flow from the Navier–Stokes equations, the grid spacing would have to be the size of the smallest turbulent eddies which are on the order of one millimeter. Because the number of grid points required is so great, this method, known as Direct Numerical Simulation (DNS), is currently limited to simple geometries and results in a computation that is extremely time and memory intensive. For this reason, the Navier–Stokes equations are time averaged to determine the turbulent stresses which can then be either modeled or predicted from mean flow quantities.

To derive the time–averaged form of the Navier–Stokes equations, it is first necessary to break the vector and scalar components of the equations up into mean

and fluctuating components. For incompressible flow, the velocity and pressure are broken down as follows:

$$u_i = \overline{u_i} + u_i' \qquad (3-1)$$

$$p = \overline{p} + p' \qquad (3-2)$$

where, $\overline{u_i}$ and $\overline{p}$ are time averaged quantities defined as:

$$\overline{A} = \frac{1}{T}\int_0^T A\,(t+\tau)\,d\tau \qquad (3-3)$$

For the average value to be independent of the integrated time step, T must be chosen to be larger than the scale of fluctuations [16]. The above expressions can then be substituted into the equations of conservation of mass (B–1), and of momentum (B–2). The result is the incompressible form of the time averaged Navier–Stokes equations.

Conservation of Mass:

$$\frac{\partial}{\partial x_j}(\varrho\overline{u}_j) = 0 \qquad (3-4)$$

Conservation of Momentum:

$$\frac{1}{\sqrt{g}}\frac{\partial}{\partial t}(\sqrt{g}\,\varrho\overline{u}_i) + \frac{\partial}{\partial x_j}(\varrho\overline{u}_j\,\overline{u}_i) = \varrho f_i - \frac{\partial\overline{p}}{\partial x_i} + \frac{\partial}{\partial x_j}\left[\mu\left(\frac{\partial\overline{u}_i}{\partial x_j} + \frac{\partial\overline{u}_j}{\partial x_i}\right) - \varrho\overline{u'_i\,u'_j}\right] \qquad (3-5)$$

The Reynolds averaged momentum equation can be, for the most part, solved for the mean velocity and pressure. The equation is complicated by the last term on the right hand side $\varrho\overline{u_i u_j}$, defined as the Reynolds turbulent stresses. This new term introduces nine variables, greatly increasing the difficulty of solving the equation. Turbulence modeling is an attempt to simplify the computation of this term. There are two methods of modeling the Reynolds stresses, eddy viscosity and non–eddy viscosity models.

3.0.1 Eddy Viscosity Models

The eddy viscosity method treats the turbulent stress term as a gradient diffusion analogous to the molecular diffusion stress term. This assumption known as the Boussinesq approximation, is that turbulence, like molecular diffusion, acts to increase diffusion. Turbulence introduces diffusion in the flow on a large scale by the movement of turbulent eddies, whereas laminar diffusion occurs on the molecular level. The Boussinesq approximation is as follows [17]:

$$\tau_t = -\varrho\overline{u'_i\,u'_j} = \mu_t\left(\frac{\partial\overline{u}_i}{\partial x_j}+\frac{\partial\overline{u}_j}{\partial x_i}\right) - \varrho\frac{2}{3}k\,\delta_{ij} \qquad (3-6)$$

where, μ_t is the turbulent or eddy viscosity and k is the turbulent kinetic energy which is defined as:

$$k \equiv \frac{1}{2}(\overline{u_1'^2} + \overline{u_2'^2} + \overline{u_3'^2}) \qquad (3-7)$$

The term containing k in equation (3–6) is absorbed in the pressure and can be eliminated. Thus, the turbulent stress term reduces to:

$$-\varrho\overline{u_i'\,u_j'} = \mu_t\left(\frac{\partial\overline{u}_i}{\partial x_j}+\frac{\partial\overline{u}_j}{\partial x_i}\right) \qquad (3-8)$$

The problem of modeling the turbulent stress term is now reduced to the evaluation of the turbulent eddy viscosity. There are several methods to accomplish this task.

Zero equation or algebraic models are methods by which eddy viscosity is determined by either setting μ_t equal to a constant or by calculating μ_t using an empirically based algebraic equation. These relations are generally functions of local flow parameters and result in predictions that are good for the geometry that they were modeled. These models, however, give inconsistent results when applied to geometries that vary from the flow configurations that the empirical constants were tuned to.

One equation models are designed to improve the generality of the turbulence model by allowing the eddy viscosity to be a function not only of local flow parameters, but also of flow upstream. This is done by solving for the turbulent velocity scale, usually chosen as $k^{1/2}$. Turbulent kinetic energy (k) can be determined by solving the equation governing this quantity. The disadvantage to this method is that there is still a need to prescribe the length scale, thus introducing empiricism. This method is less limited than the zero equation models, however, its generality is limited by the types of flow for which the turbulent length scale is determined.

Both the turbulent velocity and length scales are solved for in two equation models. The most popular of this type of method is the k–epsilon model which gives good predictions for a variety of flow configurations. However, assumptions made and empiricism required for the closure of the epsilon equation limits the model's generality. The k–epsilon model will be discussed in more detail in the following sections.

3.0.2 Non–eddy Viscosity Models

Non–eddy viscosity models do not utilize the Bousinesq approximation in modeling the turbulent stresses, rather, they attempt to either solve for the components of the turbulent stress tensor or solve the Navier–Stokes equations directly.

Reynolds stress models solve the Reynolds stress equations for the components of the turbulent stress tensor and the turbulent diffusion fluxes. This model, unlike the eddy viscosity models, account for the non–isotropic characteristics dominant in some types of flow. The disadvantage to this method

is that the additional computations and memory allocations required greatly increases the calculation time.

Algebraic stress models reduce the partial differential equations of the Reynold's stress model to a set of algebraic relations. In practice, algebraic stress models are coupled with the k–epsilon equations to determine these stresses. The consistency of algebraic stress models is increased over the k–epsilon model.

Large eddy simulation models solve the three dimensional time dependent Navier–Stokes equations to resolve the large eddy structure of the flow. Eddies are resolved directly down to the size of the grid. Smaller eddies are modeled using the eddy viscosity approach and small scale turbulence is averaged out with spatial filtered averaging. This method is extremely time and memory intensive and, thus, is not useful for industrial applications.

3.1 The k–epsilon Turbulence Model

This investigation deals with the application of an improvement to the k–epsilon model to a particular geometry. It is, therefore, necessary to explain k–epsilon in more detail than what was provided in the previous section on eddy viscosity models. In this model, the turbulent length and velocity scales are determined from the turbulent quantities kinetic energy and dissipation. By dimensional analysis, the eddy viscosity can be approximated as [17]:

$$\mu_t \equiv \propto \varrho \, V_t \, L \qquad (3-9)$$

where, $\propto$ is a proportionality constant, ϱ is the density, V_t is the turbulent velocity scale, and L is the turbulent length scale [17]. In the k–epsilon model, the turbulent velocity scale is chosen to be $k^{1/2}$, and the turbulent length scale is chosen to be

$k^{3/2}/\varepsilon$. The proportionality constant is empirically determined and is represented as C_μ. Turbulent viscosity can, therefore, be modeled as follows:

$$\mu_t = \varrho C_\mu \frac{k^2}{\varepsilon} \qquad (3-8)$$

The turbulent kinetic energy, k, and dissipation, ε, can be found from the turbulent transport equations. The turbulent kinetic energy equation can be written as [18]:

$$\frac{\partial k}{\partial t} + \overline{u}_k \frac{\partial k}{\partial x_k} = \frac{\partial}{\partial x_k}\left(\nu \frac{\partial k}{\partial x_k}\right) - \overline{u'_i u'_k}\frac{\partial \overline{u}_i}{\partial x_k} - \nu \overline{\frac{\partial u'_i}{\partial x_k}\frac{\partial u'_i}{\partial x_k}} + \overline{\frac{p'}{\varrho}\frac{\partial u'_i}{\partial x_i}} - \frac{\partial}{\partial x_k}\left(\overline{k' u'_k} + \overline{\frac{p'}{\varrho} u' \delta_{ik}}\right) \qquad (3-9)$$

1 2 3 4 5 6

#1 Rate of change of turbulent kinetic energy

#2 "Viscous" diffusion

#3 Rate of production of turbulent kinetic energy by interaction with mean strain rate

#4 Dissipation (viscous destruction) of turbulent kinetic energy

#5 Pressure strain

#6 "Turbulent" diffusion and "pressure" diffusion of turbulent kinetic energy

The pressure strain term can be eliminated because $\frac{\partial u'_i}{\partial x_i} = 0$ from the time dependent form of the continuity equation. The exact form of the turbulent kinetic energy equation is simplified to its final modeling form by the following assumptions:

- Isotropic turbulence (valid at high Reynolds numbers)

$$\varepsilon\ (dissipation) = \nu \overline{\frac{\partial u'_i}{\partial x_k}\frac{\partial u'_i}{\partial x_k}} \qquad (3-10)$$

- Apply the eddy viscosity concept to term #3:

$$-\overline{u'_i u'_k} = \frac{\mu_t}{\varrho}\left(\frac{\partial \overline{u}_i}{\partial x_k} + \frac{\partial \overline{u}_k}{\partial x_i}\right) \qquad (3-11)$$

- The "Turbulent" diffusion term can be simplified by the use of the eddy diffusivity concept and the addition of the turbulent Prandtl number, σ_k.

$$-\overline{k'u'_k} = \frac{\mu_t}{\sigma_k \varrho}\frac{\partial k}{\partial x_k} \qquad (3-12)$$

The final form of the turbulent kinetic energy equation that will be modeled is as follows:

$$\frac{\partial k}{\partial t} + \overline{u_k}\frac{\partial k}{\partial x_k} = \frac{\partial}{\partial x_k}\left[\left(\nu + \frac{\nu_t}{\sigma_k}\right)\frac{\partial k}{\partial x_k}\right] + (\Pr - \varepsilon) \qquad (3-13)$$

$$\text{where,} \quad \Pr(\text{production}) = \nu_t\left(\frac{\partial \overline{u}_i}{\partial x_k} + \frac{\partial \overline{u}_k}{\partial x_i}\right)\left(\frac{\partial \overline{u}_i}{\partial x_k}\right) \qquad (3-14)$$

$$\text{and} \quad \nu_t \text{ (turbulent kinematic viscosity)} \equiv \mu_t / \varrho$$

The turbulent kinetic energy equation is solved in conjunction with the turbulent dissipation equation. The modeled equation for epsilon is given as:

$$\frac{\partial \varepsilon}{\partial t} + \overline{u}_k\frac{\partial \varepsilon}{\partial x_k} = \frac{\partial}{\partial x_k}\left[\left(\nu + \frac{\nu_t}{\sigma_\varepsilon}\right)\frac{\partial \varepsilon}{\partial x_k}\right] + C_1\frac{\varepsilon}{k}\Pr - C_2\frac{\varepsilon^2}{k} \qquad (3-15)$$

1 2 3

#1 Rate of change of turbulent dissipation

#2 Diffusion of the turbulent dissipation

#3 Sources of dissipation

The model contains five empirical coefficients, for which a reasonable range of values are determined by analysis of simple turbulent flows. Numerical optimization is then employed to determine the best set of model coefficients. From decay of grid turbulence, C_2 is determined to be 1.80 [18]. From near wall turbulence considerations:

$$C_1 = C_2 - \frac{k^2}{\sigma_\varepsilon \sqrt{C_\mu}} \qquad (3-16)$$

In local equilibrium near wall turbulence, production equals dissipation. From this C_μ can be approximated to be 0.09 [18]. In order to prevent the eddy viscosity from becoming unbounded, the rate at which dissipation approaches zero must be slower than the rate at which turbulent kinetic energy approaches zero. This requires that the dissipation of epsilon be less than the dissipation of k. To assure this, σ_k must always be less than or equal to σ_ε. After computer optimization, the recommended set of coefficients becomes [19]:

$$C_\mu = 0.09 \quad C_1 = 1.44 \quad C_2 = 1.92 \quad \sigma_k = 1.0 \quad \sigma_\varepsilon = 1.3$$

The turbulent kinetic energy and dissipation are solved for from their respective equations and applied to the Boussinesq approximation to evaluate turbulent viscosity. The addition of the eddy viscosity to the molecular viscosity creates a greater dissipative effect in an attempt to simulate turbulent mixing. However, in areas of high shear, the rate of production of turbulent kinetic energy is much faster than that of dissipation. This causes the turbulent viscosity to be overpredicted in these regions. The dissipative nature of the k–epsilon model results in inconsistent predictions, especially in swirling and recirculating flows where conservation of the momentum of the primary stream of flow is important. Because of the assumption of isotropic flow in the closure of the turbulent transport equations, the model also fails to give accurate predictions for flows that are highly anisotropic. The k–epsilon model proves to give qualitative results for many flows, however, it suffers from a few deficiencies which render it inapplicable to more complex flows.

3.2 The Chen Modification to the k–epsilon Turbulence Model

The modification made by Chen to the k–epsilon turbulence model was motivated by the lack of success of previous modifications. As was discussed in the Chapter 2, many attempts were made to remedy the dissipative nature of the model. The approaches, however, were to deal with the model's deficiencies in predicting the features of a particular type of flow. The modifications often violate requirements imposed on the determination of the coefficients, and, in most cases, fail to make a significant improvement in predictions. In addition, these modifications lack generality and are inapplicable to flows differing from that for which they were modeled. For this reason, Chen attacks the most fundamental problem of the k–epsilon turbulence model, the overprediction of eddy viscosity in areas of high mean strain.

To correct this problem, Chen proposes an additional source term be added to the dissipation equation [10]

$$\frac{\partial \varepsilon}{\partial t} + \overline{u}_k \frac{\partial \varepsilon}{\partial x_k} - \frac{\partial}{\partial x_k}\left[\left(\nu + \frac{\nu_t}{\sigma_\varepsilon}\right)\frac{\partial \varepsilon}{\partial x_k}\right] = C'_1 \mathrm{Pr}\frac{\varepsilon}{k} - C'_2\frac{\varepsilon^2}{k} + C'_3\frac{\mathrm{Pr}^2}{k} \qquad (3-17)$$

The last term on the right side of the equation is the proposed modification. The term adds a second time scale which allows the transfer of energy between the two transport equations to react more efficiently to mean strain. This time scale will allow the rates of production of turbulent kinetic energy and dissipation to converge. The result is a decrease of eddy viscosity where the velocity gradients are high and an increase in μ_t where they are low.

The model constants C_1, C_2, and C_3, as well as the turbulent Prandtl numbers are redetermined using the original stipulations imposed on the

coefficients of the standard model, as discussed in the previous section. The coefficients were then numerically optimized resulting in the final model values:

$$\sigma_k = 0.75 \quad \sigma_\varepsilon = 1.15 \quad C'_1 = 1.15 \quad C'_2 = 1.9 \quad C'_3 = 0.25$$

Observing this final set of coefficients, it is noticed that in equilibrium flow, where production equals dissipation, dissipation can be substituted for production in the third term. The result is a source term identical to the first source term, $Pr\ \varepsilon/k$. The first and third coefficients, C'_1 and C'_3, respectively, can combine with the resulting coefficient being equal to C_1 of the original k–epsilon equation. So, in equilibrium flows, the Chen model reduces to the original k–epsilon model. In areas of high shear, however, production will not equal dissipation and the first and third terms will not be identical in form. Rather, in areas of high production, or shear, the third term will contribute to the production of dissipation more than the solitary term would have.

To assess the performance of this improvement, Chen applied his modification to a variety of flows. The cases evaluated were: fully developed turbulent channel and pipe flows, co–flowing plane and round jets, a flat plate turbulent boundary layer flow, flow over a backward facing step, and swirling flow. The modification showed improved predictions of the decay of centerline velocity and jet half width for both co–flowing jet cases and a reduction of the error in predicting the reattachment length from 28% to 2.8% for the rectangular backward facing step case. Numerical predictions of the axial velocity of the co–axial flowing jet case show significant improvement over the predictions of the standard k–epsilon model, illustrating the ability of the Chen modification to conserve swirl. The improved model predicts the mean velocity of the flat plate flow test case well, yet underpredicts the turbulent kinetic energy and shearing stress near the wall. For

the channel and pipe flows, no difference at all was seen. These last four cases perhaps indicate the inability of the wall function to correctly account for wall effects, rather than the Chen modifications failure to remedy the dissipative nature of the k–epsilon model.

In cases where wall effects have a much larger influence on the flow than diffusion, such as the four cases mentioned above, the Chen modification fails to make an improvement. This point is fortified by the predictions of flow through a rectangular duct with 90° bend, a test case modeled by the author and discussed in appendix A. The results clearly illustrate that turbulent viscosity is decreased in areas of high shear and increased in regions of low shear. This should have resulted in the improvements of velocity predictions, yet failed to do so. The problem, as speculated, is the inability of the wall function to model the effects of curvature on the flow. The Chen modification is intended to eliminate the diffusive nature of the k–epsilon turbulence model. It is not intended to attack the problems associated with k–epsilon's assumption of isotropy and use of a log–law of the wall to model near wall flows. For cases where wall effects dominate the flow, such as the rectangular elbow with 90° bend, Chen's model is unable to overcome these forces to change flow predictions. The Chen modification has been shown to improve results for swirling and recirculating flows and is unable to improve near wall predictions and turning flows. The question proposed in this study is how the Chen modification will effect predictions of flow in industrial combustor geometries, which contain combinations of swirling, recirculating and turning flows.

4.0 The Quarled Burner Test Cases

The two test cases evaluated in this study represent the basic flow physics characteristic of combustor geometries. In this chapter these characteristics will be identified and related to the flow features seen in the quarled burner cases. Included in this section is a description of the experiment. The flow conditions and locations of the experimental test stations are provided along with the boundary conditions used for computation. Details of the computational analysis are presented. Included is a description of the grid and discretization method used for the final computation.

In a combustor, it is necessary to stabilize the flame. For a flame to be stabilized, a constant supply of heat and radicals must be introduced to the incoming fuel–air mixture for combustion to occur [3]. Introducing swirl into the flow is one of the most efficient ways of accomplishing this. A flow with sufficient swirl strength will produce a large adverse pressure gradient in the direction of flow and cause a large centerline recirculation. This phenomena, known as vortex breakdown, stabilizes the flame by increasing the residence time of the fluid which allows ample time for dissipation and mixing [7]. Flow encountering a step will experience a high adverse pressure gradient which results in a

secondary recirculation. Often a combustor will incorporate a step–like geometry with swirl to ensure recirculation and flame stabilization. The function of the quarl, the ramped section prior to the expansion, is to produce a shorter, but wider recirculation zone [20]. Flow in these geometries is axisymmetric when the amount of rotation imparted on these flows is higher than that associated with the onset of vortex breakdown [21]. The basic characteristics of a combustor, swirl, recirculating flow behind a step–like structure, and a slight expansion or quarl, are represented in the two burner cases evaluated.

The experimental data for these cases is taken from a report by Harwell Laboratory [11] who obtained the data from experiments conducted by the International Flame Research Foundation (IFRF) in IJmuiden, Holland. Both cases are cold flow experiments, that is, they contain no combustion. In addition, they can be considered axisymmetric. The first quarled burner case consists of swirling flow which is expanded through a 21.4° ramp (quarl) to a slight step. The length of the chamber is 4 meters. A diagram of the geometry is shown in Fig. 9a. Experimental data is available at five locations: 0.17 m, 0.25 m, 0.34 m, 0.45 m, and 0.75 m downstream of the inlet. All but the last experimental station are located in the quarl. Both swirl and axial velocity data are given at each of the experimental locations. This case, as seen in Fig. 9b, characterizes axisymmetric swirling flow with a primary centerline recirculation zone which is caused entirely by the tangential motion of the flow. Case 1 also includes a small recirculation behind the expansion and a weak secondary centerline recirculation zone, which results in a stagnation region near the centerline.

The flow in the second case is turned through a 19.8° quarl and then expanded by a large step. The length of the chamber, which has an end

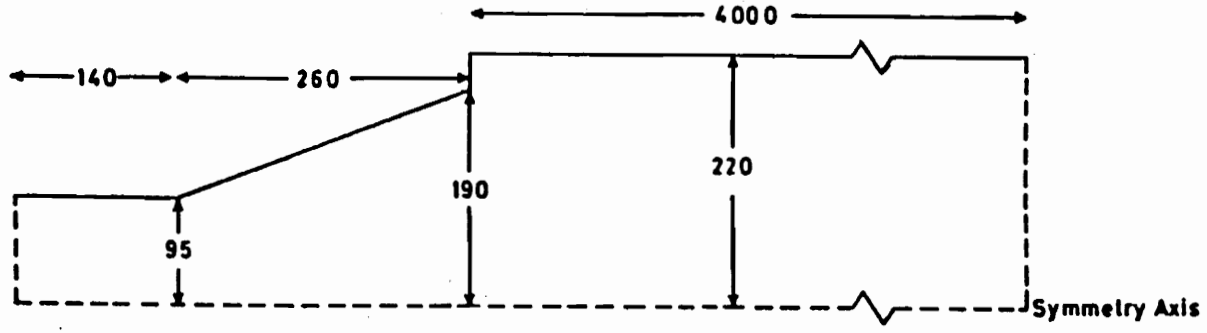

Figure 9a. Quarled Burner Case 1, Geometry [11]

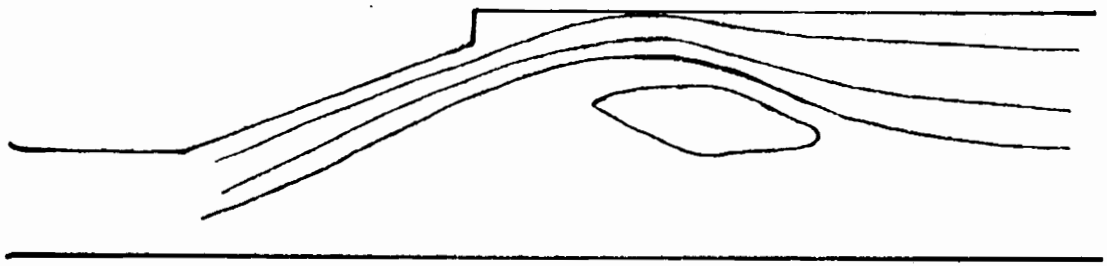

Figure 9b. Quarled Burner Case 1, Experimental Streamlines [11]

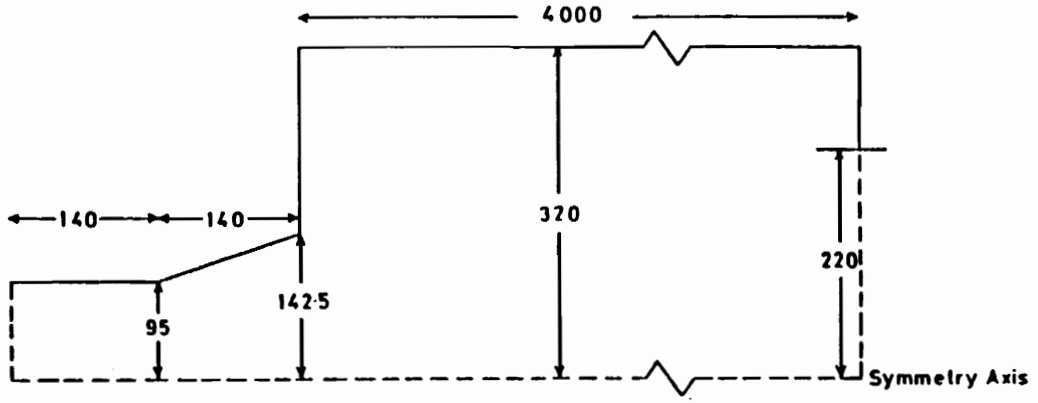

Figure 10a. Quarled Burner Case 2, Geometry [11]

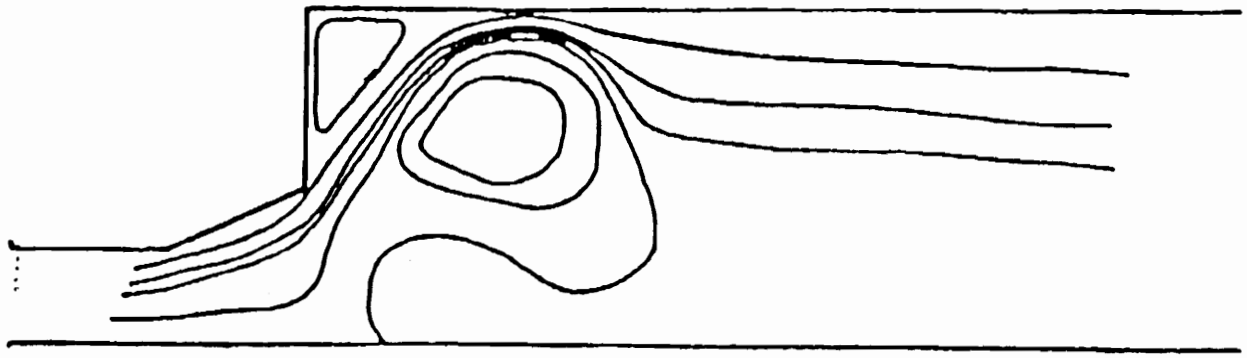

Figure 10b. Quarled Burner Case 2, Experimental Streamlines [11]

contraction, is 4 meters. The geometry of Case 2 is depicted in Fig. 10a. Experimental data for this case is available at 0.32 m, 0.45 m, 0.58 m, and 0.95 m downstream of the inlet. None of the experimental locations are located in the quarl. Swirl and axial velocity measurements are available at each station. This case demonstrates a combination of the effects of swirling flow, flow being turned through the quarl, and flow encountering a large expansion. Case 2 is characterized by a primary centerline recirculation zone, similar to case 1, and a strong secondary recirculation behind the expansion. This case also contains a secondary centerline recirculation zone, which is larger than that of case 1 and is responsible for the positive axial velocity at the centerline. Figure 10b shows experimental streamlines which illustrate the two zones of recirculation occurring in this geometry. This case better represents the geometry and flow characteristics of an industrial combustor. It is this case that is of primary interest and will best determine the applicability of the Chen modification to combustor geometries.

The meshes for the quarled burner test cases were developed using STAR–CD's pre–processor PROSTAR. The 2–D axisymmetric models used for the analysis of each case were determined to be grid independent by varying the mesh spacing. The grid for case 1 contains 287,400 cells all together: 350 cells in the inlet, 700 cells in the quarl and 1,824 cells to the exit. Figure 11 does not depict the grid to the exit so that the packing structure can be resolved. The mesh is slightly packed towards the outer radius throughout the inlet, quarl and portion of the expansion shown. This is done to better resolve the gradients, which are largest in this area of the flow. Case 2 is modeled using a grid containing 5,430 cells total (Fig. 12): 350 cells in the inlet and quarl, and 4730 cells in the

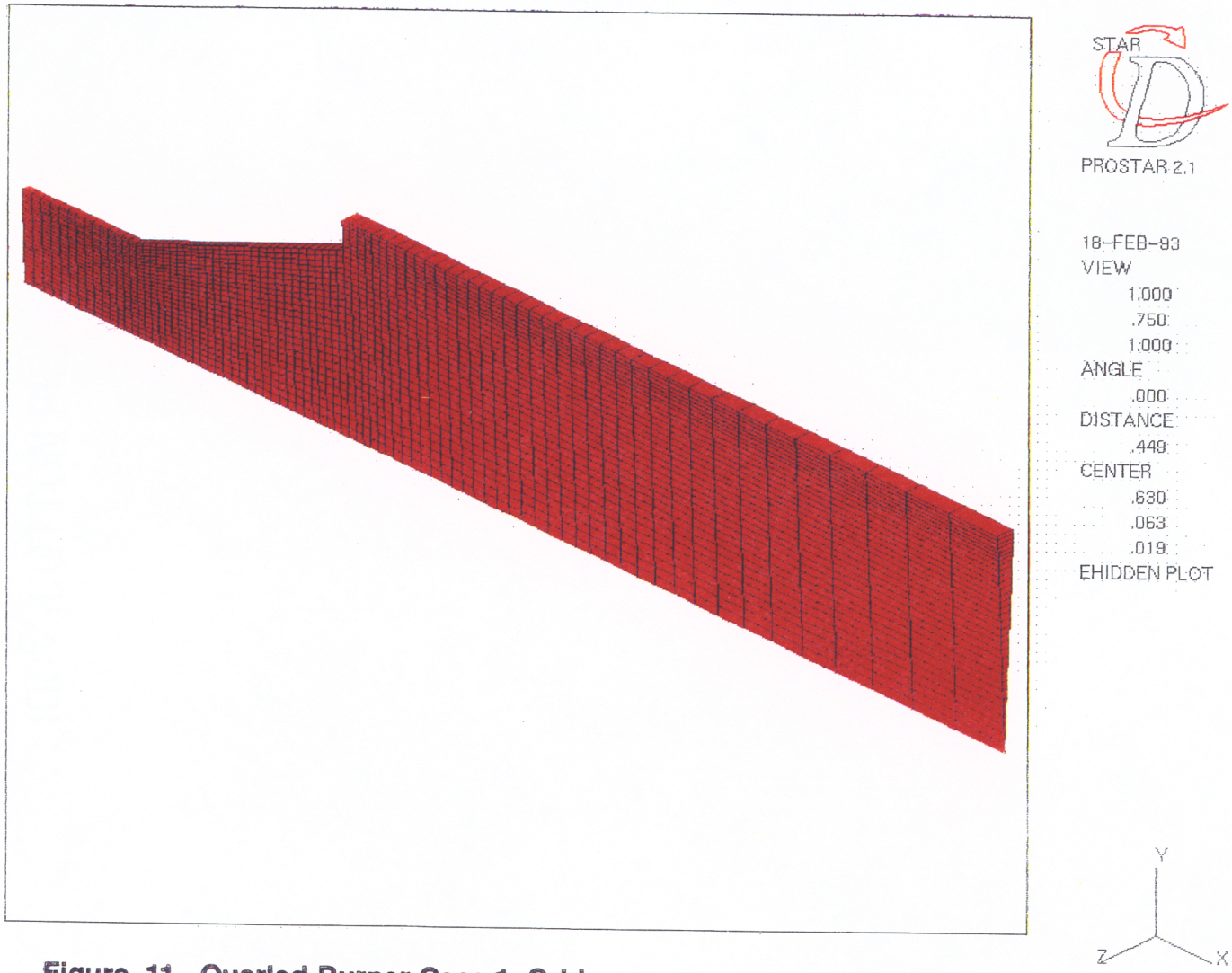

Figure 11. Quarled Burner Case 1, Grid

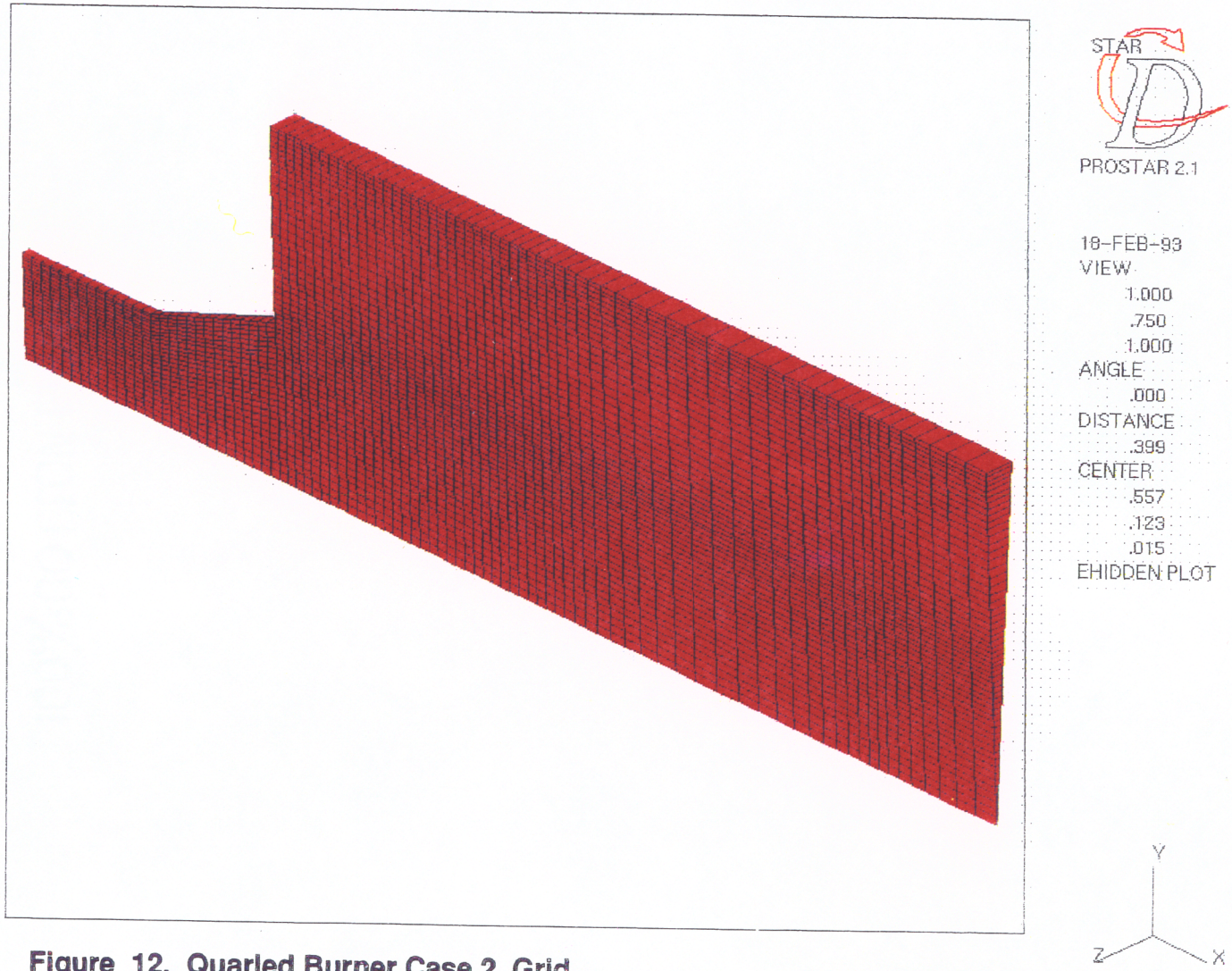

Figure 12. Quarled Burner Case 2, Grid

expansion to the exit. Again, a shortened version of the model is depicted to show grid spacing (Fig. 12). Similar to case 1, the grid is packed towards the outer radius in the inlet and quarl. In the expansion, the mesh is packed towards the outer radius and towards the center of the region. Again, this is done for better gradient resolution.

The boundary conditions, flow parameters and discretization methods are also prescribed in PROSTAR. Inlet boundary conditions for both cases are given in the report [11] for swirl and axial velocity, and turbulent kinetic energy and dissipation. The inlet axial velocity for the first case is specified as a constant value of 4.6 m/s, wheras the tangential velocity is linearly increasing from approximately zero at the centerline to 6.5 m/s at the outer radius. The turbulent kinetic energy and dissipation for case 1 are specified as 0.045 m^2/s^2 and 0.25 m^2/s^2 respectively. The inlet axial velocity for case 2 is specified as 4.9 m/s and the tangential velocity is linearly increasing from approximately zero at the centerline to 12 m/s at the outer radius. The turbulent kinetic energy and dissipation are given as 0.09 m^2/s^2 and 0.6 m^2/s^2, respectively. At the outlet the gradients of all variables normal to the exit plane are taken to be zero. Continuity need not be prescribed, as it is imposed on the flow by the solution method. A standard log law of the wall is to applied to the walls and a cyclic boundary condition, which assures the tangential and axial components of velocity and scalar values are identical for the faces prescribed, is applied to the x–y faces of the model. The axis of rotation is prescribed as a symmetry axis.

Flow in the quarled burners is assumed to be incompressible. In addition, the experiment, and, therefore, the analysis contains no reaction. Computation of the combustion reaction is not necessary for this study, as it is the ability of the

Chen modification to improve the predictions of turbulent flow in a combustor geometry that is in question.

To determine the best solution, the test cases were solved with numerous discretization schemes. Both case 1 and case 2 were solved using upwind differencing, and blended central differencing with a blending factor of 0.75, 0.9 and 0.95. The predictions change from the upwind differencing method, which is a first order scheme, to central differencing with a blending factor of 0.75. The solution changes significantly from a blending factor of 0.75 to 0.9, however, the changes from 0.9 to 0.95 are miniscule. Therefore, results from the computations using central differencing with a blending factor of 0.9 are used in this report and are presented in the following chapter.

5.0 Results

Two burner geometries are tested with Chen's modification to the k–epsilon turbulence model. The modification has been implemented into STAR–CD, a commercial CFD (computational fluid dynamics) code via a user defined subroutine. Details of the implementation and use of the Chen modification with STAR–CD can be found in appendix C. The addition of the Chen model to STAR–CD has been verified using a rectangular backward facing step test case. The case is similar to one for which Chen had shown improved results. The solution of the backward facing step case yields improved results from STAR–CD with the standard k–epsilon model. Velocity profile predictions for this computation, which are presented in appendix D, agree with the experimental data. Based on these results, the implementation of the Chen modification to STAR–CD is verified. The computational results of the quarled burner test cases, which are presented in this chapter, are compared with experimental velocity data to evaluate the improvement made by the model. In addition differences in the prediction of flow parameters, such as turbulent eddy viscosity, are presented to help evaluate the cause for changes in the velocity predictions.

5.1 Results: Case 1

Case 1 consists of a more elementary flow pattern than case two, but its consideration enables the evaluation of the Chen modification's effect on the development of a centerline recirculation induced by swirl. As seen from Fig. 13, the velocity gradients are highest in the quarled region near the outer radius. The Chen modification (Fig. 14), as predicted, decreases the turbulent viscosity by as much as 91% in this area. The region in which the eddy viscosity decreases by the greatest magnitude corresponds to the region of greatest shear. The modification decreases eddy viscosity by a lesser amount in areas of less severe velocity gradients. From the contours in Fig. 14, the pattern of flow recirculation can be seen. Moving in a radial line in the expansion from the centerline to the outer wall, the decrease in eddy viscosity decreases as the center of recirculation is approached, then increases, followed by a decrease very close to the wall. This pattern is expected, since, as the center of recirculation is approached, the momentum of the fluid decreases and stress decreases between adjacent streams of fluid. Downstream of the recirculation, the radial shear stresses drop rapidly, resulting in an increase of the turbulent viscosity.

Figure 15 shows the effect the change in eddy viscosity has on the swirl velocity. The large gradients in swirl velocity are maintained throughout the quarl, giving the velocity profile a peaked appearance in this region. Predictions at stations 2 through 4 are greatly improved over those made with the standard k–epsilon model. At station 5, the Chen modification moves the profile of swirl velocity closer to the experimental result, but fails to completely resolve the characteristic of the flow.

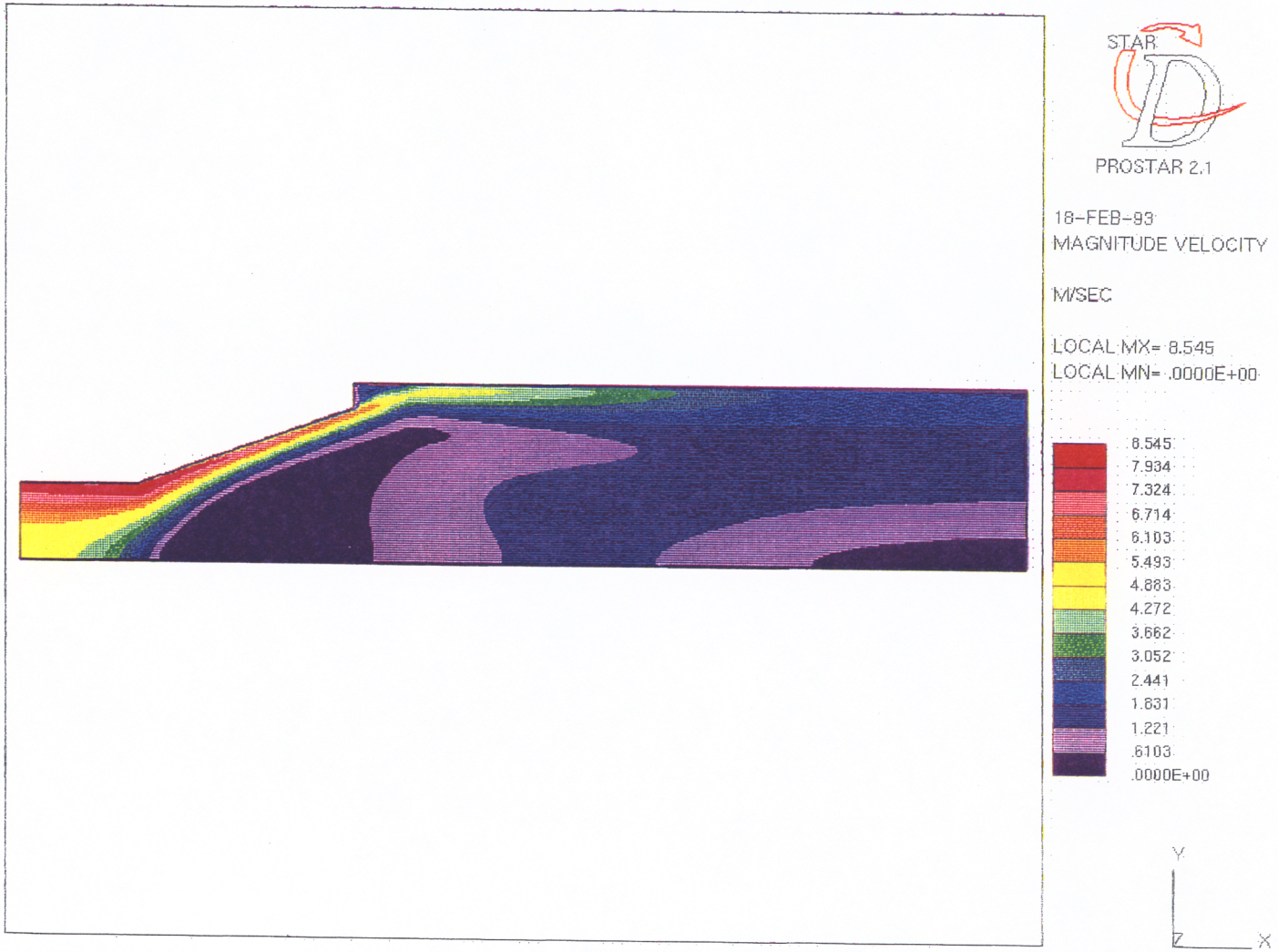

Figure 13. Quarled Burner Case 1, Velocity Magnitude Predictions with the Chen Modification

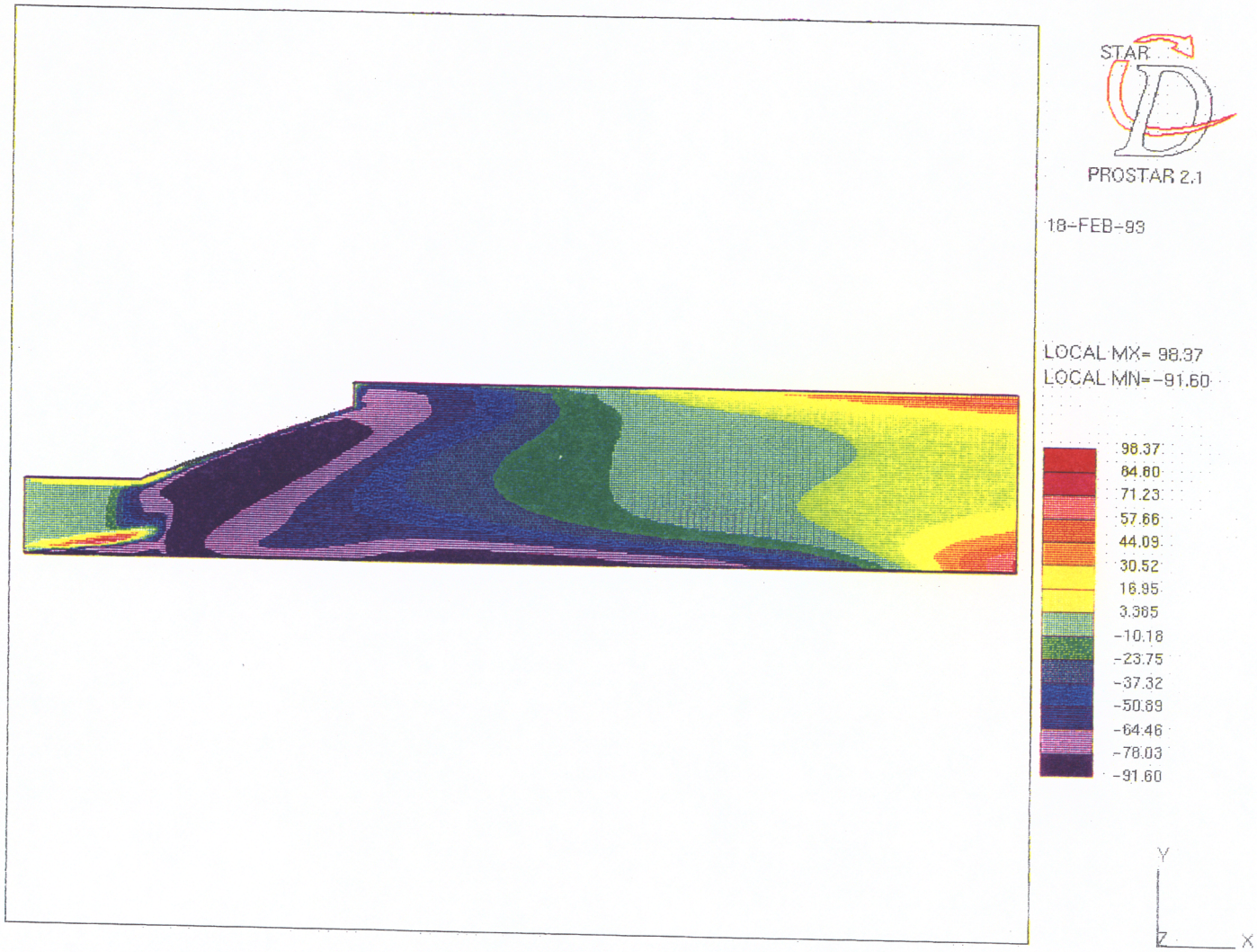

Figure 14. Quarled Burner Case 1, Percent Change Eddy Viscosity from the Standard k–epsilon Model to the Chen Modification

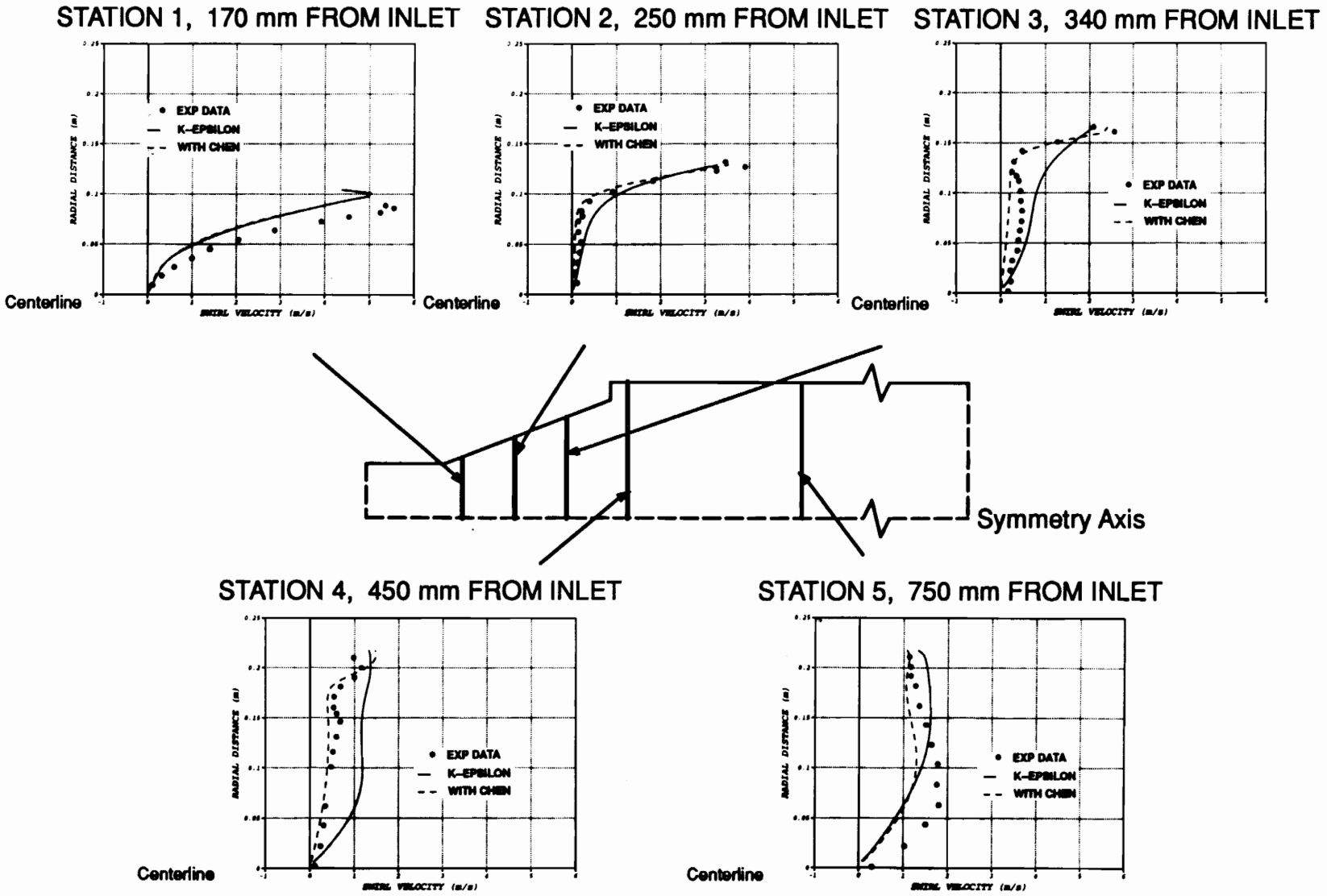

Figure 15. Quarled Burner Case 1, Swirl Velocity Predictions with the Chen Modification

The decrease of turbulent viscosity also allows the flow's axial momentum to maintain a concentrated profile in regions of high shear. Figure 16 shows predictions of axial velocity with the Chen modification more closely match the experimental data. The Chen modification increases the velocity at the centerline and predicts the peak in velocity at the outer radius. Looking back at the experimental streamlines of Case 1 (Fig. 5a), the flow is characterized by a stream of high momentum fluid that moves along the outer radius of the quarl. This stream is indicated by the peaks seen in axial and swirl velocity. The standard k–epsilon model overpredicts eddy viscosity in this region and allows the momentum of this stream to diffuse before it exits the quarl.

As a result, the stream enters the expansion at a decreased angle, causing the low pressure region which forms below it to be predicted lower than was determined experimentally. Therefore the standard k–epsilon model predicts the center of recirculation to be further into the quarl and closer to the axis of symmetry. Because the profiles of axial and swirl momentum are better preserved by the Chen model, the high momentum stream of flow enters the expansion at an increased angle, allowing the low pressure region to form further away from the centerline. The result, as seen from Fig. 17, is that the location of the center of recirculation is more accurately predicted. The comparison of the experimental, standard k–epsilon and Chen modification streamline plots illustrates the ability of the Chen model to predict the flow characteristics of this combustor geometry and, in contrast, the failure of the standard k–epsilon model to predict the placement of the recirculation zone.

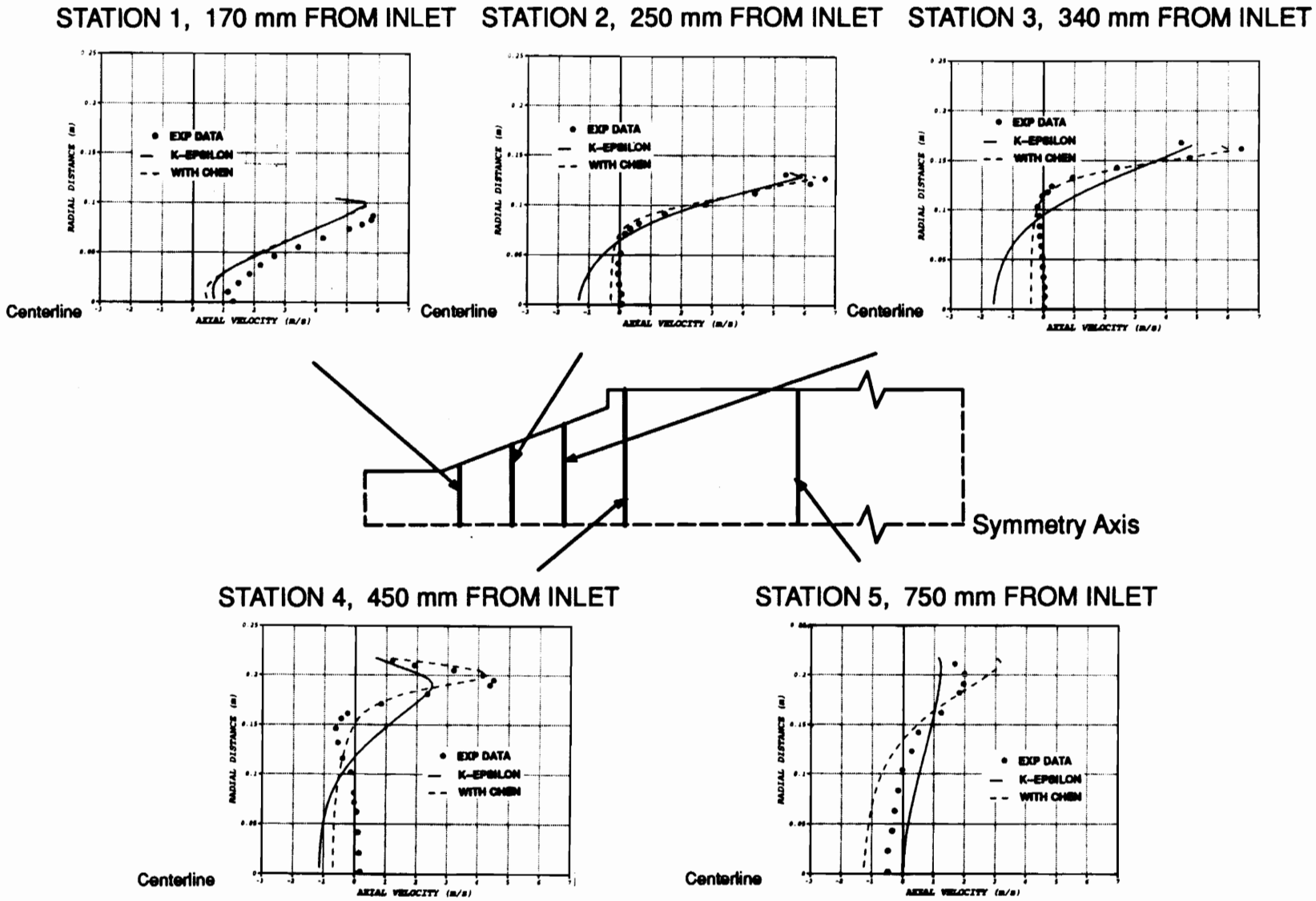

Figure 16. Quarled Burner Case 1, Axial Velocity Predictions with the Chen Modification

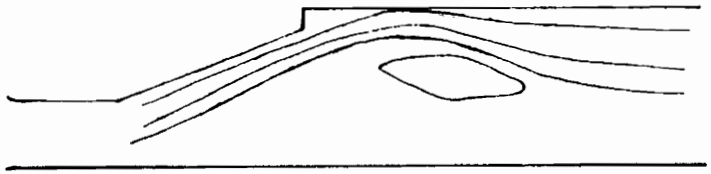

Figure 17a. Quarled Burner Case 1, Experimental Streamlines [11]

Figure 17b. Quarled Burner Case 1, k–epsilon Model Streamlines

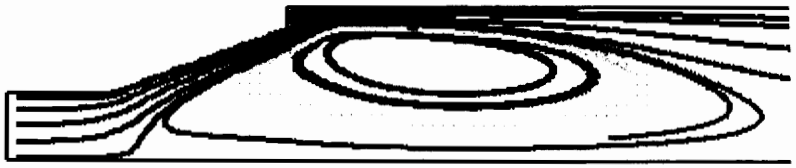

Figure 17c. Quarled Burner Case 1, Chen Modification Streamlines

6.2 Results: Case 2

Case 2, like case 1, is characterized by a centerline recirculation. However, complicating the flow is the addition of a second recirculation zone behind the expansion. A contour plot of velocity magnitude (Fig. 18) shows the region of highest velocity gradients to be at the outer radius of the quarl continuing on the same angle into the expansion. Significant gradients are also present near the walls behind the step and near the outer radius in the expansion. In regions of high strain, the Chen modification decreases the eddy viscosity from that predicted by the standard k–epsilon model. As illustrated by Fig. 19, the decrease in turbulent viscosity results in the largest change where a jet of high momentum fluid moves against fluid recirculating in the opposite direction. This 93% decrease also occurs in the quarl where fluid moving into the expansion encounters the corner of the recirculation zone. The change in viscosity decreases as the gradients become less severe and, further downstream, the percent change becomes positive. In the corner of the step, velocities are very small and the gradients seen reflect this stagnant nature. Therefore, in this region the change in turbulent viscosity is near zero and becomes positive as the corner is approached. Changes in turbulent viscosity will effect the nature of the flow. Where the eddy viscosity is increased the flow will disperse and slow down. Contrarily, where it is decreased, the flow will speed up.

The Chen modification, because it decreases turbulent viscosity in regions with high velocity gradients, maintains the peaked nature of the swirl momentum of the flow in these regions. This is particularly evident from the predictions of swirl velocity at station 1 (Fig. 20). The standard k–epsilon model diffuses the

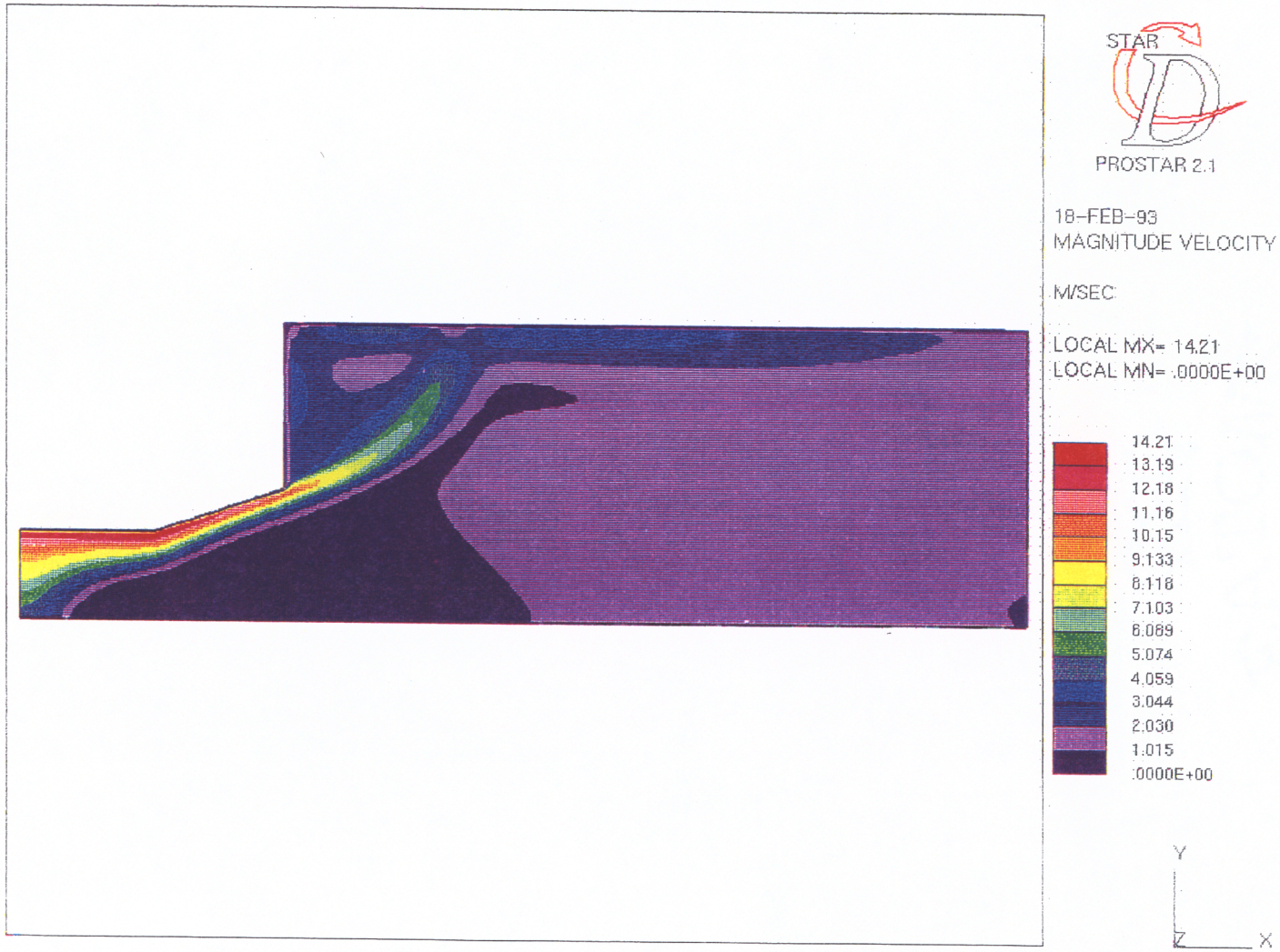

Figure 18. Quarled Burner Case 2, Velocity Magnitude Prediction with the Chen Modification

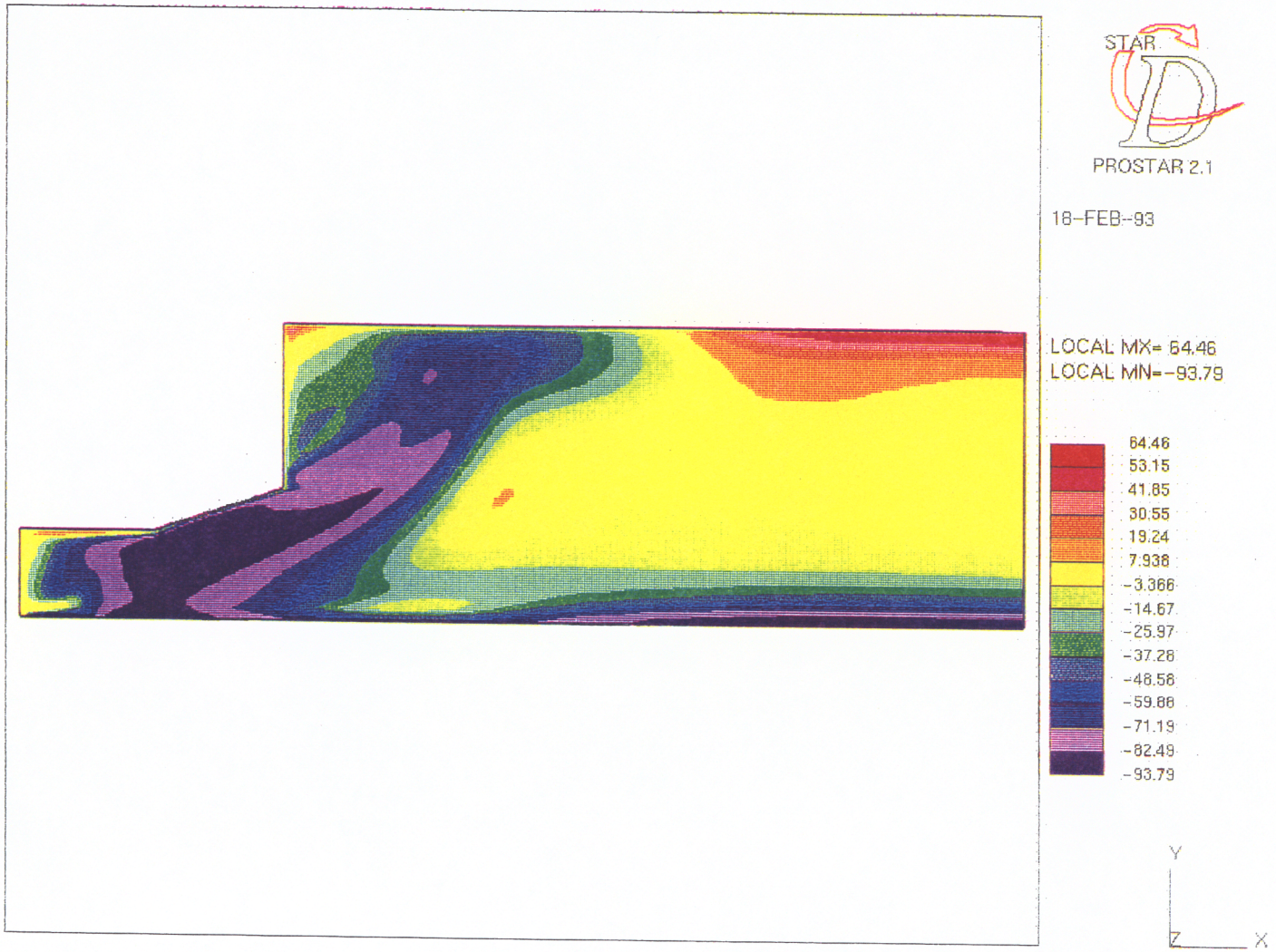

Figure 19. Quarled Burner Case 2, Percent Change Eddy Viscosity from the Standard k–epsilon Model to the Chen Modification

momentum of the jet, whereas, the Chen modification preserves its momentum, as indicated by the spike in the profile. The results of stations 2 through 4 show an improved agreement between the computational predictions and the experimental data.

The axial velocity results show similar improvements. As Fig. 21 illustrates, the Chen modification also preserves the large gradients of axial velocity in the flow. At station 1, the appearance of the jet, which was pushed against the outside radius of the quarl by the momentum of the swirl and then dumped into the expansion, is also prevalent. Because the spiked nature of the swirl momentum is preserved, the structure of this jet will remain more dense, as compared to the more diffuse profile the standard k–epsilon model produces. As a result, the spiked nature of the axial momentum of this jet is also preserved. The predictions made by Chen's modification at the remaining experimental stations also show the result of decreased eddy viscosity in this region, as the flow retains its structure.

By improving axial and swirl velocity predictions, the structure of the flow is also better predicted. The experimental, standard k–epsilon, and Chen modification streamline plots (Fig. 22) clearly indicate that the modification is able to predict the correct placement of the centerline recirculation zone and the size of the secondary recirculation behind the step. The streamline plot of the standard k–epsilon predictions show the stream that moves over the recirculation zone to be fatter than that predicted by the Chen modification, indicating the failure of the standard k–epsilon model to predict the large gradients of swirl and axial velocity seen in this region of the flow. By maintaining the concentration of the jet momentum, the Chen modification is able, as in case 1, to accurately

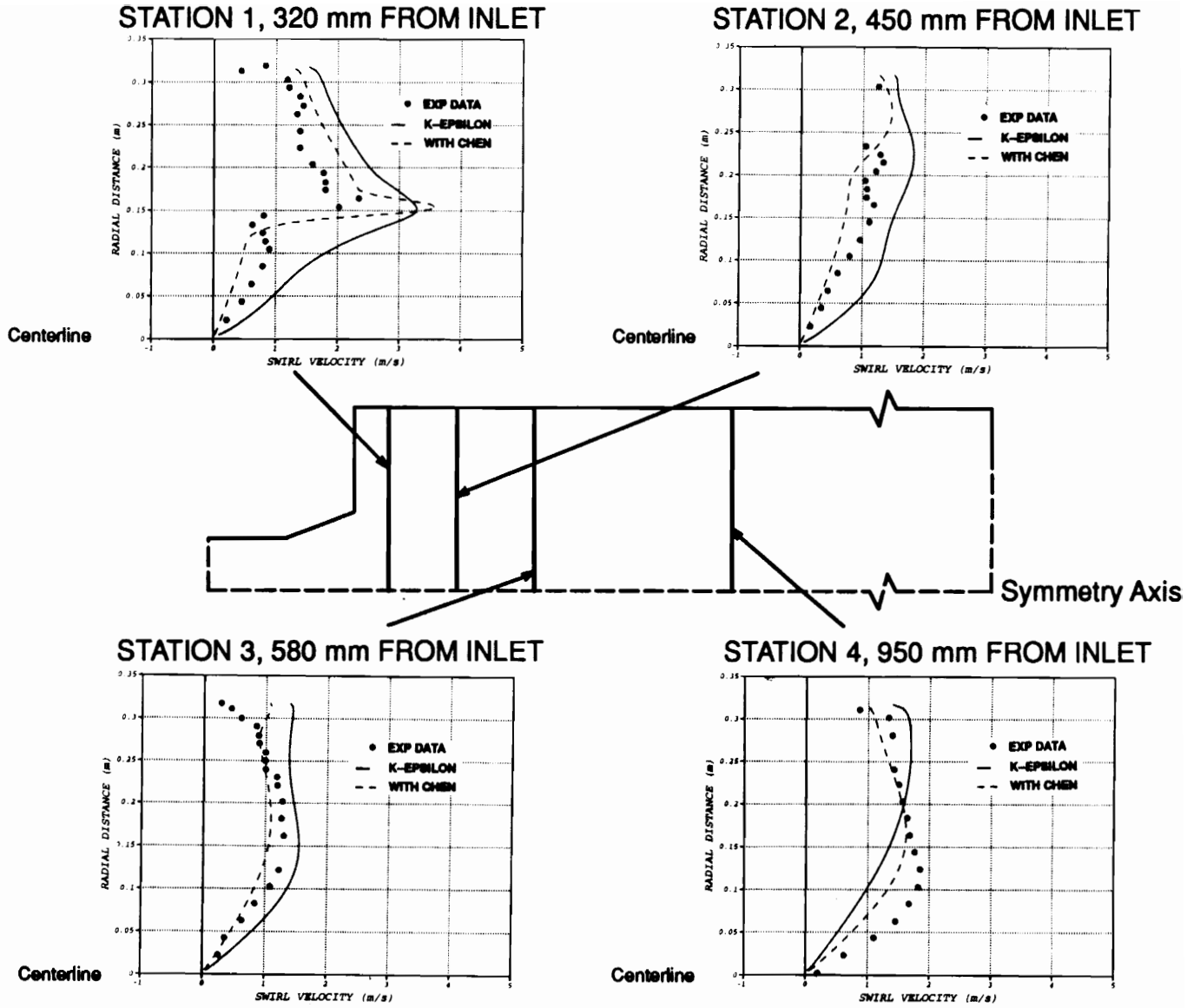

Figure 20. Quarled Burner Case 2, Swirl Velocity Predictions with the Chen Modification

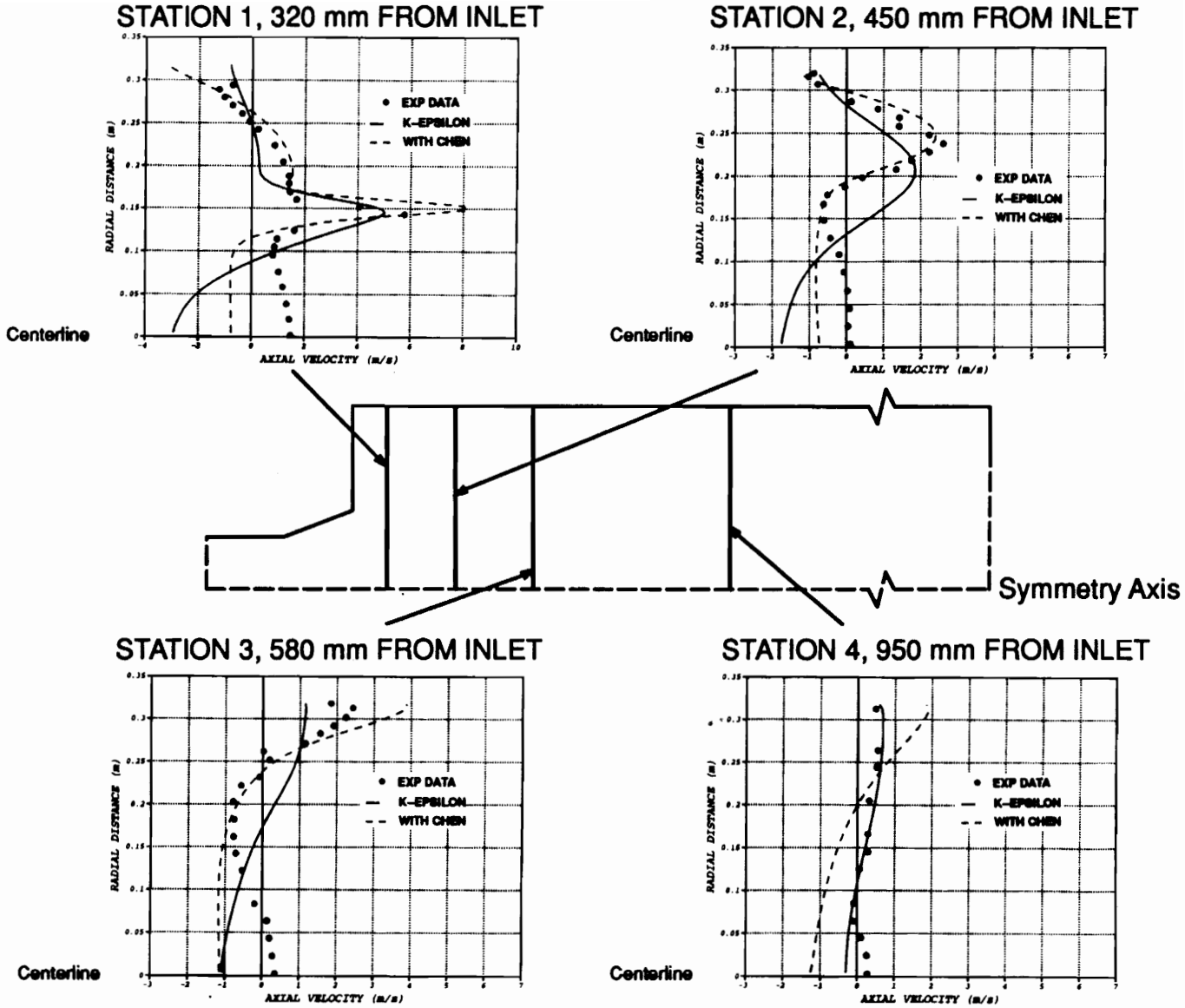

Figure 21. Quarled Burner Case 2, Axial Velocity Predictions with the Chen Modification

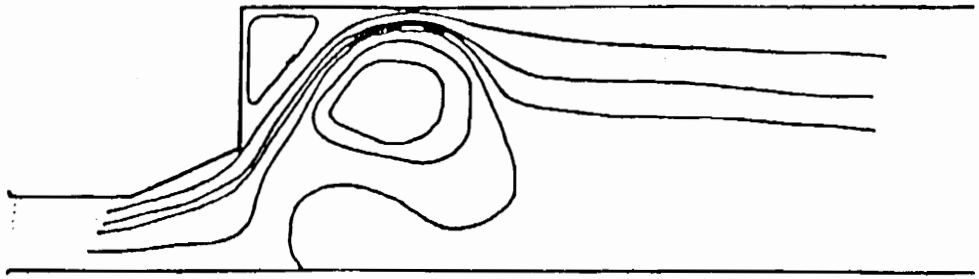

Figure 22a. Quarled Burner Case 2, Experimental Streamlines [11]

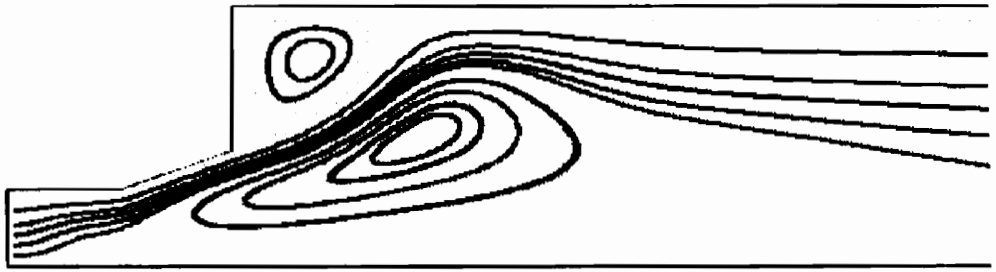

Figure 22b. Quarled Burner Case 2, k–epsilon Model Streamlines

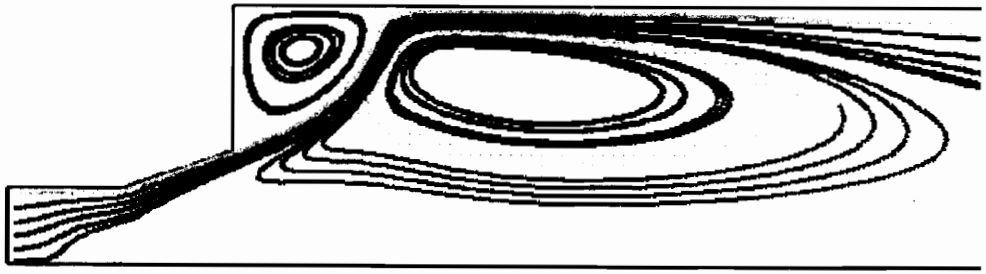

Figure 22c. Quarled Burner Case 2, Chen Modification Streamlines

predict the location of the center of recirculation. As a result, the recirculation behind the step is also decreased.

The results presented in this chapter indicate that the Chen modification improves predictions over the standard k–epsilon model of turbulence. By improving velocity predictions, a more accurate representation of the locations of the characteristic recirculation zones is obtained. The prediction of the locations of recirculation zones is important to the combustion engineer, as these are the regions where flame is held. A flame front will be located at the edge of the recirculation zone. Therefore, the prediction of the location and size of recirculation regions allows the combustion engineer to predict the location of the flame, as well as hot spots, and to determine approximately how much fuel will be burned. A more accurate representation of the turbulent structure of the flow, along with the calculation of the concentration of species, a capability of most commercial CFD codes, will also allow a better representation of the mixedness of the flow. The capability of modeling a combustor flowfield with more confidence allows the combustion engineer to make geometry and boundary condition changes to the model and predict what effect these changes will have on the system. This is an important tool in the design process which greatly decreases the number of iterations required to finalize a design.

6.0 Discussion

The Chen modification has been proven to make consistent predictions for several types of flow, including the two quarled burner test cases discussed in the previous chapter. Improvements can be attributed to the Chen model's ability to control the overprediction of turbulent viscosity in regions of high shear. Because the standard k–epsilon model overpredicts eddy viscosity in these regions, the momentum of the flow is diffused, resulting in the misrepresentation of the location and shape of flow features, such as the centerline recirculation zone, characteristic of combustor geometries. The Chen modification controls this overprediction and allows the large gradients of axial and swirl velocity in regions of high shear to be preserved. Consequently, the locations and sizes of the primary flow features are better predicted. This chapter not only addresses the mechanism that allows the Chen modification to produce better predictions, but it also addresses the cases for which it is not intended to improve predictions.

The diffusive nature of the k–epsilon model is controlled by allowing the turbulent transport equations to react more effectively to mean strain. A source term containing a second time scale is added to the dissipation equation to accomplish this task. However, this is not the only modification made to the turbulent transport equations. The empirical coefficients of the dissipation equation are also

re–evaluated and the turbulent Prandtl numbers are adjusted. The expected result is, in regions of high shear, the prediction of dissipation will increase from that predicted by the standard k–epsilon model, thereby decreasing the eddy viscosity. Figures 23 and 24 contradict this expectation by illustrating a decrease in the turbulent dissipation in regions of high shear and an increase in regions of low shear. Note that the local scale of percent change turbulent dissipation is changed in Fig. 24 for better gradient resolution. Turbulent kinetic energy, however, is decreased by approximately the same percent as dissipation in corresponding regions (Fig. 25 and 26). Since kinetic energy is squared in the numerator of the approximation for turbulent kinetic energy, given by equation 3–8, an equal change in both k and epsilon will amount to a change in the eddy viscosity of the same degree as the change in the turbulent transport quantities. The Chen modification does not randomly increase or decrease turbulent viscosity, but sensitizes both turbulent transport quantities to shear. It can be seen by reviewing Figs. 14 and 19, plots of the percent change eddy viscosity for cases 1 and 2, respectively, that the patterns of change follow the varying size of the velocity gradient.

The changes made by the Chen modification improve the predictions of the major flow characteristics for the two quarled burner test cases. However, the improvement does not extend to making exact predictions throughout the flow. The Chen modification is intended to make significant advances in eliminating the k–epsilon model's problem of yielding overly diffusive predictions in regions of high shear. It has succeeded in this task. However, it was not intended to tackle k–epsilon's inability to model anisotropy. This problem stems from the assumption of isotropic turbulence made in the closure of the turbulent transport equations. A study of swirling flow encountering an expansion by Hallett and Günther concludes that immediately downstream of the expansion, the flow is highly anisotropic, with

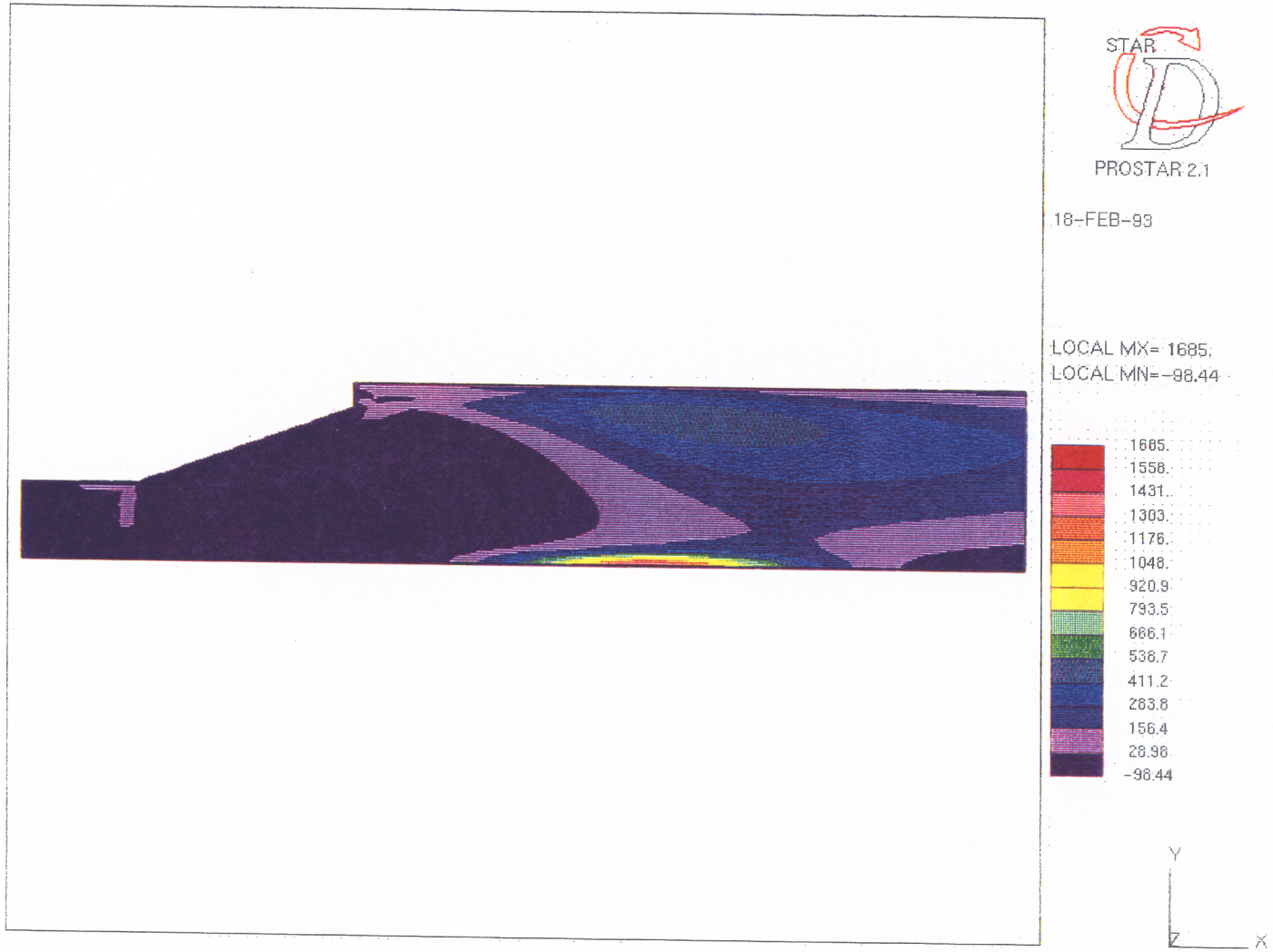

Figure 23. Quarled Burner Case 1, Percent Change Turbulent Dissipation from Standard k–epsilon to Chen Modification

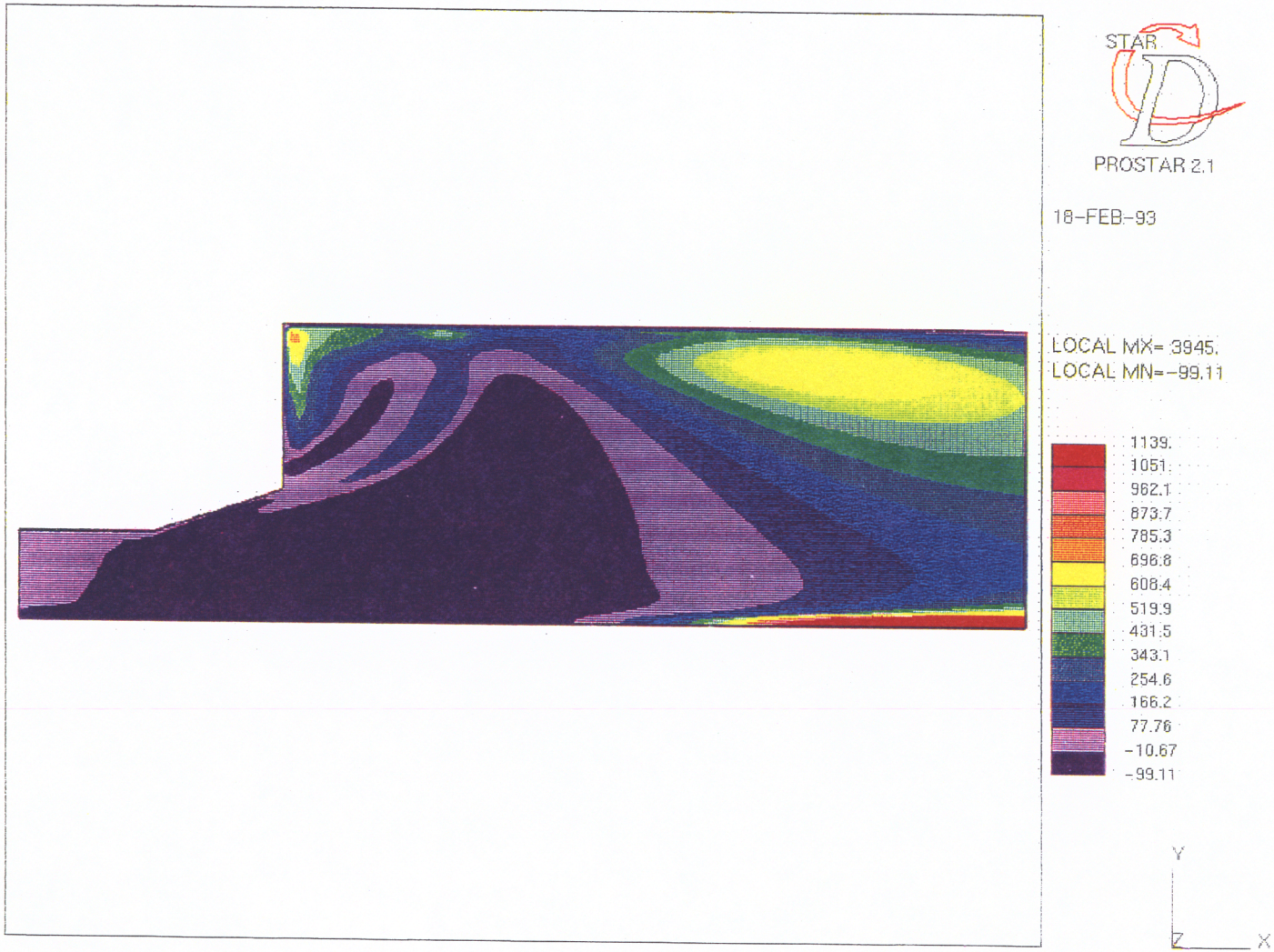

Figure 24. Quarled Burner Case 2, Percent Change Turbulent Dissipation from Standard k–epsilon to Chen Modification

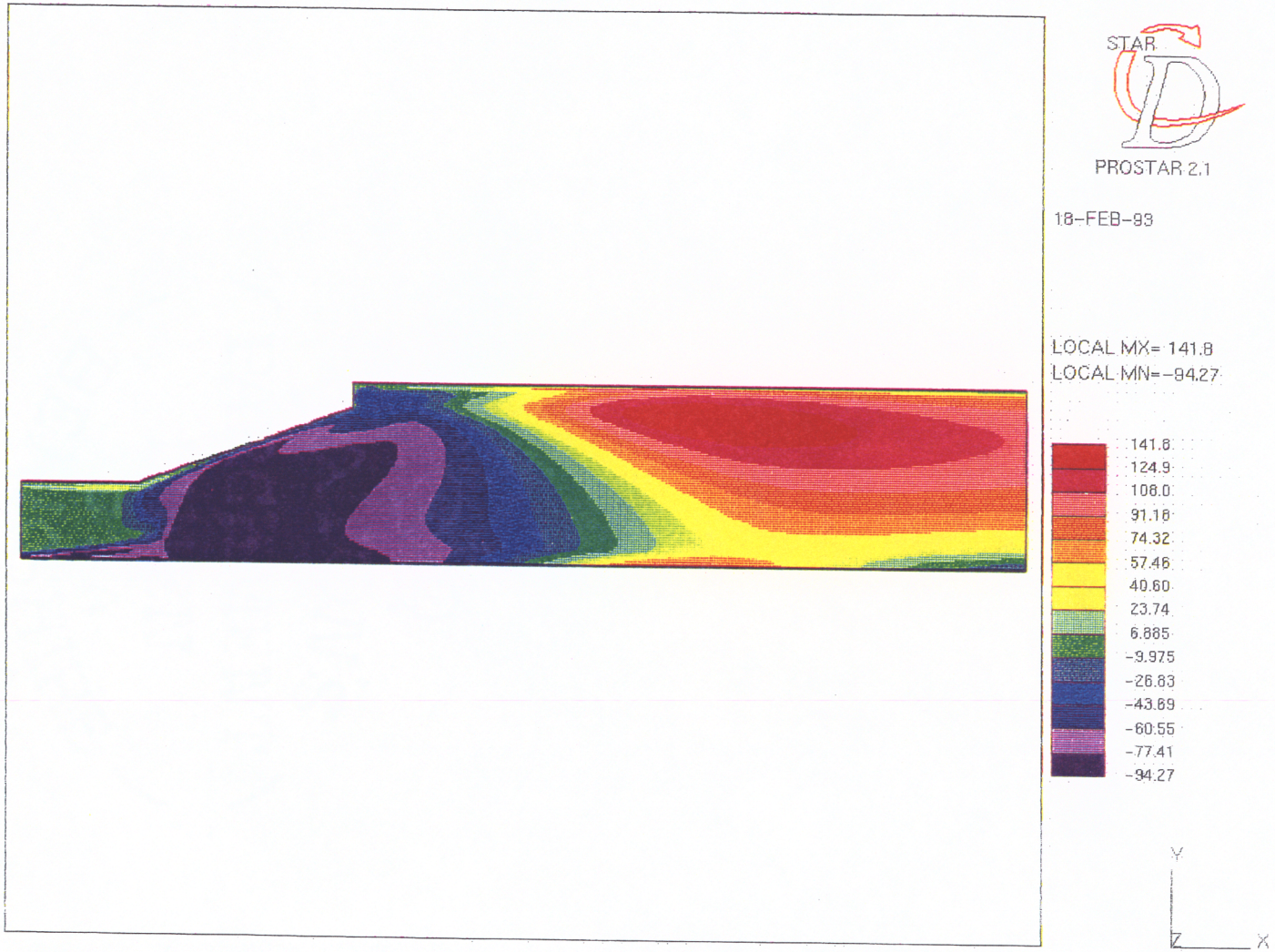

Figure 25. Quarled Burner Case 1, Percent Change Turbulent Kinetic Energy from Standard k–epsilon to Chen Modification

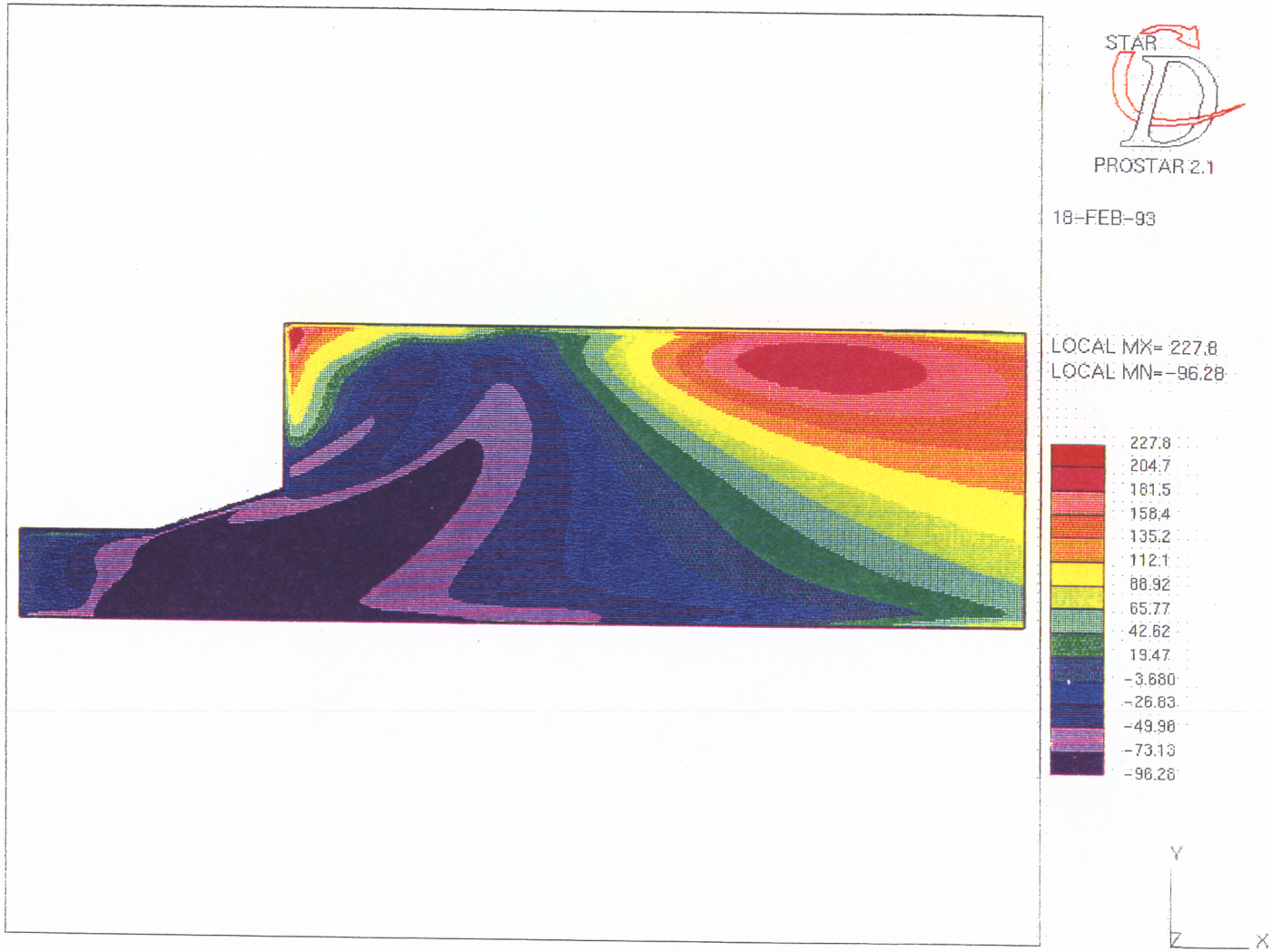

Figure 26. Quarled Burner Case 2, Percent Change Turbulent Kinetic Energy from Standard k–epsilon to Chen Modification

the fluctuations in the axial direction being much higher than those in the tangential and radial directions [7]. This would explain the inability of the Chen modification to make more exact predictions.

The greatest inconsistencies are seen in the axial velocity predictions of both cases, the second case revealing a more pronounced difference. The Chen modification makes great improvements in the axial velocity throughout the flow profile. However, it fails to predict the positive momentum measured experimentally at the centerline. In case 1 a second centerline recirculation zone counteracting the momentum of the first is present [22]. The additional recirculation zone forms a bubble inside the primary centerline recirculation and recirculates in the opposite direction, explaining the presence of a positive axial velocity at the centerline. Although it occurs in both cases, this phenomena is more apparent from the experimental streamlines of the second case (Fig. 27). The streamline which moves from the primary recirculation to the centerline forms a small bubble near the axis of symmetry. Although the presence of a second centerline recirculation zone is not specified in the experimental document, this bubble does indicate that one exists. Furthermore, Abou–Arab, Richter, and Seeger resolved an internal and an external recirculation zone in their investigation of flow in a burner model, fortifying the assumption that this flow phenomena occurs in case 2 [20]. This flow structure occurs because of the predominance of the axial fluctuation as the flow enters the expansion, and is therefore unable to be modeled by an anisotropic turbulence model, like k–epsilon. The Chen modification to the k–epsilon model, however, is able to greatly improve the predictions of the major flow structures in the quarled burner test cases and is concluded to be applicable to combustor geometries.

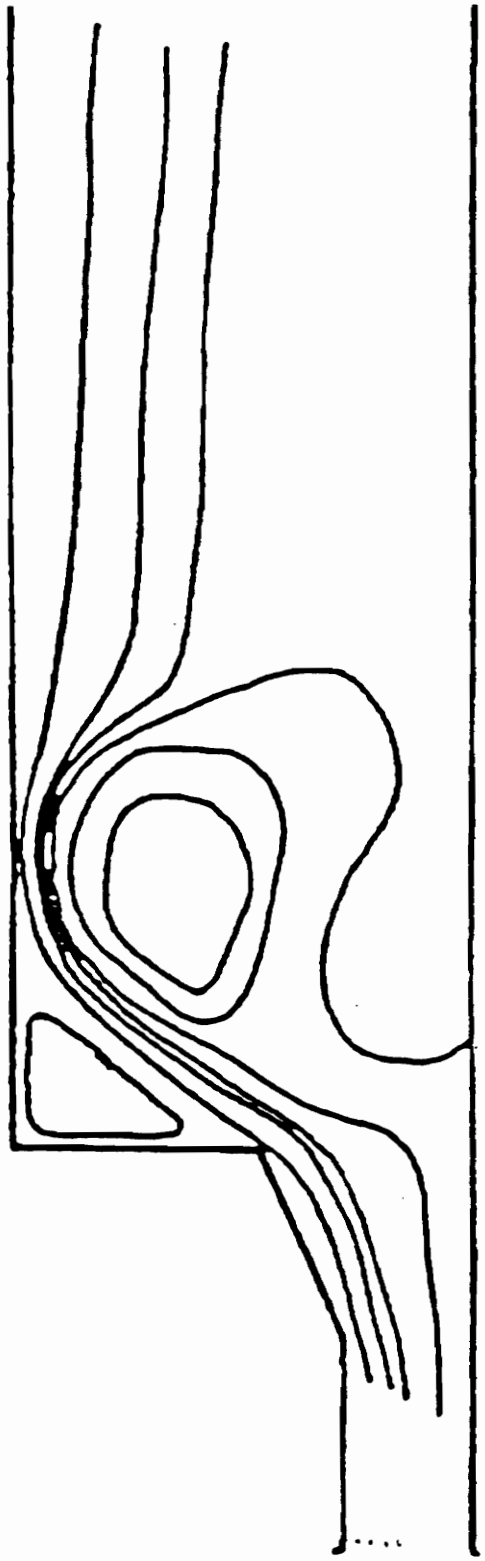

Figure 27. Quarled Burner Case 2, Experimental Streamlines [11]

As mentioned briefly before, the Chen modification failed to improve predictions for flow in a rectangular duct with 90° bend (See Appendix A). This geometry is characteristic of a strong secondary flow pattern caused by the curvature of the duct. Therefore, it is useful for evaluating the ability of a code to model a flow with strong curvature effects. The results of an evaluation of the Chen modification show no difference from the predictions with the standard k–epsilon model. However, eddy viscosity is changed. The turbulent viscosity is decreased near the outer radius of the bend and increased near the inner radius. This corresponds to the changes needed to improve the predictions. This type of flow contains a certain amount of anisotropy. However, the failure of the Chen modification to improve predictions is not primarily caused by the inability of k–epsilon to model anisotropy, but in the inability of the wall function employed to model the effects of curvature.

The k–epsilon model can not resolve flow completely to the wall. Therefore, a log–law is used to model the flow in the near wall region. The log–law, however, is not valid for all flows, resulting in inconsistent results. One of the regions where the wall function used is not valid is at points at or near separation [23]. The wall function expresses the flow in terms of wall shear [24]. In this area, the flow can not be described in this manner because, at or near separation, the flow is detached from the wall. Since the law of the wall was formulated for zero pressure gradient boundary layers, the wall function is also not valid for flows with a high adverse pressure gradient. In these instances, the wall function will predict a steeper increase in dissipation than for zero gradient boundary layers, yet experiments show that the gradient of dissipation is virtually independent of pressure gradient [14]. This effect can be seen in the case of the rectangular elbow with 90° bend. The near wall flow on the convex surface in the bend experiences an adverse

pressure gradient. Both the standard k–epsilon and the Chen modification underpredict the turbulent structure occurring near the inner radius of the bend. The overprediction of the dissipation of turbulence in this region results from the use the wall function. The effects of curvature in this area are so strong, that any changes in the viscous forces will result in negligible improvements in the prediction of the velocity. In any situation where the wall effects are the dominant force in determining the flow structure, the Chen modification will fail to make an improvement. It is not the intention of Chen to tackle the problem of the use of wall functions, and , therefore, an improvement in these situations is not expected.

The Chen modification has been shown to improve results for the two quarled burner test cases evaluated. However, the modification is not intended to attack the problem of k–epsilon's use of a log–law of the wall and it's assumption of isotropy. Therefore, the Chen modification will not resolve flow features that are a function of a high degree of anisotropy or a result of strong wall effects. As in the case of the quarled burners, the secondary centerline recirculation zone, which is an effect of anisotropic behavior was not resolved because of the assumption of isotropy made in the closure of the k–epsilon model. The Chen modification was unable to make improvements in the case of the rectangular elbow because of the inability of the wall function to predict the secondary flow patterns which occur as an effect of the curvature of the flow. Chen's model, however, is able to significantly improve predictions of the quarled burner geometries. Furthermore, it is able to accurately predict the location of the center of recirculation for both burner cases. In industrial combustor design, the prediction of the location of flow structures is of paramount importance. The Chen modification can, therefore, be considered a successful improvement to the k–epsilon model.

7.0 Conclusions and Recommendations

A modification to the k–epsilon turbulence model is proposed by Y. S. Chen. Many modifications have been made to the k–epsilon model. However, most have concentrated on improving results for specific categories of flow. Chen's approach is to attack a general problem with the k–epsilon model, rather than a specific application problem. In many flows, the pattern of inconsistencies in predictions indicates the diffusive nature of the k–epsilon model. The modification Chen proposes attempts to remedy this problem by adding a second time scale to the highly empirical turbulent dissipation equation. This extra term, which includes a coefficient whose value must be empirically determined, will allow the turbulent energy transfer mechanism to react more effectively to mean strain. The resulting effect is a decrease in eddy viscosity in regions of high shear and an increase in regions of lower shear. Chen had tested his modification on a variety of different flow types, including flow over a rectangular backward facing step and a swirling flow. The results were favorable and prove Chen's model to be general and applicable to a broad range of flows. The present study is concerned with the

applicability of the Chen modification to combustor geometries, which contain a combination of swirling, turning and recirculating flows.

The Chen modification is tested on two burner cases to evaluate its applicability to combustor geometries. In the first test case, swirling flow encounters a ramp, or quarl, before it reaches a small expansion. This geometry results in a centerline recirculation high in the expansion and extending partially into the quarled region. In the second test case, swirling flow passes through a shorter quarled region than in the first case before entering a larger expansion. The resulting flow pattern is a centerline recirculation accompanied by a second recirculation zone behind the step. The center of recirculation is, like the first case, high in the expansion, but does not extend into the quarled region. For both cases, from the velocity profiles, it is clear that k–epsilon diffuses the swirl and axial momentum, which results in the inconsistent prediction of the location of the recirculation zone for both cases. The k–epsilon model predicts the center of recirculation to be low in the expansion and further upstream.

The Chen modification improves results drastically. Comparisons of experimental and computational velocity profiles show Chen's ability to predict the peaks in swirl and axial momentum that the standard k–epsilon model fails to. This indicates that the Chen modification preserves the gradients of the swirl and axial velocity, which k–epsilon has been shown to diffuse. The result is a significantly improved prediction of the location of the recirculation zone. The size of the recirculation zone, which was overpredicted by the standard k–epsilon model, is now correctly predicted by Chen. The improvements are due to the control of the growth of eddy viscosity in regions of high shear. The standard k–epsilon model tends to overpredict eddy viscosity in these regions causing the diffusion of axial

and swirl momentum. The Chen modification is able to control this effect, which results in a decreased prediction of the eddy viscosity in regions of high shear.

The discrepancies in the predictions occur near the centerline. Experimental measurements show a slight positive velocity near the axis of symmetry. Studies of swirling flow entering an expansion show that the flow is highly anisotropic as it enters the expansion, with the axial velocity fluctuation dominating. The anisotropy of the flow gives rise to a secondary centerline recirculation which opposes the primary zone flow. Because the k–epsilon model assumes isotropy, the Chen modification is unable to capture this flow feature. It is noted that it is not the intention of Chen's model to attack k–epsilon's inability to model anisotropy. However, the isotropic assumption of k–epsilon is an important issue of concern and a subject of future research. Chen's model has decreased the negative flow near the centerline because it has correctly predicted the position of the center of the primary recirculation zone. The Chen modification has greatly improved results and has accurately predicted the position of the primary flow features.

Two problems inherent to the k–epsilon model limit the scope of improvements the Chen modification has the ability to make. One, is the inability of k–epsilon to model anisotropic flows, and the other, is the use of a wall function to predict flow near the wall. The isotropic assumption is made in the derivation of the turbulent kinetic energy equation used in the k–epsilon model. Therefore, nothing can be done to remedy this problem, except to use a model which solves for the turbulent Reynolds stresses directly. These models, discussed in chapter 3, do produce accurate results, but not without the cost of increased computational time and memory requirements. For the large and complex geometries that

industrial combustion design engineers are interested in modeling, such models are impractical. Speed and general consistency of results are of greatest importance in practical design applications. Therefore, the Chen modification proves to be the best option for modeling complex combustor geometries.

Wall functions, as seen in the case of the rectangular duct with 90° bend, can prevent the Chen modification from making improved predictions. The use of a wall function is necessary for high Reynolds number k–epsilon models, which are unable to model turbulence close to the wall. Chen implements his modification to a high Reynolds number k–epsilon model and, therefore requires the use of a wall function.

A low Reynolds number k–epsilon model does not require the use of a wall function and can model turbulence to the wall. A disadvantage to the low Reynolds number k–epsilon model is that it requires 60 to 100 grid points across the boundary layer [25]. This greatly increases the number of cells in the model, which will increase the computational time and memory requirements. Furthermore, studies show a low Reynolds number k–epsilon model to produce only minor improvements for a variety of flows [26]. A recommendation to remedy this problem is to employ the use of a one equation model at the wall. This type of model is often referred to as a two layer model. A high Reynolds number model is used in the core flow and a one equation model is used in the near wall region. In the rectangular elbow case, the wall function was unable to predict the effects of the curvature of the convex wall which experiences a high adverse pressure gradient. A one equation model, which uses an empirical length scale yields much better predictions for adverse pressure gradients than a k–epsilon model [14]. A two equation model, tested by Rodi, showed improved results for a two

dimensional boundary layer flow, separated flows, and flows with a high adverse pressure gradient [25].

It is recommended that the Chen modification be implemented within a two layer model and tested with a turning flow, similar to the rectangular duct with 90° bend, and a burner case such as the quarled burners analyzed in this study. This, along with a comparison of the Chen modification with a Reynolds Stress Model, for both a turning flow and combustor type geometry is the subject of future research.

Appendix A. Rectangular Elbow with 90° Bend

One of the complex flows Chen has suggested for future study is turbulent flow inside a strongly curved duct. In this thesis, a rectangular duct with 90° bend was chosen. This flow is of particular interest because of the generation of secondary motion, or streamwise vorticity. Secondary flow patterns occur in this geometry because of the curvature of the duct and are responsible for pressure losses and a redistribution of the streamwise velocity. The standard k–epsilon model of turbulence is unable to consistently model this flow configuration. It has been shown that the Chen modification improves predictions for several complex flows, however the modification can not be considered universally applicable. Flow in curved ducts is the subject of many studies because it occurs in many industrial applications. Thus, any method which has the potential of improved predictions should be explored.

The case chosen is an experiment performed by Tayler, Whitelaw and Yianneskis of a rectangular duct with 90° bend [27]. One of the purposes of their study was to provide detailed measurements suitable for the evaluation of numerical analysis. The data is, therefore, both comprehensive and extensive. The test configuration is a 40 x 40 millimeter duct with a 0.3 meter entrance length. The flow turns through 90° and exits through 2.0 meters. The geometry of the

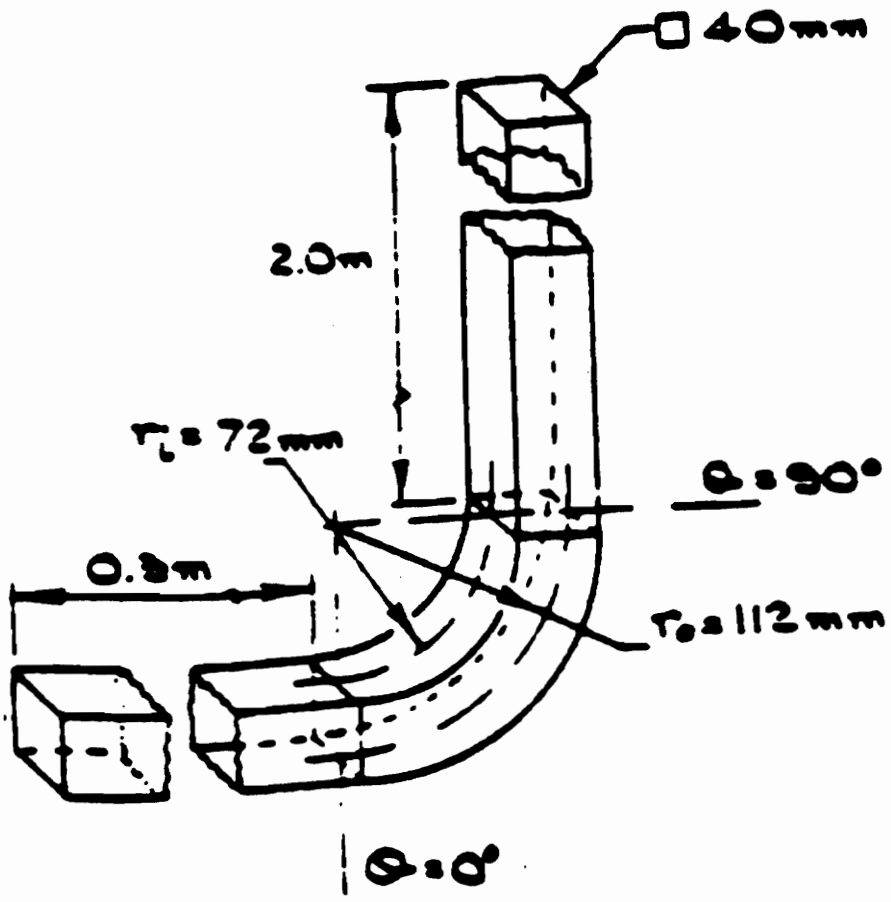

Figure 28. Rectangular Duct with 90° Bend, Geometry [33]

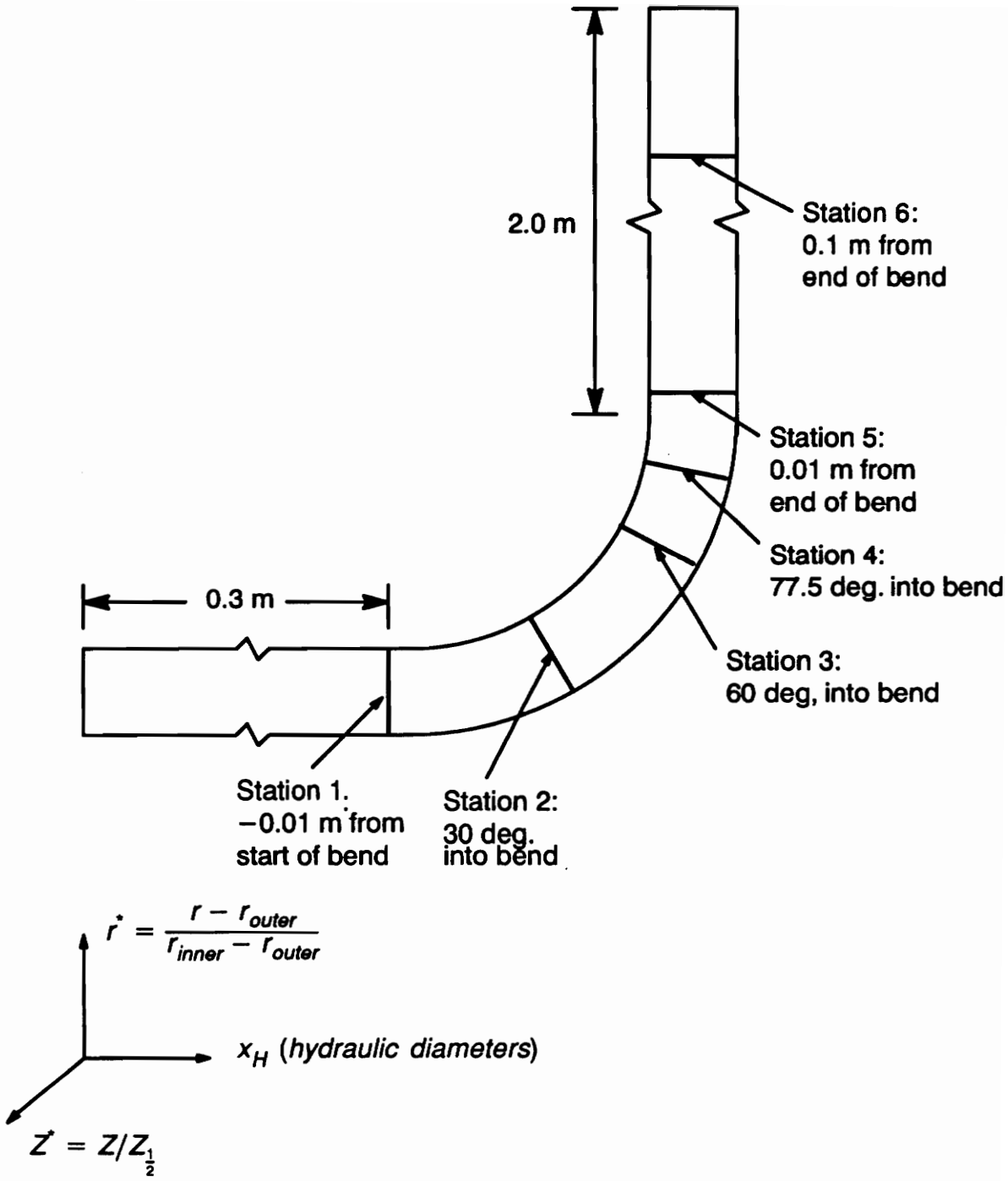

Figure 29. Rectangular Duct with 90° Bend, Experimental Locations and Nomenclature

rectangular elbow is shown in Fig. 28. Velocity measurements are taken at –0.01 meters from the bend entrance, 30°, 60°, and 77.5° into the bend, and 0.01 and 0.1 meters from the end of the bend. Each experimental station contains 50 data points, 10 points in the spanwise direction for each one of the locations in the radial direction. Fig. 29 illustrates the nomenclature used to describe the location of the experimental points and the locations of the experimental stations.

This configuration must be evaluated in three dimensions. However, the flow can be considered symmetric about the x–y plane, cutting the required number of computational cells in half. The geometry now has a 40 x 20 cross–section rather than a 40 x 40 cross–section. The mesh, shown in Fig. 30, accordingly has 20 cells in the radial direction, 10 cells in the spanwise direction and 104 cells in the streamwise direction. A mesh sensitivity study was conducted, determining the 21 x 11 x 105 mesh to be the most effective. A finer mesh violated the requirement of y^+ between 30 and 100 at walls [30], and a more course mesh was unable to model the gradients in the flow. The inlet is set with a uniform velocity profile of 1.00 m/s in the axial direction. The inlet values of turbulent kinetic energy and dissipation were approximated using the assumption of a 3% turbulent intensity and are 0.03024 m^2/s^2 and 0.43823 m^2/s^2 respectively. Gradients of all variables are set to zero at the outlet plane, while the gradients in the normal direction at the symmetry plane are set to be identically zero. The walls are treated with a standard log–law of the wall. The model is run using lower and higher order schemes, with the higher order schemes producing more consistent predictions. Therefore, the results presented are calculated with central differencing with a blending factor of 0.9.

The Chen modification, as illustrated in Figs. 31 through 36, yielded no improvement in the streamwise velocity predictions . This result is somewhat of a

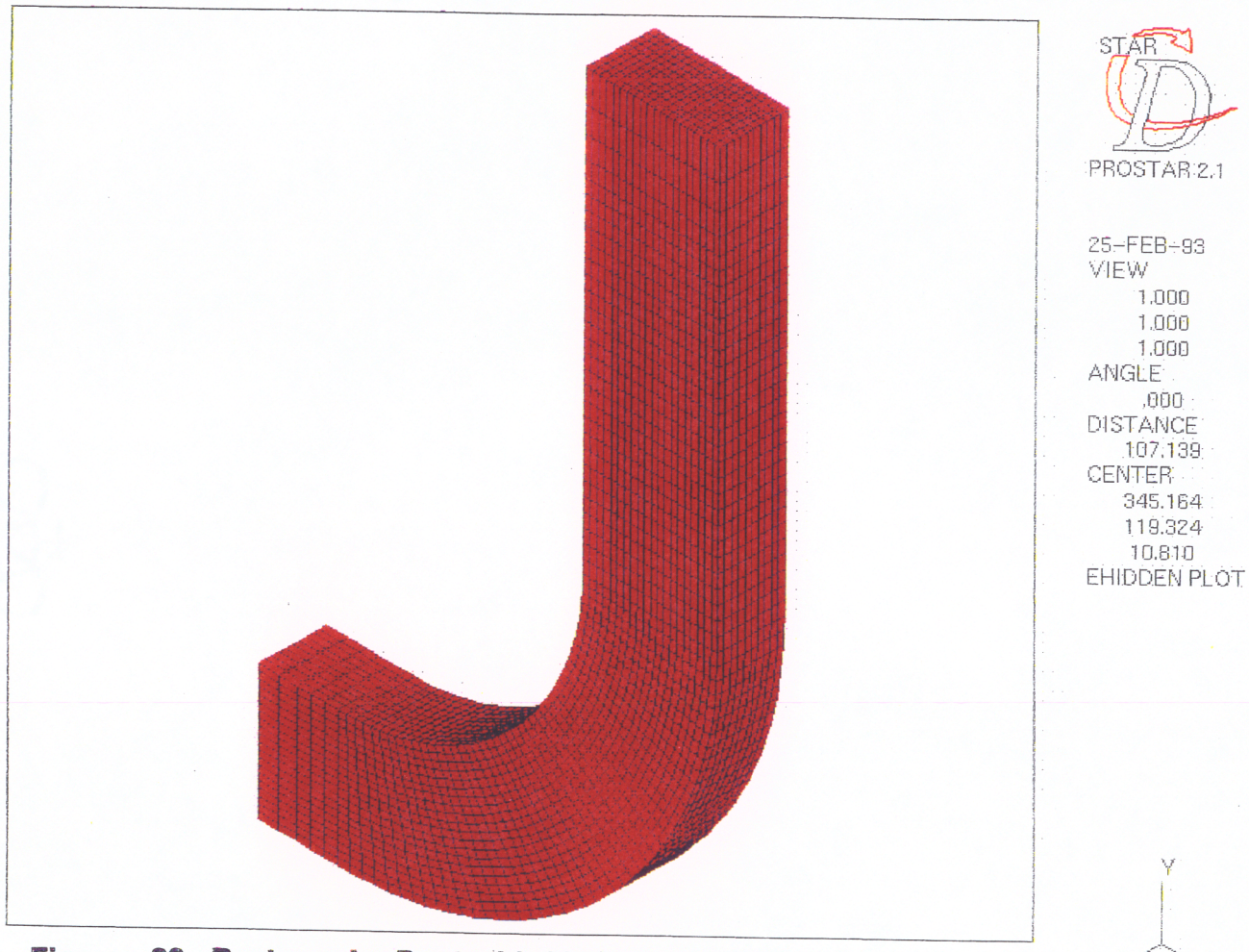

Figure 30. Rectangular Duct with 90° Bend, Mesh

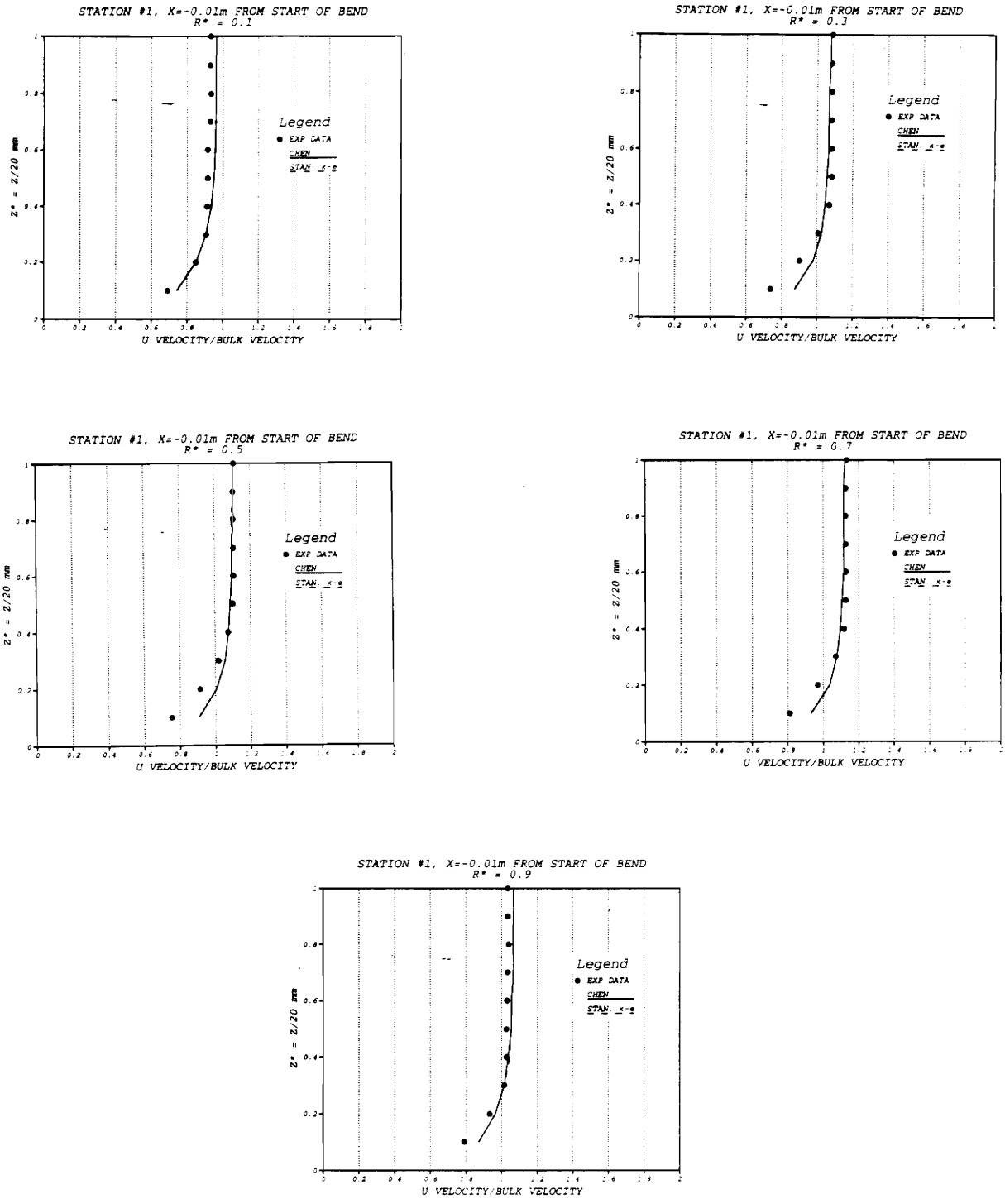

Figure 31. Rectangular Duct with 90 ° Bend, Streamwise Velocity Profiles at Experimental Station 1

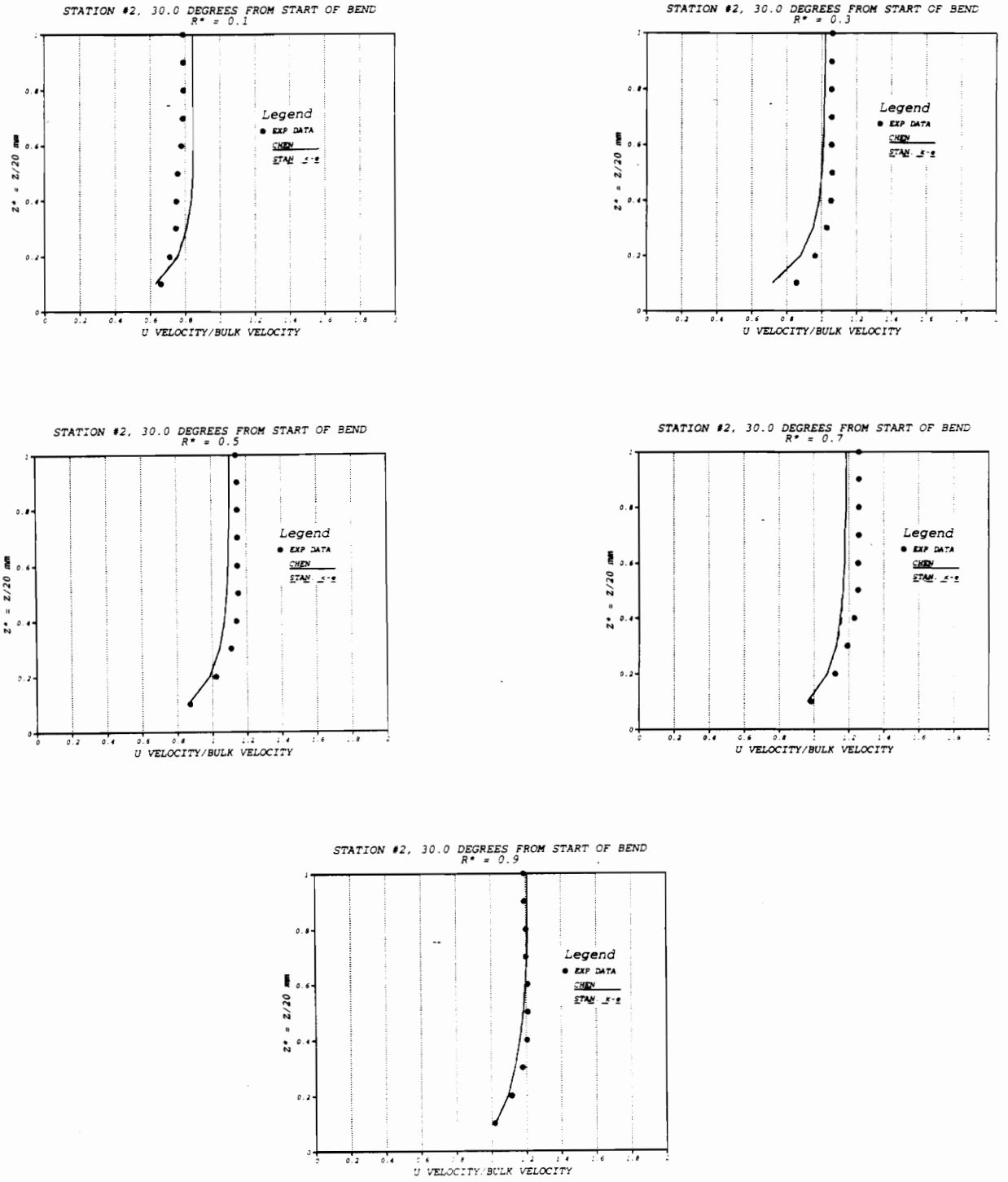

Figure 32. Rectangular Duct with 90 ° Bend, Streamwise Velocity Profiles at Experimental Station 2

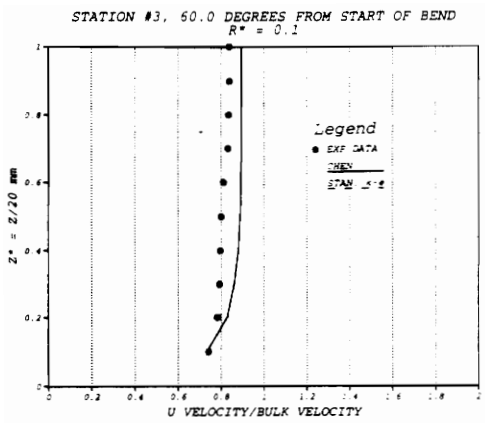

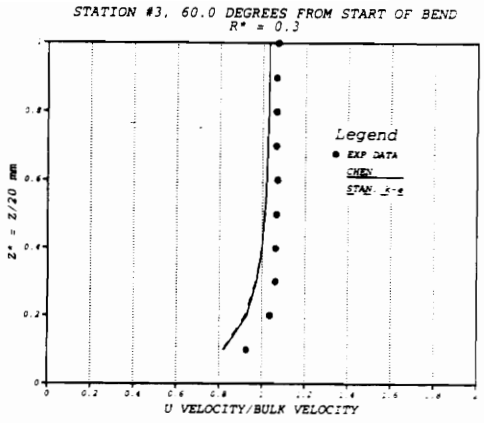

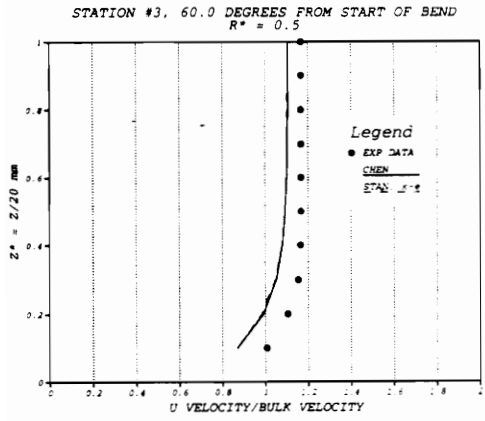

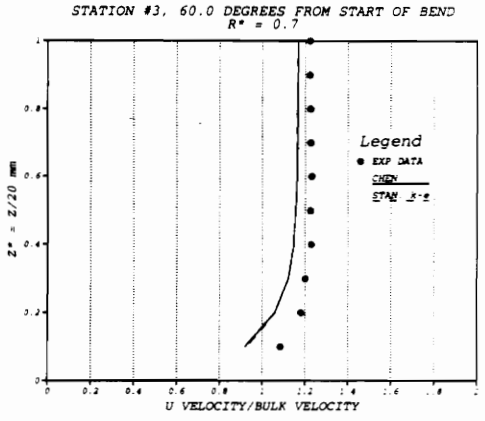

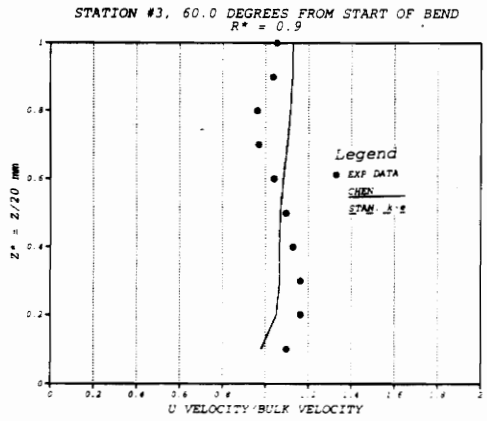

Figure 33. Rectangular Duct with 90 ° Bend, Streamwise Velocity Profiles at Experimental Station 3

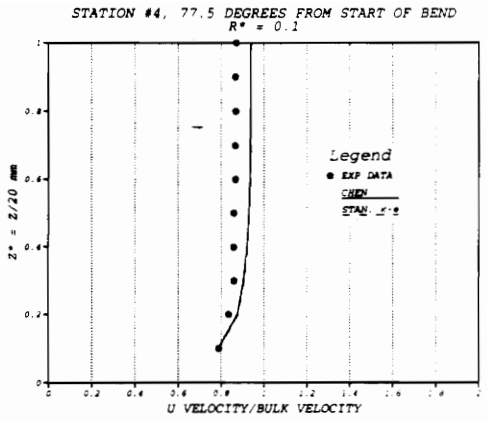

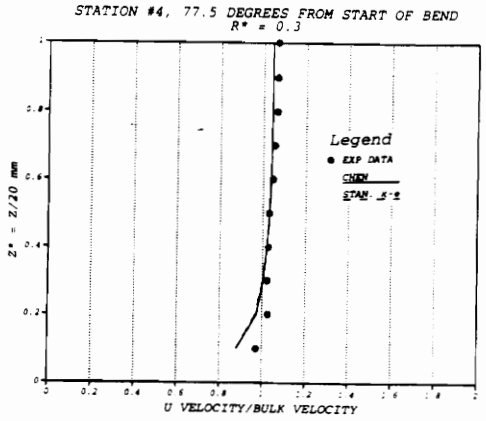

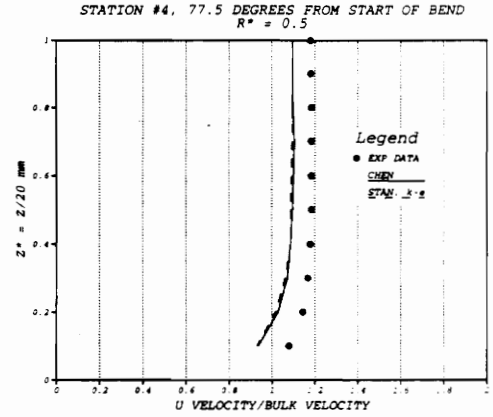

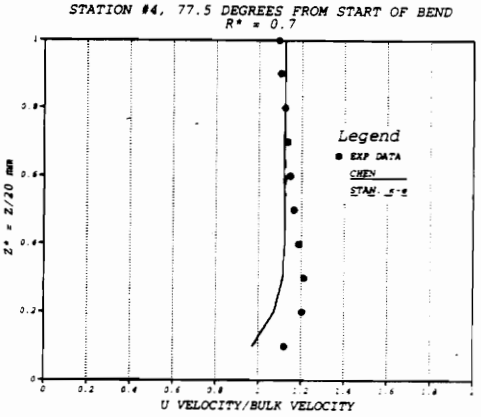

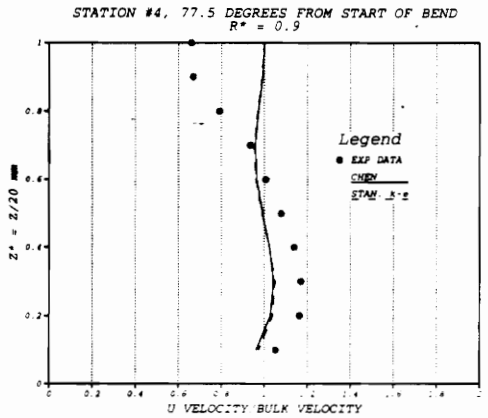

Figure 34. Rectangular Duct with 90 ° Bend, Streamwise Velocity Profiles at Experimental Station 4

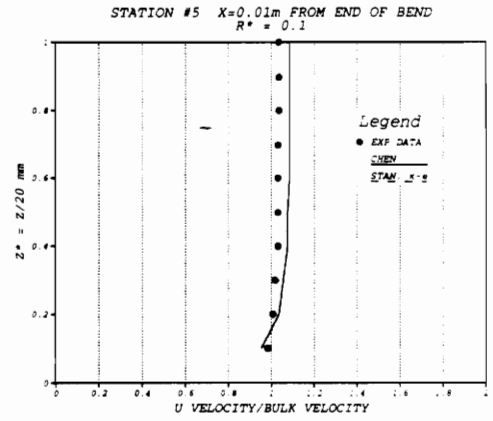

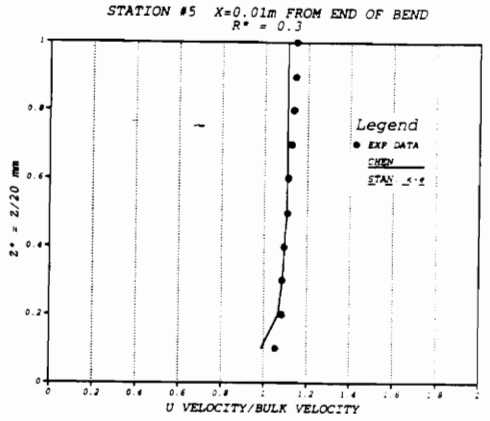

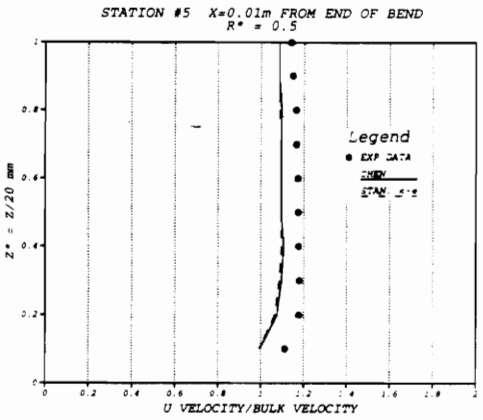

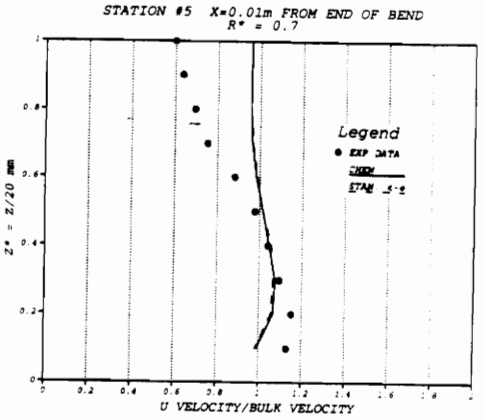

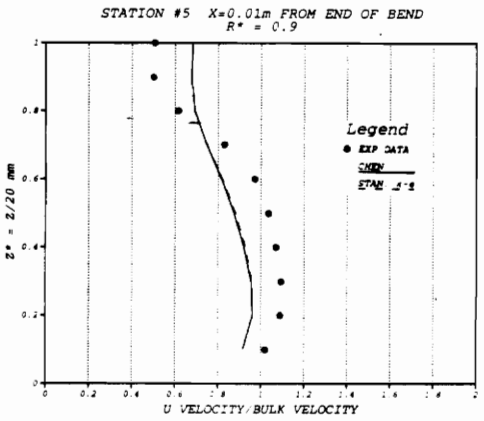

Figure 35. Rectangular Duct with 90 ° Bend, Streamwise Velocity Profiles at Experimental Station 5

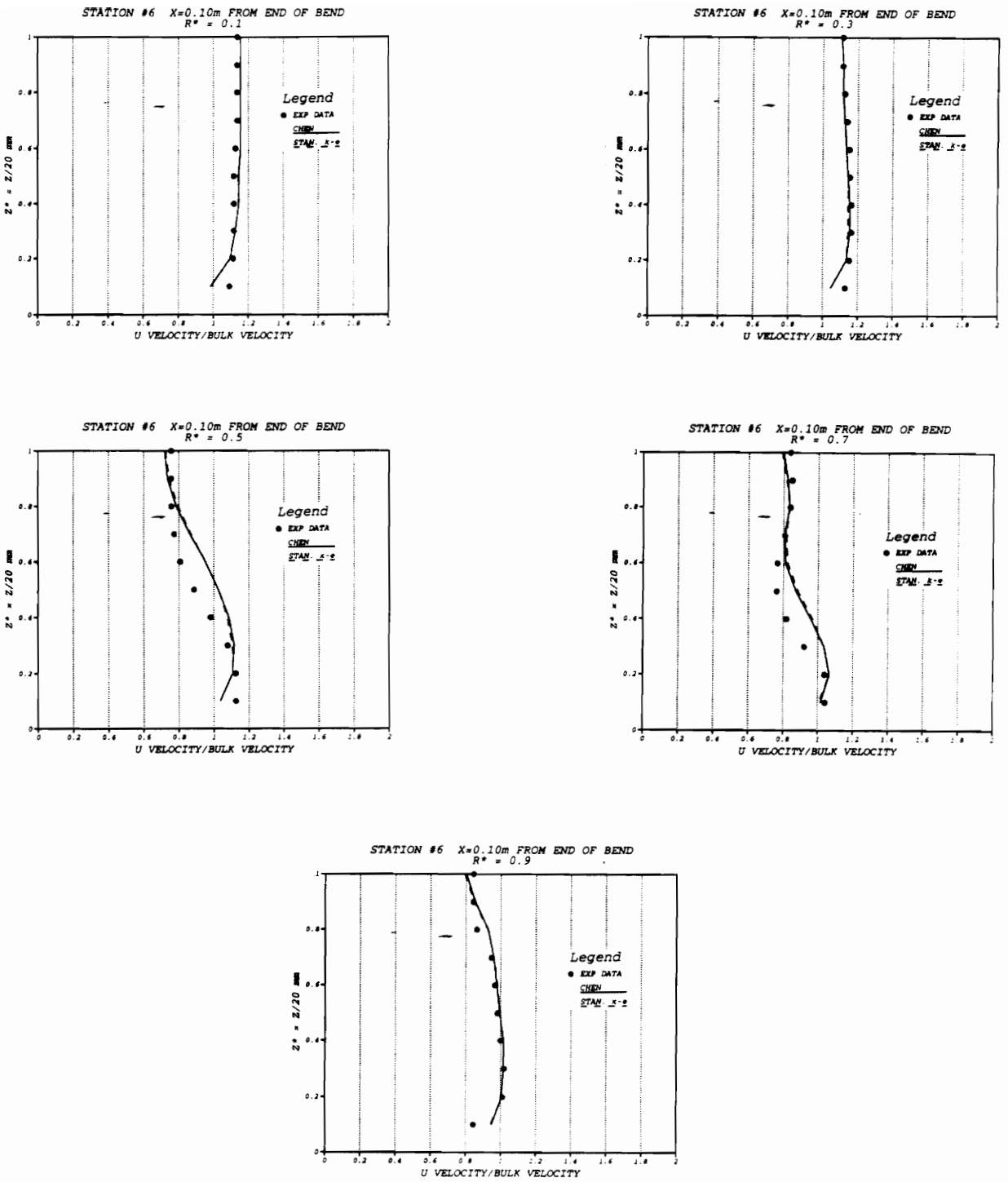

Figure 36. Rectangular Duct with 90 ° Bend, Streamwise Velocity Profiles at Experimental Station 6

surprise, as the improvements to cases previously tested by Chen were so drastic. As seen in Figs. 37 and 38, the Chen model was successful in altering the prediction of eddy viscosity, but failed to make a change in the velocity predictions. Referring back to the velocity profiles, the secondary flow structures in the region near the convex side of the bend are underpredicted. It is speculated that the reason this occurs is due to standard k–epsilon's overprediction of the eddy viscosity near the outer radius of the bend, where the flow has more momentum, and the underprediction of the eddy viscosity of the region near the inner radius of the bend where the secondary flow patterns are dominant. The Chen modification decreases the turbulent viscosity near the outer radius and increases the viscosity near the inner radius. The expected result from this prediction would be the increase in momentum of the jet moving near the concave surface, pushing it further towards the outer radius and increasing the region for development of the secondary flow. A decrease in momentum near the convex surface of the bend would be expected to increase the turbulent motion in this region and promote the generation of streamwise vorticity.

This points to two of the deficiencies, not of the Chen modification, but of the k–epsilon turbulence model. One, the inability of high Reynolds number k–epsilon, implemented in most commercial CFD codes, to model flow in the near wall region, and two, the inability of k–epsilon to model anisotropic flow. The primary problem preventing the Chen modification from making an impact on the results is the inconsistent modeling of the near wall flow. Because the high Reynolds number k–epsilon model is unable to model near wall flow, a standard log–law of the wall is used in this region. In the rectangular elbow, the flow in the near wall region on the convex wall of the bend experiences a strong adverse pressure gradient. The

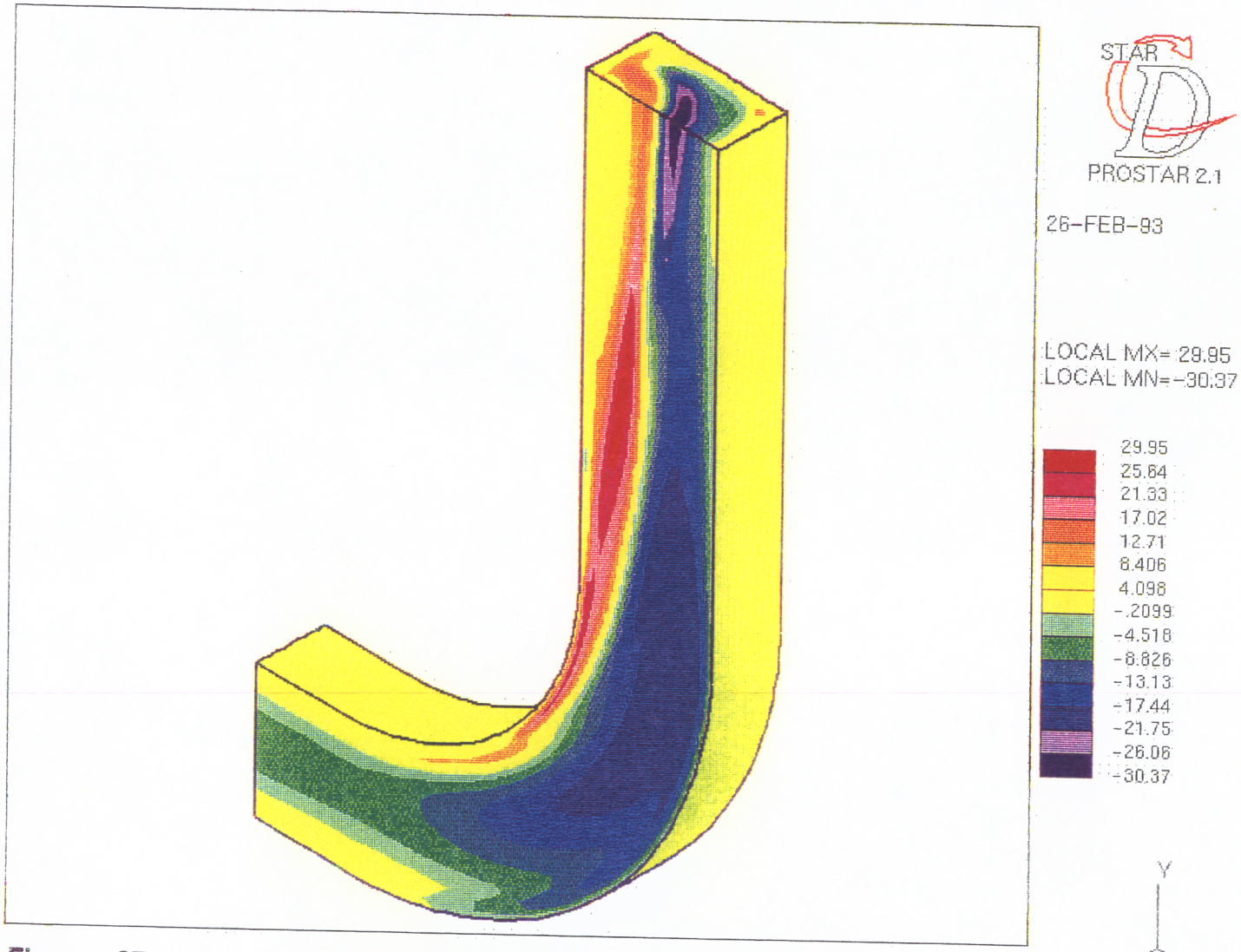

Figure 37. Rectangular Duct with 90° Bend, Percent Change Eddy Viscosity from Standard k–epsilon to Chen Modification

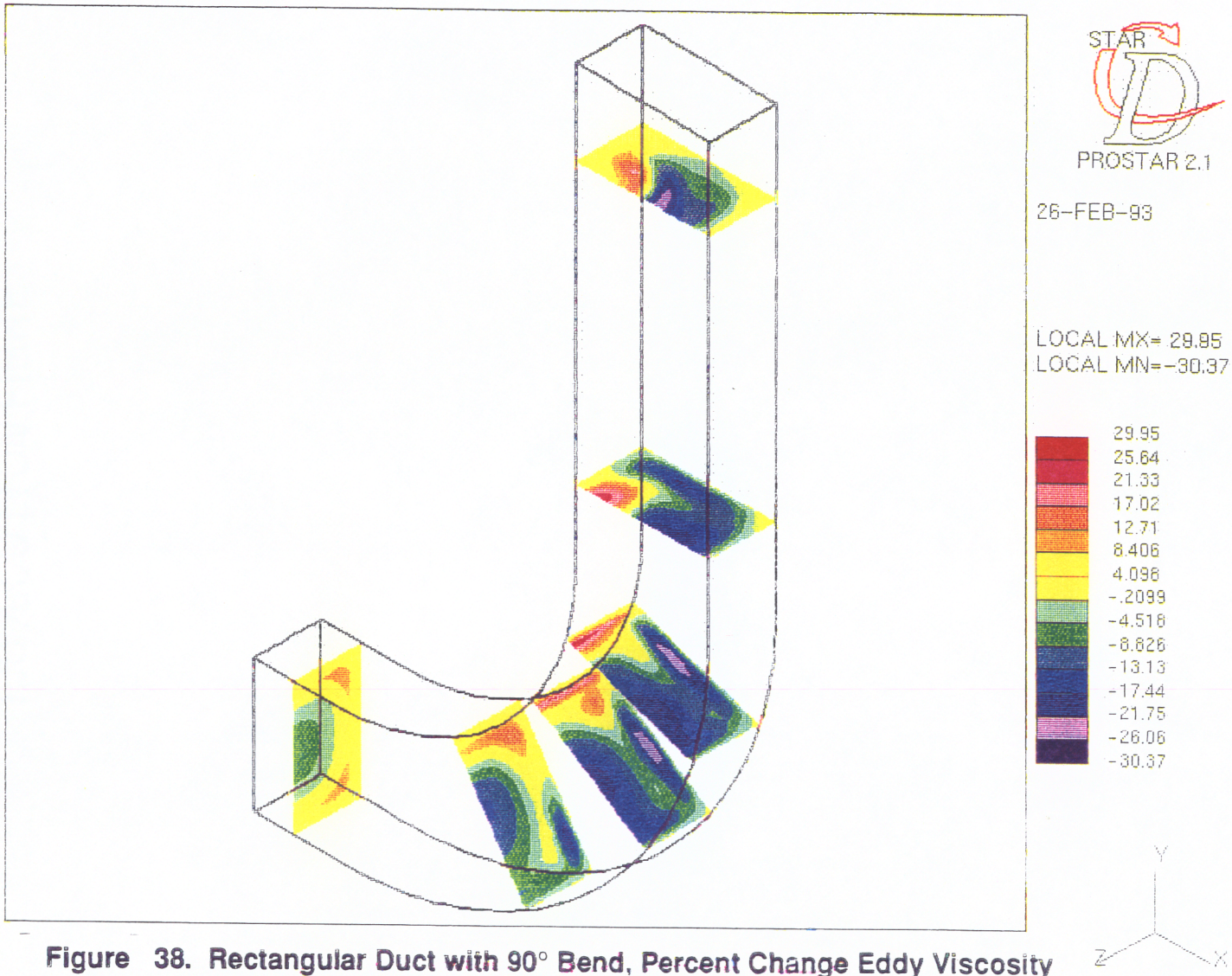

Figure 38. Rectangular Duct with 90° Bend, Percent Change Eddy Viscosity from Standard k–epsilon to Chen Modification (sections at the experimental locations)

log–law of the wall, however, is formulated for a zero pressure gradient boundary layer, rendering it inapplicable to flows with high adverse pressure gradients [14]. The log law represents flow in the near wall region as a function of the wall shear [24]. Therefore, in regions were there is no wall shear, such as separated flow, the log–law is inapplicable. Typically, the misrepresentation of the near wall flow by the law of the wall does not largely effect predictions in the core flow. The exception occurs in flows which are highly influenced by curvature, such as the rectangular elbow. The Chen modification is unable to improve predictions because the effects of curvature dominate the flow, rendering the changes in eddy viscosity useless.

The Chen modification is not universally applicable to all flow types, however, it has proven to be effective in improving predictions for many complex flows. Furthermore, while the Chen modification failed make an improvement in the case of the rectangular duct with 90° bend, it did not yield worse predictions than the standard k–epsilon model. A suggested solution to this problem is to use a two layer model in conjunction with the Chen modification. A two layer model combines the use of a high Reynolds number k–epsilon model in the core flow and a one equation model near the wall. A one equation model specifies the length scale and solves for a velocity scale from the turbulent kinetic energy equation. One equation models, which specify a length scale from empirical correlations, are ore consistent in their predictions of near wall flows than a low Reynolds number k–epsilon model [14]. In addition, the one equation model requires fewer cells in the near wall region than a low Reynolds number model, thus, greatly decreasing the computational time and memory required for the calculation. By using the one equation model coupled with the Chen modification, the speed of the k–epsilon model will be retained, while improving results in flows with strong wall effects.

Appendix B. Application Code

The Chen modification is implemented into STAR–CD, a three dimensional commercial CFD code which uses a pressure correction based scheme. A manual containing complete documentation on the mathematical modeling, numerical techniques and use of the code is available for reference through the author upon request. STAR–CD has the capability of modeling steady or transient flows, laminar or turbulent flows, and incompressible or compressible flows as well as heat transfer, mass transfer, distributed resistances (porous media), buoyancy, multiple species and non–newtonian fluids. The two implicit algorithms employed by STAR are the SIMPLE and the PISO methods. Both are pressure correction based schemes, the latter being the most recently developed method. Previous studies [28] have shown the SIMPLE method to perform better than the PISO algorithm for steady state flows and, thus, SIMPLE was chosen for the present stVGó. STAR employs a mesh generation system which has the capability of creating body fitted and non–orthogonal grids, unstructured meshes, and a range of cell shapes (hexahedra,pentahedra, tetrahedra). The mesh generation, definition of the boundary and initial conditions, and the application of additional parameters is accomplished by the pre–processing program PROSTAR. PROSTAR also acts as a post–processor, providing superb visualization and data manipulation

capabilities. The following sections contain details on the governing equations, SIMPLE, and the spatial discretization methods used in this study.

B.1 Governing Equations

The Navier–Stokes equations are comprised of the equations for conservation of mass, momentum and energy and are referred to as the governing equations of fluid flow. Only the mass and momentum equations are presented here, as the cases dealt with in this study do not require the energy equation to be solved. The equations are represented in Cartesian tensor notation for simplicity and can be applied to a specified control volume [29,30].

Conservation of Mass:

$$\frac{1}{\sqrt{g}}\frac{\partial}{\partial t}(\sqrt{g}\,\varrho) + \frac{\partial}{\partial x_j}(\varrho u_j) = 0 \qquad (B-1)$$

$$where,\ \sqrt{g} \equiv determinant\ of\ metric\ tensor$$

The first term on the left hand side of the equation represents the time rate of cçÚ vP of the density in the control volume. The second term represents the rate of mass flux out of the control volume's surface.

Conservation of Momentum:

$$\frac{1}{\sqrt{g}}\frac{\partial}{\partial t}(\sqrt{g}\,\varrho u_i) + \frac{\partial}{\partial x_j}(\varrho u_j u_i) = \varrho f - \frac{\partial p}{\partial x_i} + \frac{\partial}{\partial x_j}\left[\mu\left(\frac{\partial u_i}{\partial x_j} + \frac{\partial u_j}{\partial x_i}\right) - \frac{2}{3}\delta_{ij}\,\mu\frac{\partial u_k}{\partial x_k}\right] \qquad (B-2)$$

The first term on the left hand side represents the time rate of change of momentum in the control volume and the second term represents the rate of change of

where, $\sqrt{g} \equiv$ *determinant of metric tensor*

momentum due to convection. On the right hand side, the first term represents the body forces, the second is the surface pressure forces and the third and last term represents the viscous forces. The inclusion of the determinant of the metric tensor in both equations allows the solution in body fitted coordinates.

For turbulent flow, the u_i, p and stress tensor take on their ensemble averaged variables. The ensemble averaging of the Navier–Stokes equations for turbulent flow calculations have been discussed in chapter 3. The equations of state used by STAR to calculate density variation and molecular viscosity will not be presented, as the cases studied are incompressible and have been computed with constant laminar viscosity. Details on the method of non–dimensionalizing the equations and further details on the methods used are unavailable to the author due to the restrictions imposed by STAR–CD in their licensing agreement.

B.2 The SIMPLE Algorithm

STAR–CD employes a variant of the SIMPLE (Semi–Implicit Method for Pressure–Linked Equation) algorithm of Patankar and Spalding [31], which is the most commonly used pressure correction based scheme. The basic principle of the scheme is to predict the components of velocity by solving the momentum equations separately and then introduce a correction based on the requirement of continuity [32]. By decoupling the governing equations in this manner, the system can now be solved as a set of scalar equations rather than one vector equation. This p& 6VGW&Rends itself to a less computationally time and memory intensive

calculation than a scheme which requires the governing equations to be solved as one vector equation [29].

The procedure can be broken down into a series of steps [33]. Velocities are first predicted by guessing a pressure field and solving the continuity equations individually. The predicted velocities are defined as the difference between the actual velocity and a velocity correction. The guessed pressure, used to calculate the predicted velocities, is described in the same manner. By writing the u–momentum equation in terms of the predicted velocities, a relationship between the actual velocities and the pressure correction term can be established. In the second step, the pressure correction term is solved for by forcing the predicted velocities to satisfy continuity. Lastly, the corrected velocities are determined from the previously established relationship between the pressure correction and velocity.

The method is essentially a predictor corrector algorithm requiring iteration to converge to a steady state solution. A consequence of using this type of method is that the velocities and pressure must be under–relaxed to achieve stability. The SIMPLE algorithm of STAR–CD has been tested against various methods employed by other commercial CFD codes for the test cases used in this study and has proven to produce satisfactory results [28].

B.3 Spatial Discretisation

Spatial discretisation is the manner in which the convective and diffusive fluxes in the governing equations are represented. Fluxes are generally expressed in terms of the nodal values of the quantity surrounding the control volume node.

The two methods of spatial discretisation used in this study are upwind differencing, which is a lower order scheme, and a blended central differencing method, which uses a combination of lower and higher order schemes. The convective term, expressed as:

$$C_i = (\varrho u \Phi \cdot \vec{S})_i \qquad (B-1)$$

$$C_i = F_i \Phi_i \qquad (B-2)$$

$$where, \quad F \equiv (\varrho u \cdot \vec{S})$$

$$\Phi \equiv any\ of\ the\ dependent\ variables$$

$$and, \quad \vec{S}_i \equiv surface\ vector\ of\ face\ i$$

will be used to demonstrate the method of discretisation employed by both of the schemes used in this study, as well as the linear upwind and central differencing schemes which appear as components of the blended central differencing method.

B.3.1 Upwind Differencing

A lower order scheme like upwind differencing is easiest to solve. The method chooses the nearest upwind neighbor value for Φ_i (Fig. 39).

$$C_i = F_i \Phi_{i-1} \quad , \text{ if } F_i \geq 0 \qquad (B-3)$$

or

$$C_i = F_i \Phi_i \quad , \text{ if } F_i < 0 \qquad (B-4)$$

However simple this method may be, the method of discretisation results in a truncation error which causes a degradation of local gradients. This effect is known as numerical diffusion. Numerical diffusion can be decreased by refining the mesh. This, however, results in an increase in computational time and memory requirements.

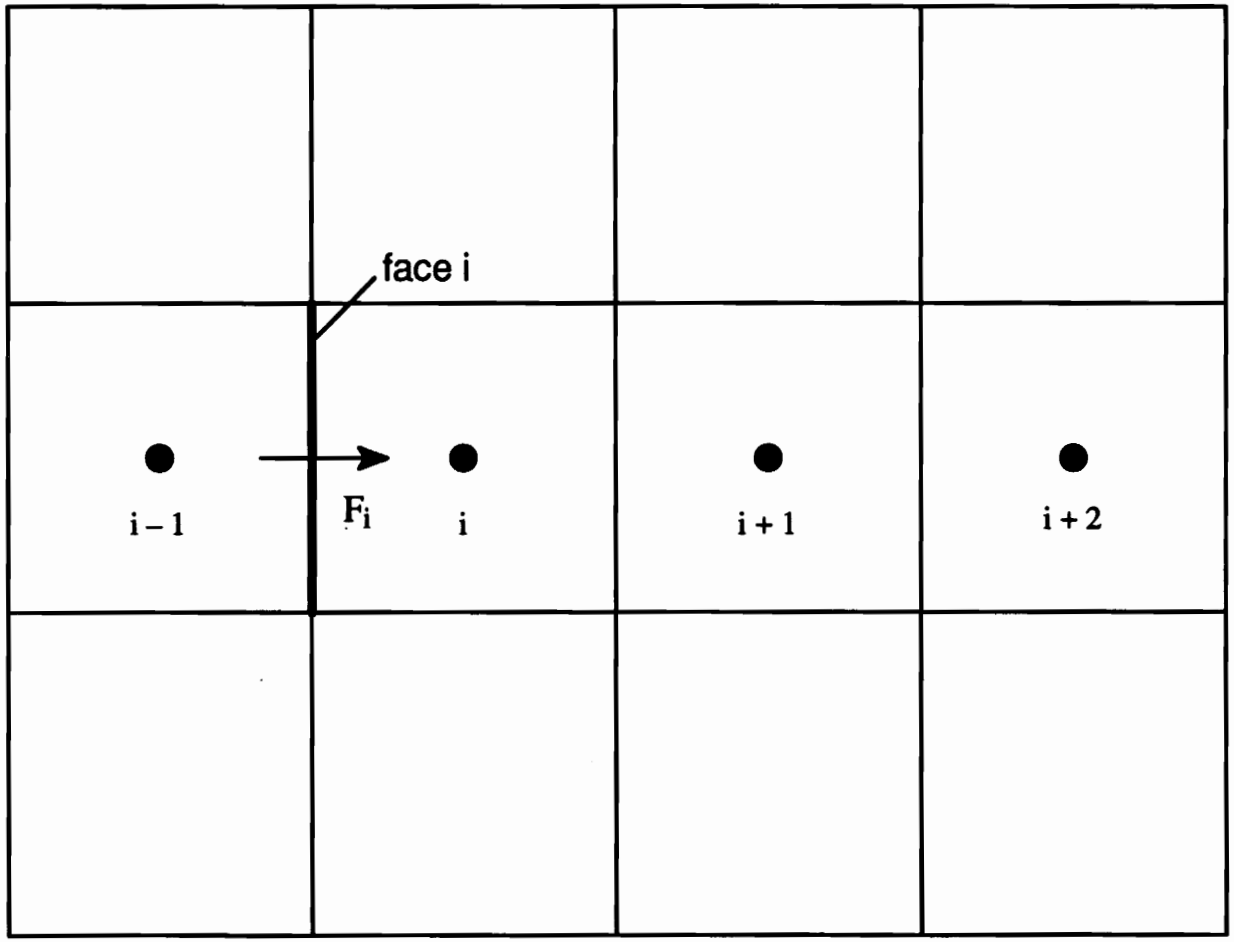

Figure 39. Node Labeling Convention For Flux Discretisation

B.3.2 Linear Upwind Differencing

Linear upwind differencing is a second order scheme which uses linear extrapolation to determine Φ_i from the two nearest upwind nodes (Fig. 39).

$$C_i = F_i \, [\Phi_i + (\Phi_i - \Phi_{i-1})] \, f_- \quad , \text{ if } F_i \geq 0 \qquad (B-5)$$

or

$$C_i = F_i \, [\Phi_{i+1} + (\Phi_{i+1} - \Phi_{i+2})] \, f_+ \quad , \text{ if } F_i < 0 \qquad (B-6)$$

where, f_+ and f_- are linear interpolation factors

This higher order differencing scheme preserves gradients more effectively than lower order methods. However, the truncation error resulting from this method of discretisation results in artificially generated spatial inconsistencies, known as numerical dispersion.

B.3.3 Central Differencing

The central differencing scheme is also a second order scheme. Unlike the linear upwind scheme, however, central differencing linearly interpolates from the node's neighbors, regardless of flow direction

$$C_i = F_i \, [\, f_+ \, \Phi_i + (\, 1 - f_+ \,) \, \Phi_{i+1} \,] \qquad (B-7)$$

where, f_+ is an interpolation factor

This scheme does reduce the amount of artificial diffusion, but, like linear upwind differencing, does produce numerical dispersion.

B.3.4 Blended Central Differencing

Blended central differencing combines the higher order schemes central differencing (CD) and linear upwind differencing (LUD) with a lower order scheme, such as upwind differencing (UD), in an attempt to control numerical dispersion.

$$C_i^{BD} = \gamma\, C_i^{CD/LUD} + (1-\gamma)\, C_i^{UD} \qquad (B-8)$$

The blending factor γ is user–specified and is taken to be uniform over the computational field. If $\gamma < 1$, the solution may be influenced by numerical diffusion.

Appendix C. Implementation and Use of the Chen Modification

The Chen modification was implemented into STAR–CD via a user defined subroutine. USORKE, the subroutine provided, is used to modify the source terms of the turbulent transport equations. In addition, a common block was added to the subroutine to change the turbulent Prandtl numbers. To employ the modification, the use of the user defined subroutine, USORKE, must be specified and the turbulent dissipation equation coefficients, $C_{\varepsilon 1}$ and $C_{\varepsilon 2,}$ must be changed in the pre–processing program PROSTAR. A more detailed description of the implementation of the Chen modification to the k–epsilon turbulence model into STAR–CD and its use is included in the following sections.

C.1 Modifying the User Defined Subroutine USORKE

To implement the Chen modification into STAR–CD, the source terms of the k–epsilon equation and the turbulent Prandtl numbers must be changed. This is done through USORKE, a subroutine which can be modified to suit the user's purpose. The source terms are formulated in the user defined subroutine and passed back to STAR–CD. These terms replace the standard k–epsilon source terms. Because the source terms are expressed as functions of the turbulent

transport properties, they must be linearized to be evaluated. The source terms can be linearized as:

$$S = S_1 - S_2 \Phi \qquad (C-1)$$

The source terms of the Chen modification are given as [10]:

$$C_1 \mathrm{Pr} \frac{\varepsilon}{k} - C_2 \frac{\varepsilon^2}{k} + C_3 \frac{\mathrm{Pr}^2}{k} \qquad (C-2)$$

where, the third term is the addition made by Chen. The compressibility terms can be defined as:

$$A_{comp1} = \frac{2}{3}\left(\mu_t \frac{\partial u_i}{\partial x_i} + \varrho k\right)\frac{\partial u_i}{\partial x_i}$$

and,

$$A_{comp2} = C_4 \, \varrho \varepsilon \frac{\partial u_i}{\partial x_i}$$

The source terms of the compressible turbulent dissipation equation can now be written as follows.

$$S = \varrho C_1 \frac{\varepsilon}{k} \mathrm{Pr} - A_{comp1} \frac{\varepsilon}{k} - C_2 \, \varrho \frac{\varepsilon^2}{k} - A_{comp2} \, \varepsilon + C_3 \frac{\mathrm{Pr}^2}{k} \qquad (C-3)$$

The modification can be linearized in the same manner as the k–epsilon model. The only restriction being that S_1 and S_2 must always be positive. With this in mind, the source terms of the turbulent dissipation equation can be linearized as follows:

$$S_1 = \varrho C_\mu \frac{k}{\mu_t} \left[C_1 \varrho \, \mathrm{Pr} - \min(0.0, \; A_{comp1}) - \min(0.0, \; A_{comp2}) \; k \right] + C_3 \frac{\mathrm{Pr}^2}{k} \qquad (C-4)$$

and,

$$S_2 = \varrho C_2 \left(C_\mu \, \varrho \frac{k}{\mu_t}\right) + \max(0.0, \; A_{comp2}) + \max(0.0, \; A_{comp1}/k \qquad (C-5)$$

where,

$$\varrho C_\mu \frac{k}{\mu_t} = \frac{\varepsilon}{k} \qquad (C-6)$$

and, the min and max functions simply take the minimum or maximum value of the arguments. Arranging the source terms in this manner assures that S_1 and S_2 will be positive.

The gradients necessary to calculate production, as well as the compressibility terms are passed to the subroutine from the main program along with the values of turbulent kinetic energy, dissipation and effective viscosity from the previous time step. The values of C_1 and C_2 for the Chen modification are also passed to the subroutine, but are defined again with C_3 to ensure their correct values are used. The turbulent Prandtl numbers are changed in the subroutine and passed back to the main program via a common block taken from STAR–CD. This common block was made available to the author by Computational Dynamics. A listing of the modified subroutine is given on the following pages.

C.2 Use of the Chen Modification with STAR–CD

To use the Chen modification with STAR–CD, the user must enter PROSTAR, STAR–CD's pre and post processor. The use of the user defined subroutine USORKE must be specified and can be done by issuing the command "rsource n y n n n n". The source coefficients for the turbulent dissipation equation $C_{\varepsilon 1}$ and $C_{\varepsilon 2}$ must be change to the values specified by Chen. This can be done by issuing the command "coke 0.09 1.15 1.9". These changes must be saved in the problem file, which is accomplished by the command "prob 10". Important to remember is to include the modified version of USORKE in the file ufile.f and to specify the inclusion of this file when compiling.

```
C*************************************************************************
      SUBROUTINE USORKE(IPHI,IP,ICTID,IMAT,IPOR,X,Y,Z,U,V,W,P,TE,ED,
     *                  VIS,T,DEN,SC1,SC2,SC3,sVISCOS,sPREF,sTREF,sDENSIT,
     *                     CV,big,sSMALL,ITER,sTIME,GENP,GB,DUMY,DUDX,
     *                     DVDY,DWDZ,DUDY,DVDX,DUDZ,DWDX,DVDZ,DWDY,S1P,S2P)
C*************************************************************************
c      big replaces GREAT
c
C      IMPLICIT DOUBLE PRECISION (A-H,O-Z)
      COMMON/USR001/INTFLG(100)
C-------------------------------------------------------------------------
c      common block added to determine the values of the arrays
c      PRLINV and PRTINV and to modify them.
C-------------------------------------------------------------------------
      COMMON /MAINR/
     *      G,SOR(12),RESOR(12),SNORIN(12),PRLINV(12),PRTINV(12),
     *      URF(12),DENSIT,SORMAX,VISCOS,GREAT,SMALL,HAF,ZERO,ONTR,
     *      TWTR,SMAL1,SMAL2,SMAL3,SMAL4,SMAL5,SMALS,SGREAT,C1,C2,C3,
     *      C4,CAPPA,CMU,CMU25,CMU75,ELOG,REY,DIS,TIN,ZMIN(3),ZMOUT(3),
     *      CPH,CPS,TREF,ENREF,TENOM,EDNOM,WMOL,WM1,WM2,
     *      WM3,BETA,PREF,PREPP,UGC,GRAVX,GRAVY,GRAVZ,PRANL,OMEGA,XO1,
     *      YO1,ZO1,XO2,YO2,ZO2,DCOS1,DCOS2,DCOS3,SC1IN,SC2IN,SC3IN,
     *      HR1,HR2,HR3,URFR,URFDPW,RESMAX(12),DTNORM,FLAVG,TIME,DT,
     *      DTIN,RESNOC,RESOC,LSC(12),GG(12),RMAX, ONE,PONE,POONE,
     *      SNORV(3),GVALO(12),GVAL(12),ARAVG,SWBLF,CUNO,SORCMX(12)
c
c*****open a file to print Prandtl numbers to
c
c
c
c*****write iteration number to file
c
c      write(1,*) iter
c
c*****If iteration is one, print Prandtl numbers to a file
c
c        write(1,20)
c 20     format(2x,'Entering subroutine')
c
c      if(iter.eq.2) then
c          write(1,25)
c 25       format(2x,'PRLINV',2x,'PRTINV')
c        do 30 i=5,7
c 30       write(1,*) PRLINV(i),PRTINV(i)
c      endif
c
c*****Change Prandtl numbers to values specified by Chen
c*****PrTE = 0.75  PrDISS = 1.15
c
        PRTINV(5) = 1./0.75
        PRLINV(5) = PRTINV(5)
        PRTINV(6) = 1./1.15
        PRLINV(6) = PRTINV(6)
c*****Define coefficients used by Chen
        const1 = 1.15
        const2 = 1.9
        const3 = 0.25
c
C-------------------------------------------------------------------------
C    This subroutine enables user to specify source term (per unit volu-
```

```
C     me) for turbulence kinetic energy (if IPHI=1) and/or its dissipation
C     rate (if IPHI=2) in linearized form:
C
C          Source for kin. energy = S1P-S2P*TE, (W/m**3)
C          Source for dissipation = S1P-S2P*ED, (W/m**3/s)
C
C     where S1P and S2P can be functions of all the other parameters in
C     parameter list (which cannot be changed in this subroutine).
C
C     If k or/and epsilon is to be fixed to a given value PHI, then the
C     following may be used:
C
C          S1P=GREAT*PHI
C          S2P=GREAT,
C
C     where PHI stands for TE or ED and can be a constant or an arbitrary
C     function of the parameters in the parameter list.
C
C     ** Parameters to be returned to STAR:  S1P,S2P
C
C-----------------------------------------------------------------------
C
C      Sample coding:  k-epsilon model (same as in standard STAR coding)
C
c234567
CC----SOURCE TERMS FOR TURBULENT KINETIC ENERGY
       IF(IPHI.EQ.1) THEN
         GEN=2.*(DUDX**2+DVDY**2+DWDZ**2)+
      *         (DUDY+DVDX)**2+(DUDZ+DWDX)**2+(DVDZ+DWDY)**2
         VIST=VIS-sVISCOS+sSMALL
         GEN=GEN*VIST
cc----compressibility term
          divuvw=dudx+dvdy+dwdz
          acomp=2./3.*(vist*divuvw+den*te)*divuvw
cc----assemble source terms
         S1P=GEN-min(0.,acomp)
         S2P=0.09*DEN**2*TE/VIST+max(0.,acomp/te)
       ENDIF
C
CC----SOURCE TERMS FOR TURBULENT ENERGY DISSIPATION RATE
       IF(IPHI.EQ.2) THEN
         VIST=VIS-sVISCOS+sSMALL
         TERM=0.09*DEN*TE/VIST
         GEN=VIST*(2.*(DUDX**2+DVDY**2+DWDZ**2)+
      *           (DUDY+DVDX)**2+(DUDZ+DWDX)**2+(DVDZ+DWDY)**2)
c-----compressibility terms
          divuvw=dudx+dvdy+dwdz
c
c-----acomp1 without Chen's modification
c          acomp1=0.96*(vist*divuvw+den*te)*divuvw
c
c-----acomp1 with Chen's modification
          acomp1 = 2./3.*const1*(vist*divuvw+den*te)*divuvw
c
          acomp2=0.377*den*divuvw
cc----assemble source terms
c-----Without Chen's modification
c         S1P=(1.44*GEN-min(0.,acomp1)-min(0.,acomp2)*te)*term
c-----With Chen's modification
         S1P = (const1*GEN-min(0.,acomp1)-min(0.,acomp2)*te)*term
```

```
     .            +const3*gen**2./den/te
        S2P=const2*DEN*TERM+max(0.,acomp2)+max(0.,acomp1/te)
       ENDIF
C-----------------------------------------------------------------
       RETURN
       END
```

Appendix D. Qualifying Case: Rectangular Backward Facing Step

To qualify the implementation of the Chen modification to STAR–CD, the code was tested with a rectangular backward facing step. This geometry is similar to one tested by Chen, but contains more comprehensive experimental data. Flow approaching a backward facing step encounters a large adverse pressure gradient. As a result, a large recirculation zone forms behind the step. This case is an excellent demonstration of the ability of the Chen modification to control the dissipative effects regularly seen with the use of k–epsilon.

The case chosen is an experiment done by Vogel and Eaton [12]. The test configuration is a 3.8 centimeter two dimensional rectangular backward facing step with a 1.25 expansion ratio, as seen in Fig. 40. The flow is allowed to develop through a 2.5 meter entrance section. A porous bottom wall allowed for the variation of the boundary layer thickness at the test section entrance. The experimental data used in this study is for an inlet boundary layer thickness of 4.05 cm. The corresponding reference free stream velocity, which is defined as the free stream velocity measured at the inlet, is 11.3 m/s with a step height Reynolds number of 28,000. The inlet velocity profile, which is measured at 3.8 step heights upstream

of the step, agrees well with a standard log–law of the wall. The parameters describing the profile are included in the report, and are as follows:

Reference conditions:	U_{ref} = 11.3 m/s
	Re_H = 28,000
Boundary layer parameters (measured at x/H = –3.8):	
Boundary layer thickness	δ_{99} = 4.05 cm
Momentum thickness	Θ = 0.468 cm
Momentum thickness Reynolds number	Re_Θ = 3370
Shape factor	H = 1.389
Skin friction (log–law fit)	C_f = 0.00312

The reattachment point for this inlet profile is measured at 6 2/3 step heights downstream of separation. The exit length of the experimental apparatus is 2.5 meters, allowing the flow to again become fully developed after reattachment. Mean velocity profiles are available at 2.2, 3.0, 3.73, 4.467, 5.2, 5.93, 6.67, 7.4 and 8.865 step heights downstream of separation.

A grid independent solution was determined by varying the mesh density. The best solution is used in this study. The final grid for the rectangular backward facing step, as shown in Fig. 41, is two dimensional with 50 x 50 cells upstream of the step and 80 x 60 cells downstream of the step. To yield a consistent representation of the near wall flow, y+ must be between 30 and 100 [30]. For this reason, the grid is packed away from the walls and towards the center. The mesh is also slowly expanded downstream of the step, as the gradients are not as large in this region.

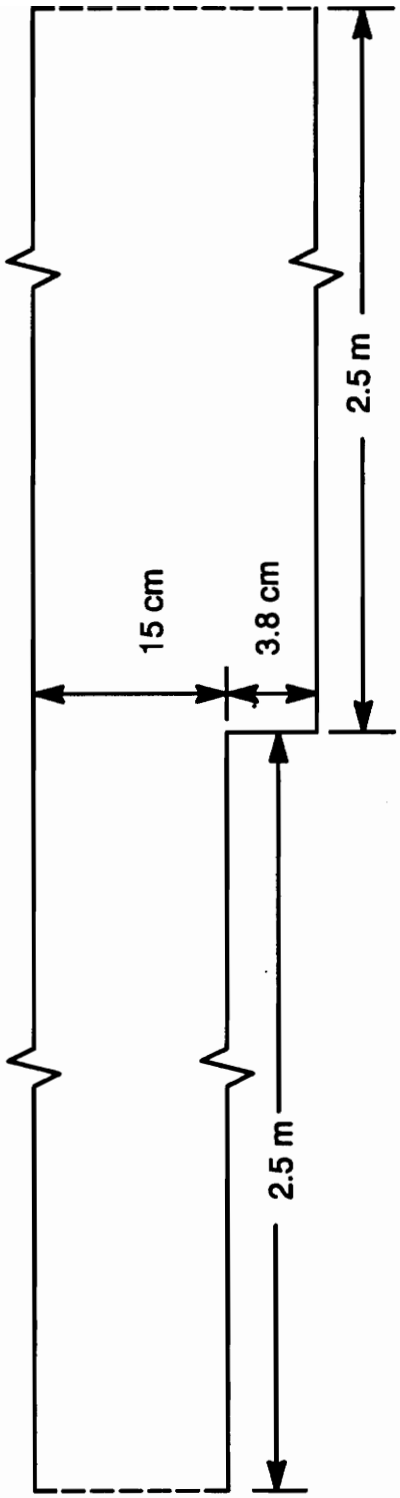

Figure 40. Rectangular Backward Facing Step, Geometry

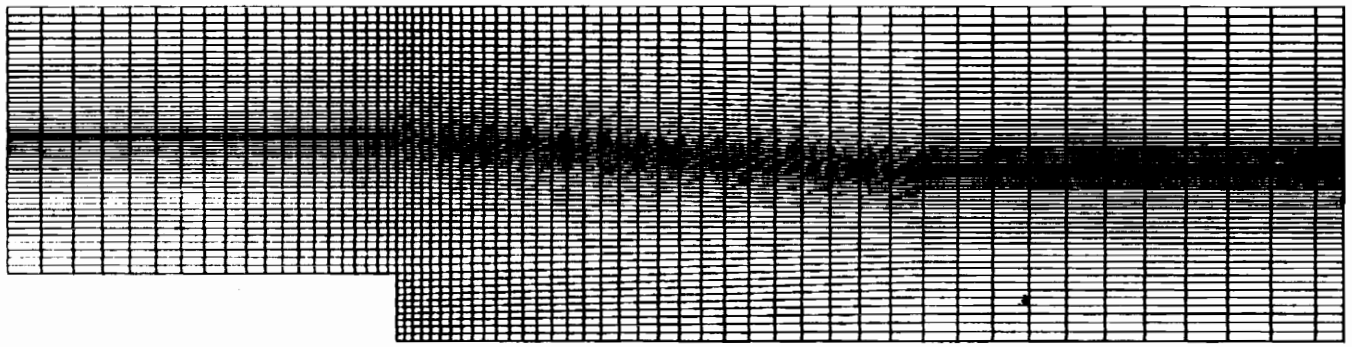

Figure 41. Rectangular Backward Facing Step, Mesh

The inlet condition is set at 3.8 step heights upstream of the expansion in accordance with the log–law of the wall given in the report. Computation is begun at 2.5 meters upstream of the step. A uniform inlet velocity and turbulence properties were given at this point and adjusted to fit the log–law parameters given for the inlet conditions. The turbulent parameters, k and ε, are determined based on the assumption of a freestream turbulence level less than 0.2%, and a turbulent to laminar viscosity ratio of 10. The values are uniform across the inlet and are given as: $k_{in} = 6.577 \times 10^{-4}$ m^2/s^2 and $\varepsilon_{in} = 2.6 \times 10^{-4}$ m^2/s^2. The inlet velocity is determined to be 10.457 m/s, which yields a boundary layer thickness of 3.95 cm at 3.8 step heights upstream from the step, a 2.5% error. This error is considered to be acceptable. Furthermore, the report by Vogel and Eaton [12] concluded that boundary layer thickness at the entrance to the step has little effect on the reattachment length, the primary characteristic of the flow. At the outlet plane, a standard outlet boundary condition is set with a flow split of 1.0. The outlet boundary condition in PROSTAR sets the gradients of all variables to zero on the specified plane or set of cell faces. The faces of the model in the x–y plane are defined as symmetry planes, which denotes the normal component of velocity and all other variables to be identically zero. The walls are treated as non–permeable. The flow in the near wall region is resolved with the use of a standard log law of the wall, the disadvantages of which were discussed in chapter 6.

This case was run with an upwind differencing scheme and blended central differencing. Final results for blended central differencing scheme with a blending factor of 0.95 are presented in this report, as they were found to yield the most consistent results. Both the Chen modification and STAR–CD with it's original k–epsilon scheme are evaluated for this test case.

The Chen modification greatly improves velocity predictions for this case. Figures 42 through 44 compare the axial velocity profiles of the Chen modification and the standard k–epsilon model. At experimental station 2, x/H = 3.0, the standard k–epsilon solution is beginning to reattach, whereas, the Chen modification is still separated and more closely models the flow. At station 5, k–epsilon predicts the flow to be reattached. At this point the Chen modification still predicts the flow to be separated. It is not until station 7 that the Chen model predicts the flow to reattach. Station 7, conveniently, is at 6 2/3 step heights downstream of separation, representing the experimental point of reattachment. Standard k–epsilon predicts reattachment to occur at 5.04 step heights, a 24.4% error, whereas the Chen model predicts the reattachment length to be 6.79 step heights, a 1.8% error. Figures 45 and 46 show the recirculation zones of the standard k–epsilon model and the Chen model, respectively. Clearly indicated is the lengthening of the recirculation region behind the step by the Chen modification.

The modification is able to make such a significant improvement in predictions because of its ability to control the dissipative effects of the k–epsilon model. Figure 47 indicates a decrease in the eddy viscosity in the recirculation zone and the region directly above it. A jet of high momentum fluid flows over the recirculation zone. This results in high gradients in the region where the jet and recirculation zone meet. The Chen modification allows the turbulent energy transfer mechanism to react more effectively to shear. The result is a decrease of the turbulent eddy viscosity in high shear regions. The Chen model predicts a lower eddy viscosity in the jet stream allowing the fluid to maintain its momentum. The jet will not react to the low pressure region created by the recirculation, and will resist

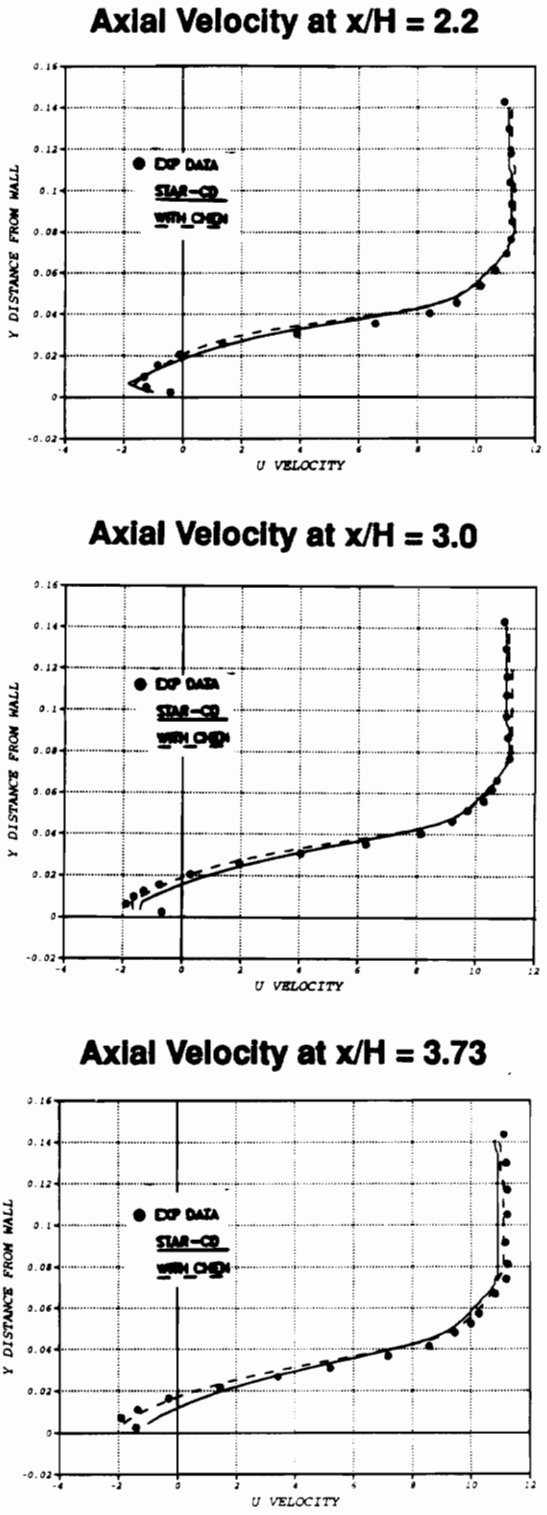

Figure 42. Rectangular Backward Facing Step, Axial Velocity Profiles

Axial Velocity at x/H = 4.467

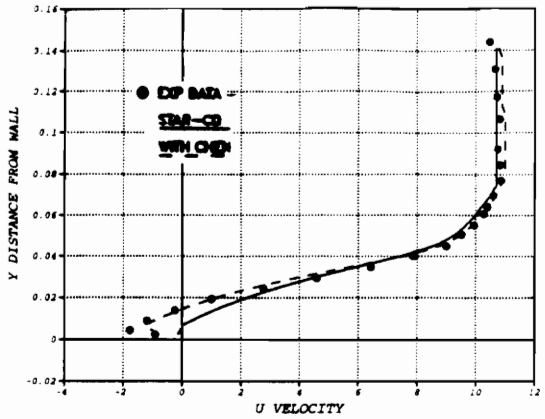

Axial Velocity at x/H = 5.2

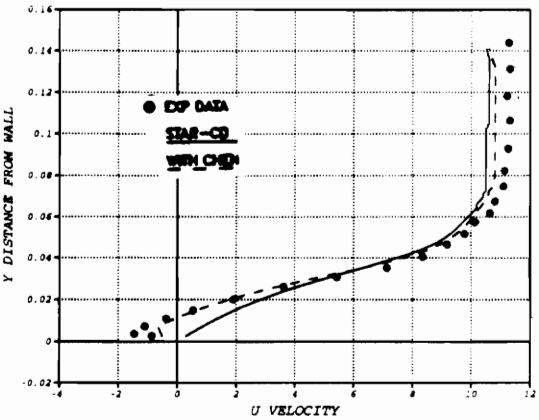

Axial Velocity at x/H = 5.93

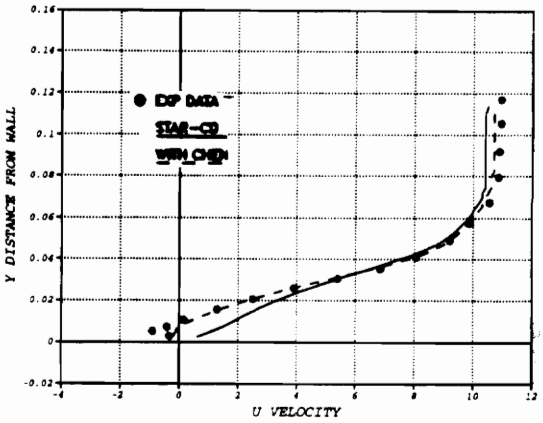

Figure 43. Rectangular Backward Facing Step, Axial Velocity Profiles

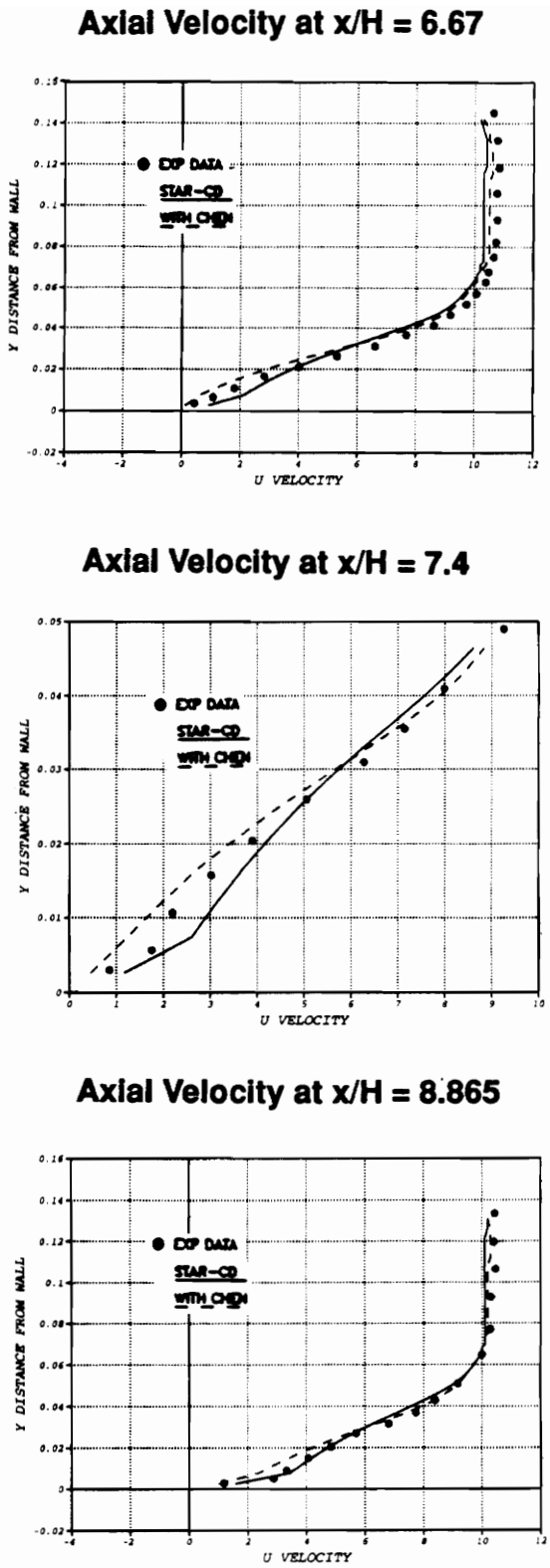

Figure 44. Rectangular Backward Facing Step, Axial Velocity Profiles

turning. The fluid is turned more slowly and the point of reattachment is extended. The converse of this argument is an explanation for the underprediction of the reattachment point by the standard k–epsilon model.

Improved results for the rectangular facing step test case prove the implementation of the Chen modification to STAR–CD to be a success. In addition to this case, the Chen modification was also run with several other cases, further verifying the implementation's success. One of these applications is the rectangular elbow with 90°, which has been discussed in appendix A.

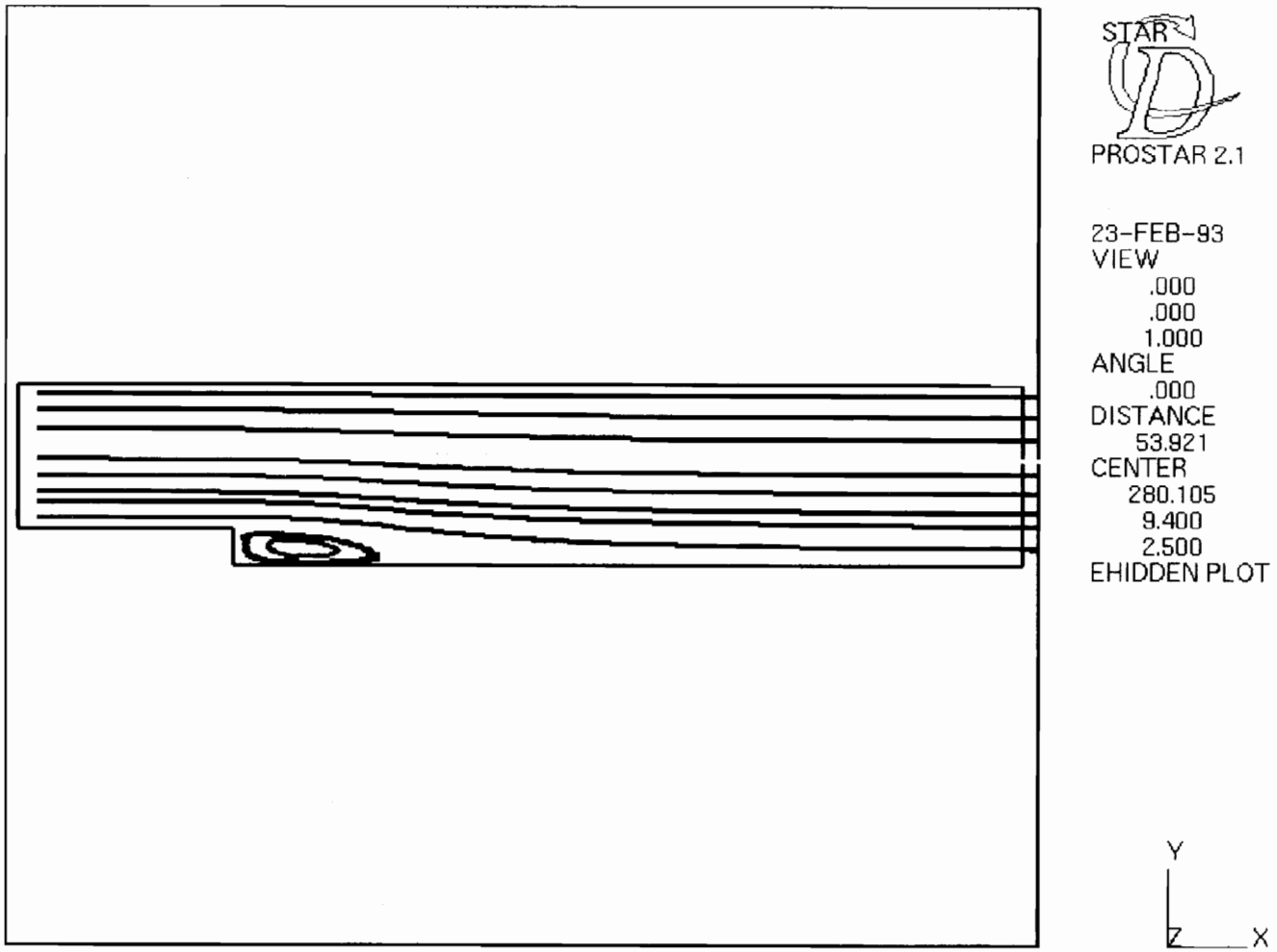

Figure 45. Rectangular Backward Facing Step, k–epsilon Model Streamlines

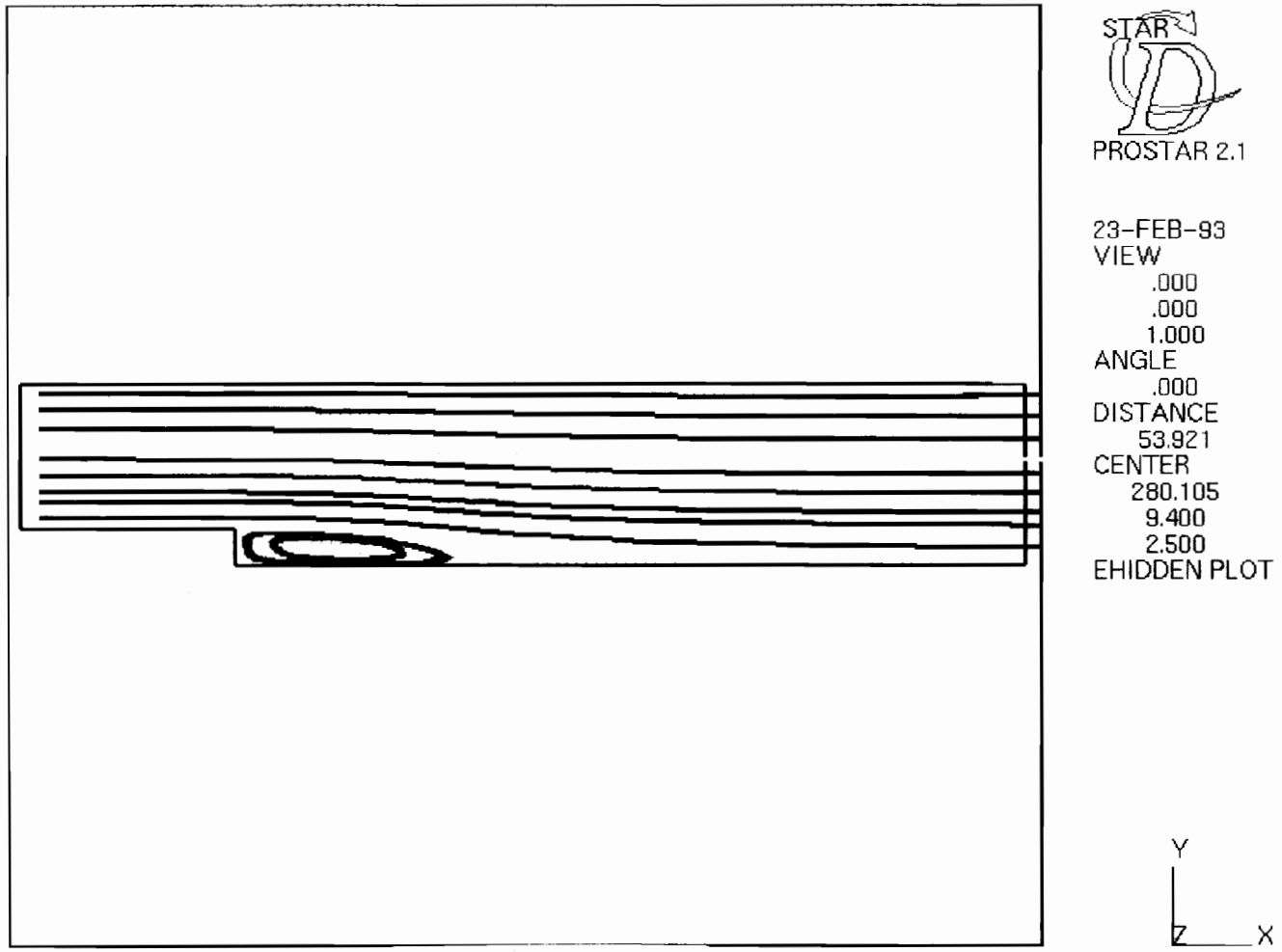

Figure 46. Rectangular Backward Facing Step, Chen Modification Streamlines

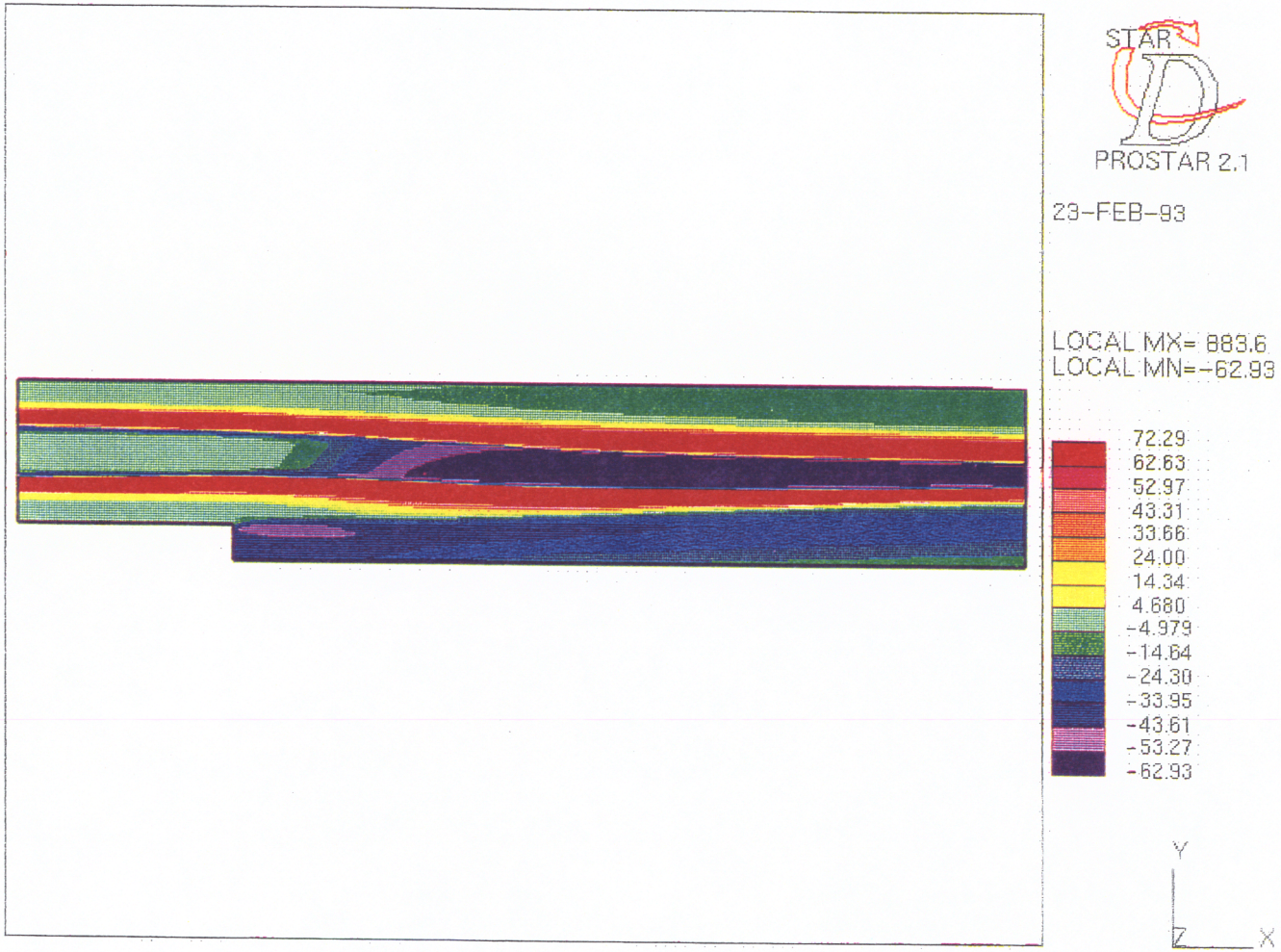

Figure 47. Rectangular Backward Facing Step, Percent Change Eddy Viscosity from Standard k–epsilon to Chen Modification

References

1. Verhoff, A., Melnik, R. E. , and Carter, J. E., "Industry Warms to CFD," *Aerospace America*, Vol. 30, No. 2, February 1992, pp. 32–35.

2. O'Connor, L., "Computational Fluid Dynamics: Giving A Boost to Engine Design," *Mechanical Engineering*, Vol. 114, No. 5, May 1992, pp. 44–50.

3. Lefebvre, A. H., *Gas Turbine Combustion*, Hemisphere, New York, 1983, pp. 107 –151.

4. Washam, R. M., Combustion Engineer, Gas Turbine Design and Development Engineering, General Electric Power Generation, Schenectady, NY, Personal Communication, January 1993.

5. Corr, R. A., Combustion Engineer, Gas Turbine Design and Development Engineering, General Electric Power Generation, Schenectady, NY, Personal Communication, January 1993.

6. Lefebvre, A. H., *Gas Turbine Combustion*, Hemisphere, New York, 1983, pp. 126–127.

7. Hallett, W. L. H., Günther, R., "The Turbulent Structure of Swirling Flow in A Sudden Expansion," *Fourth Symposia on Turbulent Shear Flows*, 1984, pp. 19.25–19.28.

8. Korane, K. J., "The Changing State of CFD," *Machine Design*, Vol. 62, No. 15, July 26, 1990, pp.83–85.

9. Moin, P., "The Computation of Turbulence," *Aerospace America*, Vol. 30, No. 1, January 1992, pp. 42–47.

10. Chen, Y. S. and Kim, S. W., "Computation of Turbulent Flows Using an Extended k–ε Turbulence Closure Model," NASA CR–179204, October 1987.

11. Clarke, D. S., Moore, J. R., and Wilkes, N. S., "Prediction of Turbulent Swirling Flows Through Quarled Burners Using Reynolds Stress Turbulence Models," *Harwell Laboratory Publication*, AERE R 13726.

12. Vogel, J. C., Eaton, J. K., "Combined Heat Transfer and Fluid Dynamic Measurements Downstream of a Backward–Facing Step," *ASME Journal of Heat Transfer*, Vol. 107, November 1985, pp. 922–929.

13. Sloan, D. G., Smith, P. J., and Smoot, L. D., "Modeling of Swirl in Turbulent Flow Systems," *Progress in Energy and Combustion Science*, Vol. 12, No. 3, 1986, pp. 163–250.

14. Pourahmadi, F. and Humphrey, J. A.,"Prediction of Curved Channel Flow with an Extended k–ε Model of Turbulence,"*AIAA Journal*, Vol. 21, No. 10, October 1983, pp. 1365–1373.

15. Rodi, W. and Scheuerer, G., "Scrutinizing the k–ε Turbulence Model Under Adverse Pressure Gradient Conditions," *ASME Journal of Fluids Engineering*, Vol. 108, June 1986, pp. 174–179.

16. Hinze, J. O., *Turbulence*, McGraw–Hill Inc., New York, 1975, p. 6.

17. White, F. M., *Viscous Fluid Flow*, McGraw–Hill Inc., New York, 1991.

18. Braaten, M. E., "An Introduction to Boundary Layer Theory and Turbulence Modeling," Power Generation Engineering Course Notes, Fluid Mechanics Program, General Electric Research and Development Center, Schenectady, NY.

19. Launder, B. E., and Spalding, D. B. ,"Numerical Computation of Turbulent Flows," *Methods in Applied Mechanics and Engineering*, Vol. 3, pp. 269–289.

20. Abou–Arab, T. W., Richter, W., and Seeger, M., "Experimental Investigation of Turbulent Isothermal Flow in a Two Dimensional Furnace Model," *International Journal of Engineering Fluid Mechanics*, Vol. 4, No. 1, 1991, pp. 111–126.

21. Dellenback, P. A., Metzger, D. E., and Neitzel, G. D., "Heat Transfer to Turbulent Swirling Flow Through A Sudden Axisymmetric Expansion," *Journal of Heat Transfer*, Vol. 109, August 1987, pp. 613–620.

22. Benim, A. C., "Finite Element Analysis of Confined Turbulent Swirling Flows," *International Journal for Numerical Methods in Fluids*, Vol. 11, 1990, pp. 697–717.

23. Kim, S. W., "A Near Wall Turbulence Model and Its Application to Fully Developed Turbulent Channel and Pipe Flows," NASA TM–101399, November 1988.

24. Schlichting, H., *Boundary Layer Theory,* McGraw–Hill Inc., New York, 1968, pp. 553–559.

25. Rodi, W., "Experience with Two–Layer Models Combining the k–ε Model with a One–equation Model Near the Wall," *AIAA Paper*, AIAA – 91 – 0216, 1991.

26. Brankovic, A. and Stowers, S. T., "Review of Low Reynolds Number Turbulence Models for Complex Internal Separated Flows," *AIAA Paper*, AIAA – 88 – 3006, 1988.

27. Taylor, A. M. D. P., Whitelaw, J. H., and Yianneskis, "Curved Ducts With Strong Secondary Motion: Velocity Measurements of Developing Laminar and Turbulent Flow," *Journal of Fluids Engineering*, Vol 104, September 1982, pp. 350–359.

28. Battaglioli, J. L., Advanced Technologies Engineer, Gas Turbine Design and Development Engineering, General Electric Power Generation, Schenectady, NY, Personal Communication, August 1992.

29. Anderson, D. A., Tannehill, J. C., and Pletcher, R. H., *Computational Fluid Mechanics and Heat Transfer*, Hemisphere, New York, 1984, pp. 185–186.

30. STAR–CD Users Manual, Computational Dynamics Inc., Olympic House, 1991, pp. 4.3–5.3.

31. Patankar, S. V., *Numerical Heat Transfer and Fluid Flow*, Hemisphere, Washington D. C., 1980, pp.121–133.

32. Raithby, G. D., and Schneider, G. E., "Numerical Solution of Problems in Incompressible Fluid Flow: Treatment of the Velocity – Pressure Coupling," *Numerical Heat Transfer*, Vol. 2, 1979, pp. 417–440.

33. VanDoormaal, J. P. and Raithby, G. D., "Enhancement of the SIMPLE Method for Predicting Incompressible Fluid Flow," *Numerical Heat Transfer*, Vol. 7, 1984, pp. 147–163.

Vita

The author was born February 23, 1969 in Albany, New York. She resided in Newtonville, New York for her entire youth and graduated from Shaker High School in 1987. From there, the author went on to study mechanical engineering at the University of Buffalo where she was a member of Chi Omega Fraternity. She graduated Cum Laude and with engineering honors in May 1991. In the fall of 1991, she began work on a Masters of Science in Mechanical Engineering at Virginia Polytechnic Institute and State University. Persistent to work in the field of computational fluid dynamics (CFD), she struggled with the reality of a lack of funding in this field. In July 1992 General Electric Power Generation offered to sponsor her graduate work in CFD. The author, destined to return to New York, moved back home to live with her parents and conduct her research at General Electric's Main Plant facility in Schenectady. In fall 1993 she will move to Ithaca, New York where she will pursue a Doctorate in Mechanical Engineering at Cornell University.

Heather L. Relation